Copyright Warning & Restrictions

The copyright law of the United States (Title 17, United States Code) governs the making of photocopies or other reproductions of copyrighted material.

Under certain conditions specified in the law, libraries and archives are authorized to furnish a photocopy or other reproduction. One of these specified conditions is that the photocopy or reproduction is not to be "used for any purpose other than private study, scholarship, or research." If a, user makes a request for, or later uses, a photocopy or reproduction for purposes in excess of "fair use" that user may be liable for copyright infringement,

This institution reserves the right to refuse to accept a copying order if, in its judgment, fulfillment of the order would involve violation of copyright law.

Please Note: The author retains the copyright while the New Jersey Institute of Technology reserves the right to distribute this thesis or dissertation

Printing note: If you do not wish to print this page, then select "Pages from: first page # to: last page #" on the print dialog screen

NJIT
New Jersey's Science &
Technology University

The Van Houten library has removed some of the personal information and all signatures from the approval page and biographical sketches of theses and dissertations in order to protect the identity of NJIT graduates and faculty.

ABSTRACT

Conditional Artificial Dielectric:
Optically Controlled Microwave Modulator

by
Jose Manuel Jimenez

A conditional artificial dielectric with embeddings of either CdS, GaAs or Si in PMMA form the dielectric material of a microstrip in a homodyne microwave detection system. The system consists of a Michelson or Mach-Zehnder interferometers with the microstrip placed in one arm. The index of refraction of the microstrip substrate is modulated by chopped incident light causing amplitude and phase variations in the incoming RF signal. Those variations are detected by mixing the light modulated microwave carrier(information channel) with the unmodulated carrier (reference channel) in the interferometer. The output is sensed by the square law detector and a lock-in amplifier synchronized with the light modulating frequency.

CONDITIONAL ARTIFICIAL DIELECTRIC: OPTICALLY CONTROLLED MICROWAVE MODULATOR

by
J. Manuel Jimenez

Thesis Submitted to the Faculty of the Graduate Division of the New Jersey Institute of Technology in Partial Fulfillment of the Requirements for the Degree of Masters of Electrical Engineering
Department of Electrical and Computer Engineering
January 1992

APPROVAL PAGE

Artificial dielectrics:
Optically controlled microwave modulator

by
J. Manuel Jimenez

Dr. Haim Grebel, Thesis Adviser
Professor of Electrical and Computer Engineering, NJIT

Dr. John Hensel, Committee Member
Professor of Physics, NJIT

Dr. Eugene Gordon, Committee Member
Professor of Electrical and Computer Engineering, NJIT

BIOGRAPHICAL SKETCH

Author: J. Manuel Jimenez

Degree: Master of Science in Electrical Engineering

Date: December, 1991

Undergraduate and Graduate Education:

- Master of Science in Electrical Engineering, New Jersey Institute of Technology, Newark, NJ, 1991
- Bachelor of Science in Electrical Engineering Technology, New Jersey Institute of Technology, Newark NJ, 1989
- Bachelor of Science in Industrial Engineering, E.U.T.I.Z, Saragosse, Spain, 1986

Major: Electrical Engineering

ACKNOWLEDGMENT

The author wishes to express his sincere gratitude to his supervisor, Dr. Haim Grebel for his guidance and moral support throughout this research.

Special thanks to professors Edip Niver and John Hensel for the borrowed equipment and for the valuable suggestions.

And finally thanks to all members and students of the Optical Waveguide laboratory for their help and collaboration.

TABLE OF CONTENTS

Page

1. INTRODUCTION

2. THEORY

2.I Optical absorption 4
2.II Classical dispersion theory of bound electrons 6
2.III Conditional Artificial dielectric waveguides 7
1. Mathematical analysis of artificial dielectrics 8
2.IV Microstrip theory and design 10
1. Static analysis 10
1. Characteristic Impedance 12
2. Dynamic analysis 13
3. Characterization of a microstrip with the s-parameters 15
1. The scattering matrix 15
2. Variation of the scattering matrix due to incident light on the microstrip 16
2.V Interference of waves 17
1. Microwave Mach-Zenhder interferometer 17
2. Microwave Michelson interferometer 18
2.VI Homodyne detection systems 19
1. Amplitude modulation 20
1. Low level or square law detection: Doubble Side Band with Carrier(DSBWC) 20
2. Low level or square law detection Double Side Band With Carrier Suppression(DSBSC) 21
3. High level or linear detection (DSB modulation) 21
4. Phase measurements(DSB amplitud Modulation) 22
5. lock-in amplifiers 23
2. Phase modulation 24
3. Simultaneous phase and Amplitude modulation 25

3. MATERIALS AND EXPERIMENTAL METHODS

3.1 Substrate fabrication 27
1. Inhibitor removal 27
2. Catalyst selection and polymerization 27
3. Addition of semiconductor clusters 28
4. Molding the monomer 28
3.2 Microstrip fabrication 30
3.3 Absorption in CdS, GaAs and Si 35
3.4 Measurement of the relative permittivity and permeability 36
3.5 Microstrip launching characterization 37
3.6 Microstrip DC measurements 39

3.7 Microstrip S-Parameters measurements 39
3.8 Homodyne detection measurements 42
1. Mach-Zenhder and Michelson interferometers 42

4. RESULTS

4.1 Absorption in the CdS, GaAs and Si doped substrates 48
4.2 Substrates permittivity and permeability results 51
4.3 Microstrip design considerations results 52
1. Network Analalyzer results 55
4.4 Homodyne detection results (lock-in measurements) 71
1. Phase response of the GaAs, Siand CdS samples 71
2. Detection with partial suppression of the carrier in the information channel 73
3. Response for the different light sources 75
4. GaAs and CdS frequency response 75
5. Response of the detection function of the amplitud of the reference channel 79
6. Detection at different carrier frequencies 79
7. Michelson Interferometer detection 82
1. Phase Measurements in the lock-in amplifier 82
2. Phase measurements in the power meter 87

5. DISCUSSION

5.1 Substrate and microstrip considerations 89
5.2 Homodyne detection considerations 92
1. Phase response for the GaAs, Si and CdS samples(lock-in measurements) 92
1. Mach-Zehnder interferometer 92
2. Michelson interferometer 94
3. Frequency response considerations 96
2. Phase measurements in the power meter 99

6. CONCLUSIONS AND SUGGESTIONS

REFERENCES

LIST OF TABLES

Table 1. Actual dimensions of the fabricated microstrips

Table 2. Values of Zo , Zin , and S11 expected from the design considerations for all the microstrips

Table 3. S-Parameters for all the microstrips, measured in the network analyzer at 3 Ghz in darkness

Table 4. S-Parameters variations from dark to the illumination condition, measured in the network analyzer.

FIGURES

FIG. 1. Optical detectivity and absorption for various semiconductor materials.

FIG. 2. Structure of a microstrip transmission line.

FIG. 3. Effective dielectric constant as a function of frequency for microstrip transmission lines.

FIG. 4. Two-port network schematic.

FIG. 5. Basic model of the Mach-Zehnder interferometer.

FIG. 6. Basic model for a microwave Michelson interferometer.

FIG. 7. Molding for the substrate polymerization.

FIG. 8. Quantitative dimensions and structure of the microstrip.

FIG. 9. Setup used for electroplating the microstrip.

FIG. 10. Formation of the conductive coatings in the microstrip by copper evaporation.

FIG. 11. Setup used to measure the absorption of the different substrates.

FIG. 12. Coaxial measurement setup.

FIG. 13. Coaxial to microstrip launcher transition.

FIG. 14. Systems to determine the variation of the S-parameters when light is applied to the microstrip.

FIG. 15. System used to measure the spectrum of the white light source.

FIG. 16. Basic homodyne system to detect amplitude and phase modulation caused by a blue light laser modulated by a mechanical chopper.

FIG. 17. Light transmittance (T) and light attenuation (L) of copper film versus wavelength with film thickness as a parameter.

FIG. 18. Basic homodyne system to detect amplitude and phase modulation caused by a white light source.

FIG. 19. Alternative Michelson interferometer to detect amplitude and phase modulation caused either by a white light or blue light laser.

FIG. 20. Absorption of CdS, GaAs, and Si substrates

FIG. 21. Spectrum of the white light source

FIG. 22. Boundary conditions

FIG. 23. S11(2.99-3 Ghz) and S22 (2.99-3 Ghz) values of
the a)PMMA, b)CdS, C)Si1, d)Si2, e)GaAs in polar or
Smith chart representation

FIG. 24. Variation of the phase and linear magnitude of
the S11(2.99-3 Ghz) parameter as the a)CdS and b)GaAs microstrips are
illuminated

FIG. 25. Variation of the phase and linear magnitude of
the S21(2.99-3 Ghz) parameter as the a)CdS and b)GaAs microstrips are
illuminated

FIG. 26. Zooming of the phase response to observe
the sign of the variation in a long range sweeping

FIG. 27. Phase response over the sweeping between 1 and
3 Ghz.

FIG. 28. Homodyne detection response function of the
phase shifted in the Mach-Zehnder interferometer for
CdS and GaAs

FIG. 29. Detection with partial suppression of the
carrier in the information channel

FIG. 30. Difference in detection for the white light source and for the blue light
laser in the CdS sample

FIG. 31. Frequency response for the CdS and GaAs
samples

FIG. 32. Difference in detection for 50 and 200 Hz

FIG. 33. Response of the system to attenuation in
the reference channel

FIG. 34. Difference in the response for 10 and 10.2 Ghz
carrier frequencies.

FIG. 35. Difference in the response for the Michelson
and Mach-Zehnder homodyne detection systems

FIG. 36. Response of the Michelson homodyne detection
for CdS and GaAs as a function of the attenuation of the information channel

1. INTRODUCTION

Controlling optoelectronic devices, such as lasers, optical modulators, and photodiodes, with modulated electromagnetic fields is a very well-known phenomenom. In this thesis, a system is proposed that reverses the elements and the microwave carrier is controlled by light.

During the 1940's, artificial dielectrics were used in microwave systems as filters, quarter and half plate transformers and other uses. Those artificial dielectrics consisted of a large number of conducting obstacles arranged in a three dimensional pattern supported by a lightweight binder or filler, simulating a large scale model of a dielectric [1.1].

The artificial dielectrics lost their usage with the advent of improved techniques for the uses cited. However, with the introduction of semiconductors, new considerations again focused attention on conditional artificial dielectrics.

In conditional artificial dielectric waveguides, the conducting obstacles have been replaced by clusters of optically active semiconductors. When light is incident over the waveguide the clusters become highly conductive, due to the creation of electron-hole pairs by the absorption of light. A microwave signal with a wavelength much longer than the size of the clusters applied to the dielectric will induce charges created by the light forming clusters dipoles which will oppose the applied field. The newly created field opposing the field applied will have the same effect as an increase in the relative permittivity of the artificial dielectric. The same is true of the permeability, where the induced magnetic field produced by the incident electromagnetic wave, since the clusters act as magnetic dipoles, will oppose the normal component of the applied field (considering that the propagating field is a TEM mode). Therefore, the index of refraction, which is directly proportional to the relative permittivity and permeability, increases with the absorption of light. When light is not incident in the dielectric, no dipoles can be induced since there are no free charges moving in the dielectric. Therefore, the index of refraction will be much lower, since there are no induced fields opposing the microwave signal.

Experiments were carried out using CdS, GaAs and Si clusters embedded in polymethyl methacrylate (PMMA) to form the conditional artificial dielectric. Absorption measurements were performed to detect the peak absorption region for the different substrates.

The artificial dielectrics formed the substrate of a microstrip. The S-parameters of the microstrip were identified with the network analyzer, and the variation of the S-parameters when light both from a 442 nm. laser and from a white light source was incident in the waveguide. We observed that the GaAs and CdS samples showed changes in the linear magnitude and in phase for all the S-parameters. However for the Si substrate none of the S-parameters showed any variation.

The system designed to control the microwave signal was based on the same principle as for laser light modulation, but all the elements were reversed. In an electroptical modulator, the input beam is divided into two branches by an optical coupler. Then, a birefringe crystal is placed in the path of one of the divided beams. Under the effect of a microwave signal, the crystal controls the amplitude and the phase of the beam. The two beams will then converge and interfere together. The amplitude obtained will be a function of the amplitude and phase delay produced by the electrically modulated birefringe crystal [1.2].

Other optical modulators are based on the Mach-Zehnder and Michelson interferometers, where again the input beam is divided, and after that, the phase of one arm is controlled by the changes of the optical length of one of the arms. This produces different interference patterns with the unmodulated arm, which are a function of the changes produced in the length of the mechanically or electrically modulated arm. The two interferometers are based in the same principle. The only difference between them is the way both are divided and combined.

Geometries of both the Mach-Zehnder and the Michelson interferometers were evaluated in the optically controlled microwave modulator. As described before, the elements were reversed. Here, the optical carrier was replaced by a microwave carrier; and the microwave controller was replaced by a modulating light. The actual system consisted of placing a phase and amplitude controller in one branch, and the other branch had the artificial dielectric waveguide, with the embedded substrate made into the microstrip. Incident light from a laser or from a white source changed the index of refraction of the waveguide, which also changed the characteristic impedance and the electrical length of the microstrip. This produced a phase shift in the incoming microwave signal and a change in the amplitude. Then, at the interference point in the interferometer, a change in the interference of the two incoming waves was produced. This change was controlled by the intensity of the incident light into the microstrip. The two waves

were mixed and sensed in a square law detector and their output was detected by a lock-in amplifier which was synchronized with the modulating frequency of the light. Therefore, a modulated laser or other light source controlled the interference of the divided and combined microwave signal.

The phase response of the homodyne detection system for the CdS and the GaAs samples is typical of a double side band with carrier (DSBWC) amplitude modulation, with amplitude and phase errors plus the deviation from a perfect sinusoidal signal and a shift of the extrema, all of which is due to some phase modulation. The Si sample, as expected from the measurements in the network analyzer, did not show any response.

The reminder of this thesis is divided as follows:

The second section of this paper presents some theoretical background on optical absorption, artificial dielectrics, microstrip parameters and homodyne detection systems.

The third section describes the process of fabricating the microstrip, the systems used to measure the microstrip parameters, and the systems built as interferometers.

The fourth section shows the experimental results.

The fifth section discusses the results obtained and compares them to the expected results.

The sixth section summarizes the project and the conclusions drawn from it and gives ideas for improvements in the system and for future research.

2. THEORY

2.I. OPTICAL ABSORPTION.

The illumination of a semiconductor produces absorption of photons that will generate pairs of electrons and holes, by exciting electrons from the valence band to the conduction band. This process is determined by the characteristic bandgap energy (Eg) of the semiconductor and the photon energy $h \bullet f$, where h is the Plank constant and f is the light frequency. If the photon energy is equal to the bandgap energy, the electron-hole pairs are produced and if it is greater, the additional energy ($h \bullet f - Eg$) is dissipated as heat. On the other hand, for $h \bullet f$ less than Eg, a photon will be absorbed only if there are available states in the forbidden bandgap due to chemical impurities or physical defects [2.1].

Illuminating the semiconductor from a light source with $h \bullet f$ greater than Eg and a power density from the incident electromagnetic wave of P, as the wave travels through the semiconductor, the incremental fraction of the photons absorbed is proportional to the incremental absorber thickness. Therefore, the incremental power density absorbed within an incremental distance ^x is given by α P(x) ^x, where α is the absorption coefficient. Having a sample of pure dielectric with a defined absorption coefficient, from the continuity of power, one obtains

$$P(x + \hat{}x) - P(x) = [d(P(x))/dx] \; \hat{}x = -\alpha \; P(x) \; \hat{}x \quad (2.I.1)$$

where the negative sign indicates decreasing intensity of the power of the incident wave due to absorption. The solution of this equation with the boundary conditions $P(x) = P_o$ at x = 0 is

$$P(x) = P_o \; \exp(-\alpha \bullet x) \qquad (2.I.2)$$

To find the value of the absorption coefficient [2.2] consider a dielectric with a density of atoms in the excited state (level 2 of N_2) and in the ground state (level 1 of N_1). If a light with intensity I is incident in the sample, it will create ($N_1 \bullet W_i$) and ($N_2 \bullet W_i$) density of transitions per unit time from level 2 to 1 and from level 1 to 2, where W_i is the transition rate defined as:

$$W_i = \frac{c^2 \; I}{8\pi n^2 h f^3 t_{spont}} \; g(f) \qquad (2.I.3)$$

t_{spont} : Spontaneous lifetime
n : Index of refraction
$g(f)$: normalized lineshape

The density of net power generated is

$$P = (N_2 - N_1) W_i h f \qquad (2.I.4)$$

The variation of the incident intensity as it propagates through the dielectric is

$$\frac{dI}{dx} = (N2 - N1) \frac{c^2 \, g(f)}{8\pi n^2 f^2 t_{spont}} I \qquad (2.I.5)$$

By comparison with (2.II.1), the absorption coefficient is

$$\alpha = (N2 - N1) \frac{c^2 \, g(f)}{8\pi n^2 f^2 t_{spont}} I \qquad (2.I.6)$$

The condition for absorption is that $N_2 < N_1$. Figure 2.1 [2.3] shows the absorption of some of the optically active dielectrics as a function of wavelength.

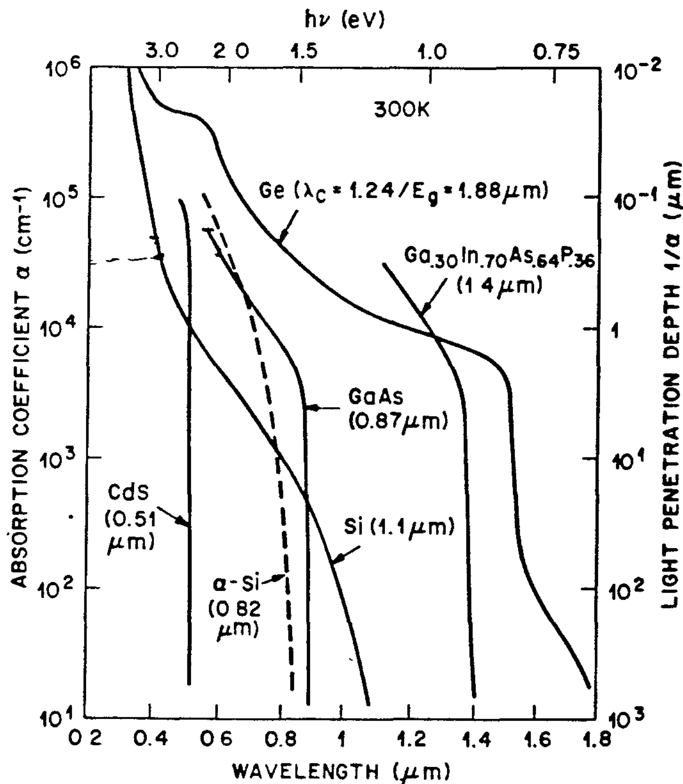

Fig 1. Optical absorption for various dielectrics

2.II CLASSICAL DISPERSION THEORY FOR BOUND ELECTRONS

As stated before, if the frequency of the incident electromagnetic field f is near a characteristic frequency of an atomic transition of the atoms of the molecular cluster, the system will acquire large dipole moments that oscillate at f. This dipole moment will contribute to the total field. This will have the effect of changing the phase velocity of the incident field or the real part of ϵ, since $v_p \equiv (\mu \epsilon)^{-1/2}$.

Choosing the applied field to be in the x-direction, the equation of motion of an atomic oscillator [2.4] is

$$m_e \ddot{x}(t) = - e E_x(t) - k x(t) - m_e g \dot{x}(t) \quad (2.II.1)$$

m_e : electron mass
e : electron charge
$E_x(t)$: time varying electromagnetic field
$x(t)$: deviation of the electron from its position
k : restoring force constant
g : damping coefficient

$E_x(t)$ and $x(t)$ have the same harmonic time dependence of the form $\exp(j2\pi f t)$, so it is implied that

$$E_x(t) = E_{xo} \exp(j2\pi f t), \text{ and } x(t) = x_o \exp(j2\pi f t) \quad (2.II.2)$$

Then, substituting (2.II.2) into (2.II.1)

$$x_o = - \frac{e E_{xo}}{m_e [4\pi^2 (f_o^2 - f^2 + jgf/2\pi)]} \quad (2.II.3)$$

f_o : $\sqrt{(k/m_e)}$
x_o : charge displacement

If N_o is the density of atoms per unit volume , the polarization resulting from the charge displacement is

$$P_{xo} = -N_o e x_o = \epsilon_o X E_{xo} \quad (2.II.4)$$

where the susceptibility X is defined as

$$X = - \frac{N_o e x_o}{\epsilon_o E_{xo}} \quad (2.II.5)$$

Substituting x_o/E_{xo} from (2.II.3) into (2.II.5), separating the imaginary and real parts of the result and using

$$1 + X = \epsilon_r \qquad (2.II.6)$$

to deduce the real and imaginary parts of the electrical relative permittivity

$$\epsilon_r = \epsilon_r' - \epsilon_r'' \qquad (2.II.7)$$

where

$$\epsilon_r' = 1 + \frac{N_o\ e^2}{m_e\ \epsilon_o} \frac{(f_o^2 - f^2)}{4\pi^2 (f_o^2 - f^2)^2 + f^2\ g^2} \qquad (2.II.8.a)$$

$$\epsilon_r'' = \frac{N_o\ e^2}{m_e\ \epsilon_o} \frac{f\ g\ /\ 2\pi}{4\pi^2 (f_o^2 - f^2)^2 + 2\pi\ f^2\ g^2} \qquad (2.II.8.b)$$

the effective permittivity is defined as [2.4b]

$$\epsilon_{eff} = \epsilon + \frac{\sigma}{j\ 2\pi f} \qquad (2.II.9)$$

Thus, if there is an imaginary part ϵ_r'', this represents the presence of the conductivity σ. We can see from equation (2.II.8) that at $f = f_o$ there will be resonance since there is a pole in the complex permittivity function. Thus, for an electromagnetic wave incident in the dielectric (in our case the dielectric clusters) at that frequency, the complex permittivity will increase dramatically, producing the same increase in the conductivity of the dielectric.

2.III CONDITIONAL ARTIFICIAL DIELECTRIC WAVEGUIDE

An artificial dielectric is a composite material consisting of macroscopic elements (usually small compared with the wavelength) of a highly polarizable material dispersed uniformely throughout some supporting, background dielectric. The supporting medium may be a lightweight material such a Poly(methyl methacrylate). The properties of the highly polarizable material in the elements may be modeled by classical dispersion theory, (see section 2.II). Under the action of an applied electric field, [2.5] the charges on each conducting obstacle are displaced so as to set up an induced field that will cancel the applied field at the obstacle surface. The obstacle is electrically neutral so that the dominant part of the induced field is a dipole field. Thus, all of those obstacles have the same function as the molecules of the normal dielectric, simulating a

dipole moment. The addition of all the forces of those dipoles produces a net dipole polarization P per unit volume. Considering E as the average net field in the medium, the displacement D is given by

$$D = \epsilon_o E + P = \epsilon E \qquad (2.III.1)$$

Where ϵ now represents the permittivity of the composite medium. Thus, for the case of an applied electric field, there is an enhancement in permittivity over the background permittivity ϵ_o of the supporting medium. In the same manner, if a magnetic field is applied to the conducting obstacle, it will induce a circulating current, so that the induced magnetic field will cancel the normal component of the applied field at the obstacle surface. These induced currents act as magnetic dipoles.

Then the artificial dielectric shows magnetic and electric dipole polarization. The induced magnetic dipoles oppose the inducing field. Thus, when a magnetic field is applied it will decrease the permeability of the dielectric from μ_o to μ, where $\mu < \mu_o$.

The index of refraction n is defined as

$$n = \sqrt{(\epsilon \ \mu / \epsilon_o \ \mu_o)} \qquad (2.III.2)$$

Therefore, the presence of a magnetic field will decrease the index of refraction.

Only for obstacles that offer spherical symmetry in a cubical or random lattice, are isotropic properties in the dielectricachieved.

2.III.1 MATHEMATICAL ANALYSIS OF ARTIFICIAL DIELECTRICS

R.E. Collin [2.5] approached the analysis of artificial dielectrics using Lorentz theory. This theory considers only dipole interaction between obstacles, and produces accurate results for obstacle spacing limited to less than 0.1 of the field wavelength.

The induced dipole moment is proportional to the field

$$p = \alpha_e \epsilon \ (E_o + E_1) \qquad (2.III.1.1)$$

α_e :Electrical polarizability of a conducting particle
ϵ :Host material permittivity
E_o :External field
E_1 :Interactive field between the induced dipole.

The total polarization of suspended particles in the polymer per unit volume is

$$P = N \ \alpha_e \ \epsilon \ (E_o + E_1) \qquad (2.III.1.2)$$

N : Number density of electron dipoles

The interactive field E_1 is proportional to p

$$E_1 = C\ p/\epsilon_o \qquad (2.III.1.3)$$

C : Interaction constant between dipoles

Substituting Eq. (2.2.3) into (2.2.2) and (2.2.1), one obtains

$$p = \frac{\alpha_e\ \epsilon_o\ E_o}{1 - \alpha_e\ C} \qquad (2.2.4a)$$

$$P = \frac{N\ \alpha_e\ \epsilon_e\ E_o}{1 - \alpha_e\ C} \qquad (2.2.4b)$$

The average displacement flux in the same direction as the applied field is

$$D_a = \epsilon_o\ E_a + P = \epsilon_{eff}\ E_a = K\ \epsilon_o\ E_a \qquad (2.2.5)$$

E_a: Average value in the component of the applied electric field of the total field in the medium.
K: Relative dielectric constant in the Ea direction
ϵ_{eff}: effective permittivity

then

$$\epsilon_{eff} = 1 + \frac{P}{E_a} = 1 + \frac{P}{(E_o + E_{pa})} \qquad (2.2.6)$$

E_{pa} : Average dipole field in the direction of Ea produced for all the particles.

The dipole field produced by all particles can be expressed as a Fourier series where the induced potential ϕ in the direction of the applied field is an odd function in that direction (call it y), and is even in the other orthogonal directions (call them x,z)

$$E_{py} = -\sum_{n=1}^{\infty} \sum_{m=1}^{\infty} \sum_{s=1}^{\infty} A_{nms} \frac{2m\pi}{b} \cos(\frac{2n\pi}{a}x) \cos(\frac{2m\pi}{b}y) \cos(\frac{2s\pi}{c}z) \qquad (2.2.7)$$

a, b, c : Distances between obstacles in the x, y, and z directions.
A_{nms} : Amplitude coefficients.

From Eq. (2.2.7) the average induced field is zero since cosine terms have a zero average.

Substituting $E_{py} = 0$ into (2.2.6), one obtains

$$\epsilon_{eff} = \epsilon \left(1 + \frac{N \alpha_e}{1 - \alpha_e C}\right) \tag{2.2.8}$$

Similarly, the effective permeability achieved is

$$\mu_{eff} = \mu \left(1 + \frac{N \alpha_m}{1 - \alpha_m C}\right) \tag{2.2.9}$$

α_m : Magnetic polarizability of a conducting particle,
C : interaction constant between the magnetic dipoles.

When a dielectric is illuminated by a light source with wavelength above the limit of the semiconductor's band gap energy, electrons are produced that act as free carriers in the semiconductor's clusters. From that principle we have inferred that those carriers make the semiconductor clusters act similarly to the conductive obstacles in an artificial dielectric, described previously, and that a similar approach could approximate the model for the embedded substrates. Thus, when light is incident in the substrate, the short lifetime of the carriers will create electric dipoles that will tranform the waveguide into an artificial dielectric. Therefore, the artificial dielectric is "conditioned" to its state by the incident light. The changes will be noticeable by the variation of the permittivity constant between the two states, light and no light. When light is incident in the substrate the index of refraction increases from the state where light is not applied.

2.IV MICROSTRIP THEORY AND DESIGN

1. STATIC ANALYSIS

The microstrip is a strip transmision line which consists of a thin metallic strip pasted on a dielectric layer which is in turn a coating on a ground plane. A

drawing of its cross section, together with the coordinate system to be used, is shown in Fig. 2

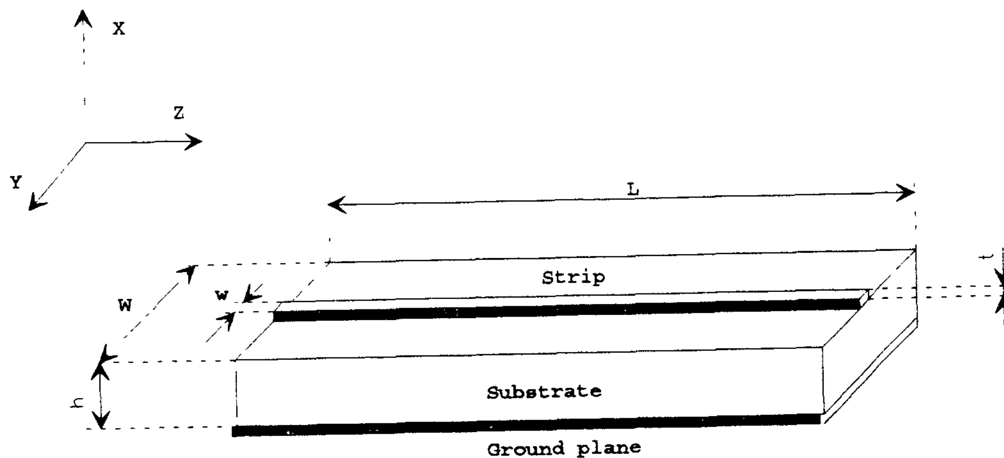

Fig 2. Structure of a microstrip transmission line

The static analysis [2.6] at low frequencies can be valid when the cross section dimensions of the microstrip are much smaller than the wavelength of the transmitted signal.
If the substrate has a $\epsilon = \epsilon_r \epsilon_o$ and $\mu = \mu_r \mu_o$, using Maxwell's equations in the air/dielectric boundary value, one obtains the parameters of the microstrip. From the boundary conditions, continuity of the tangential component of the electric field along the dilectric - air interface yields

$$E_y|_{diel} = E_y|_{air} \qquad (2.IV.1.1)$$

Using Maxwell's equation

$$(\nabla \times H)_y|_{diel} = \epsilon_r \; (\nabla \times H)_y|_{air} \qquad (2.IV.1.2)$$

Expanding the equation, and since D_x the normal component is continuous across the boundary, one obtains

$$\epsilon_r \, \partial H_z / \partial x|_{air} - \partial H_z / \partial x|_{diel} = (\epsilon_r - 1) \partial H_x / \partial z \qquad (2.IV.1.3)$$

ϵ_r is bigger than one and H_x is not zero, thus the previous equation implies that the left hand side in the equation is not zero, what implies that H_z is also not zero.

This demostrates that the longitudinal component of H exist. Similar arguments will show that E_z is also a non zero quantity.
Only the fringing components E_y and H_y at the dielectric-air interface lead to the non TEM propagation mode of the microstrip. Nevertheless, this fringing componenets are much smaller than the main field under the strip going through the substrate. Thus the difference from the TEM propagating mode is small. Another way to explain this effect in the static analysis (propagating wavelength much bigger than the width and height of the microstip), is that the right hand side of (2.IV.1.3) is too small, indicating that the longitudinal field components tend to zero.

The problem could be focused more deeply, taking into account frequency, thickness in the conductive surfaces, inhomogeneities in the substrate, etc., that could be solved from other methods, like the finite difference method or the sub-ares method. Those methods would give a more accurate solution than the one presented.

2.IV.1.1 CHARACTERISTIC IMPEDANCE

The characteristic impedance of a lossless line is defined as

$$Z_o = \sqrt{(L/C)} \qquad (2.IV.1.1.1)$$

and for a strip line as

$$Z_o = 1/(c \sqrt{\epsilon_r}\, C_o) \qquad (2.IV.1.1.2)$$

For microstrip lines, avoiding discontinuities, considering a strip of zero thickness and at lower frequencies,one could state the following wide-ranging equations [2.7]:
for $w/h \geq 2$:

$$Z_o = \frac{376.7}{\sqrt{\epsilon_r}} \left[\frac{w}{h} + 0.8825 + 0.1645 \left[\frac{\epsilon_r - 1}{\epsilon_r^2} \right] + \frac{\epsilon_r + 1}{\pi \epsilon_r} \left[1.4516 + \ln\left(\frac{w}{2h} + 0.94\right) \right] \right]^{-1} \qquad (2.IV.1.1.3)$$

and for $w/h \leq 2$

$$Z_o = \frac{119.9}{\sqrt{(2(\epsilon_r + 1))}} \left[H' - \frac{\epsilon_r - 1}{2\epsilon_r + 2} \left[0.4516 + \frac{0.2416}{\epsilon_r} \right] \right]$$

where $H' = \ln \{4h/4 + [(4h/4)^2 + 2]^{\frac{1}{2}}\}$ (2.IV.1.1.4)

and the effective relative permittivity for wide lines with $w/h \geq 1$, is

$$\epsilon_{eff} = \frac{\epsilon_r + 1}{2} + \frac{\epsilon_r - 1}{2} \left[1 + \frac{12\ h}{w} \right]^{-0.5} \quad (2.IV.1.1.5)$$

2.IV.2 DYNAMIC ANALYSIS OF THE MICROSTRIP PARAMETERS

The presence of the dielectric in the microstrip allows the wave to be TEM mode only at zero frequency. Also, due to boundary conditions involving transverse inhomogeneity in the dielectric and the presence of the microstrip, no pure TE or TM modes can exist. Thus, a hybrid-mode solution, due to mode orthogonality for surface waveguides, enables a given arbitrary field to be expanded into a series of TE and TM modes, or quasi-TEM mode.

The previous static analysis was based on quasi-static assumptions that require predominantly transverse electromagnetic fields, but the static anaysis is inadequate for higher frequencies. Above the static frequency

$$f_{stat} = \frac{21.3}{(w + 2h)\ \sqrt{(\epsilon_r + 1)}} \quad (2.IV.2.1)$$

dispersion can not be neglected [2.8].

Many people have tried to establish a relation between the microstrip parameters and frequency [2.8], [2.9], [2.10] and [2.11]. The equations derived in [2.9] are

$$\epsilon_{eff}(f) = \epsilon r - \frac{\epsilon r - \epsilon_{eff}(0)}{1 + (f/f_t)^2} \quad (2.IV.2.2)$$

where $f_t = [\epsilon_r/\epsilon_{eff}(0)]^{\frac{1}{2}}\ [Z_o/2\mu_o h]$ (2.IV.2.3)

As presented in [2.12], the frequency dependence of the characteristic impedance $Z_o(w)$ could have either increasing or decreasing slope. The characteristic impedance propagating in the fundamental mode is defined as

$$Z_o(P,I) = 2\, P_{av} / I_z^2 \quad \text{and} \quad Z_o(P,V) = V_x^2 / 2P_{av} \qquad (2.IV.2.4)$$

Above the static frequency (equ. 2.IV.2.1) and due to dispersion, these two definitions contradict each other since they give different results for the characteristic impedance. But since the equation function of the current is less frequency dependent than the equation function of the voltage, the value of the characteristic impedance above the dispersion frequency has been characterized following the current dependent equation. The relation given in [2.13] gives a factor to approximate the value of the characteristic impedance as the frequency increases, given by

$$Z_o(w) = Z_o(0)\ [\epsilon_{r,eff}(0)/\epsilon_{r,eff}(f)]^{\frac{1}{2}} \qquad (2.IV.2.5)$$

The plots showing the variation of permittivity and characteristic impedance extracted from [2.13] are shown in Fig 3.

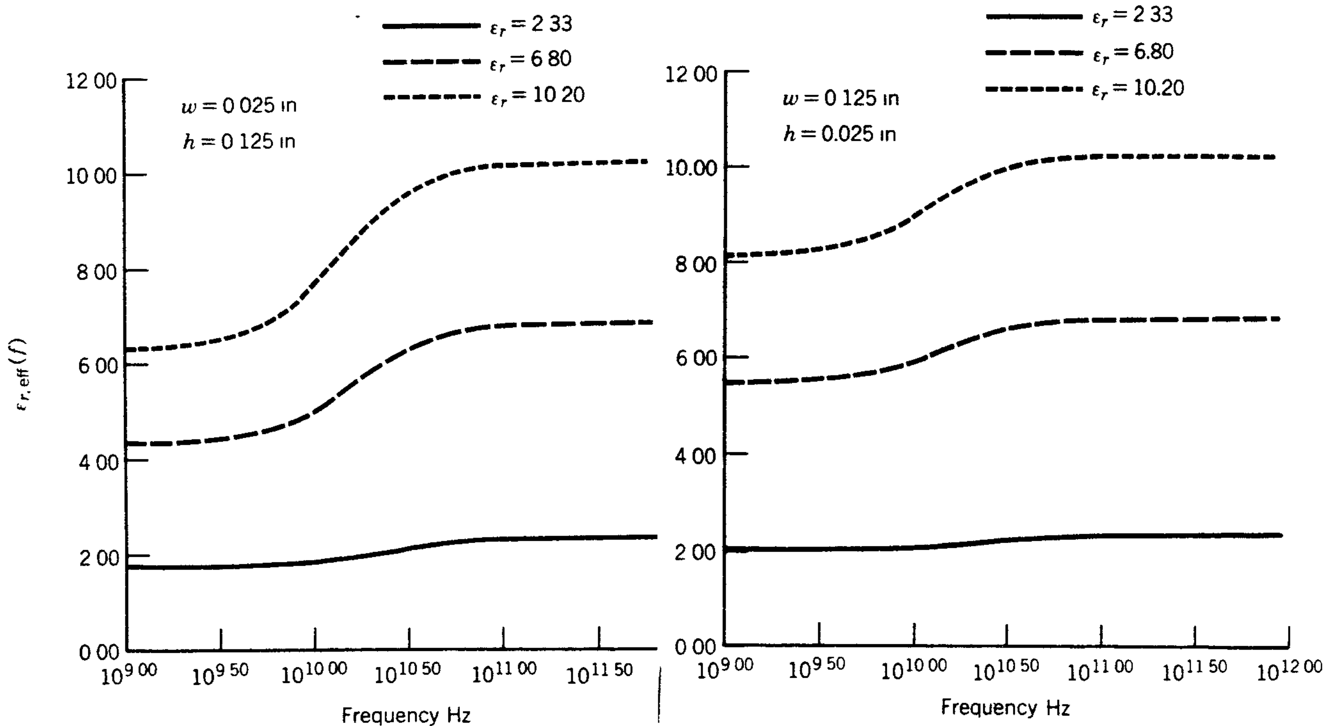

Fig. 3: Effective dielectric constant as a function of frequency for microstrip transmission lines

2.IV.3 CHARACTERIZATION OF A MICROSTRIP WITH THE S-PARAMETERS

2.IV.3.1. THE SCATTERING MATRIX

In a two-port network as in Fig 4

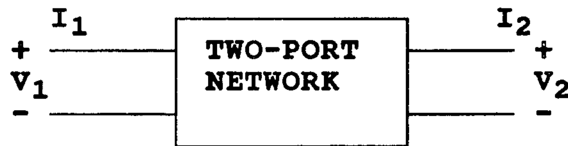

Fig 4: Two port network schematic

The S-parameters are defined as

s_{11} = Input reflection with a matched load at the output

s_{21} = Forward transmission with a matched load at the output

s_{12} = Reverse " " "

s_{22} = Output reflection with a matched load at the input

Or $s_{11} = \Gamma_{in}$, $s_{21} = T_f$, $s_{12} = T_r$, $s_{22} = \Gamma_{out}$

and $T_f = 1 + \Gamma_{in}$; $T_r = 1 + \Gamma_{out}$

where $\Gamma_{in} = Z_{in} - Z_l / Z_{in} + Z_l = |\Gamma| \Theta°$ (2.IV.3.1.1)

Z_{in} : Input impedance
Z_l : Matched impedance.

Z_{in} varies, commencing in the input plane of the microstrip

and progressing towards the matched load by the relation

$$Z_{in} = Z_o \frac{Z_l \cos(\beta l) + jZ_o \sin(\beta l)}{Z_o \cos(\beta l) + jZ_l \sin(\beta l)} = Z_o \frac{Z_l + jZ_o tg(\beta l)}{Z_o + jZ_l tg(\beta l)}$$

(2.IV.3.1.2)

Zo : Characteristic Impedance
βl : Electrical length of the microstrip

A variation in the electrical length or in the characteristic impedance will produce a change at the input impedance and in the S-parameters.

2.IV.3.2. INCREMENTAL VARIATION OF THE SCATTERING MATRIX DUE TO INCIDENT LIGHT IN THE MICROSTRIP

If a change in the magnitude and phase of the S-parameters is produced, the increment of the scattering matrix is

$$S - S' = \begin{bmatrix} s_{11} & s_{12} \\ s_{21} & s_{22} \end{bmatrix} - \begin{bmatrix} s_{11}' & s_{12}' \\ s_{21}' & s_{22}' \end{bmatrix} = \begin{bmatrix} \hat{s}_{11} & \hat{s}_{12} \\ \hat{s}_{21} & \hat{s}_{22} \end{bmatrix} \qquad (2.IV.3.2.1)$$

Just considering port one, since the microstrip is symmetrical, only s_{11} and s_{21} will be considered.

When light is applied to the microstrip, it will produce variations of the s-parameters. These variations are due to a variation in the charateristic impedance $F(\epsilon)$ and/or in the electrical length of the microstrip. These changes will be related to a variation of the absolute value and the phase of the reflection and transmission coefficients

$$\hat{s}_{11} = |\hat{\Gamma}| \; \hat{\Theta}_{11} \qquad \text{and} \qquad \hat{s}_{21} = |\hat{T}| \; \hat{\Theta}_{21}$$

$$s_{11}' - s_{11} = \frac{Z_1 - (Z_o + F(\epsilon)) \dfrac{Z_1 + j(Z_o + F(\epsilon))tg((\beta+\beta')l)}{(Z_o + F(\epsilon)) + jZ_1 tg((\beta+\beta')l)}}{Z_1 + (Z_o + F(\epsilon)) \dfrac{Z_1 + j(Z_o + F(\epsilon))tg((\beta+\beta')l)}{(Z_o + F(\epsilon)) + jZ_1 tg((\beta+\beta')l)}} - \frac{Z_1 - Z_o \dfrac{Z_1 + jZ_o \, tg(\beta l)}{Z_o + jZ_1 tg(\beta l)}}{Z1 + Zo \dfrac{Z_1 + jZ_o \, tg(\beta l)}{Zo + jZ1tg(\beta l)}} \qquad (2.IV.3.2.2)$$

z_o is function of the permittivity as defined in (2.IV.1.1.3) and (2.IV.1.1.4), β is defined as

$$\beta = \frac{2\pi f \sqrt{(\epsilon_r \mu_r)}}{c_o} \qquad (2.IV.3.2.3)$$

Thus, a change in the permittivity or permeability of the substrate will produce a variation in the amplitude and phase of the transmission and reflection coefficients.

2.V INTERFERENCE OF WAVES

If two wavefronts are traveling at the same frequency and past a given point, the total amplitude of the displacement at that point is given by the sum of the individual displacements. If the waves have the same polarization and modal configuration as waves propagating in a coaxial cable, the total field can be determined by vector addition [2.14].

Consider two waves at the same frequency, but with different magnitudes in their complex representation

$$\begin{aligned} U_1 &= u_1 \exp i(2\pi f + \Phi_1) \\ U_2 &= u_2 \exp i(2\pi f + \Phi_2) \end{aligned} \qquad (2.V.1)$$

u : amplitude
f : carrier frequency
Φ : phase component

The total amplitude is given by

$$\begin{aligned} U_t &= u_1 \exp i(2\pi f + \Phi_1) + u_2 \exp i(2\pi f + \Phi_2) \\ &= [u_1 \exp i(\Phi_1) + u_2 \exp i(\Phi_2)] \exp i2\pi f t \end{aligned} \qquad (2.V.2)$$

and the intensity of this wave is

$$I \approx U_t U_t^* = u_1^2 + u_2^2 + 2 u_1 u_2 \cos(\Phi_1 - \Phi_2) \qquad (2.V.3)$$

2.V.1. MICROWAVE MACH-ZEHNDER INTERFEROMETER

Interferometers are accurate measurement systems that determine the changes in the amplitude and phase of the interference of two waves when one of them is being phase or amplitude-modulated. A basic model is the Mach-Zehnder interferometer, a basic model of which is in Figure 5

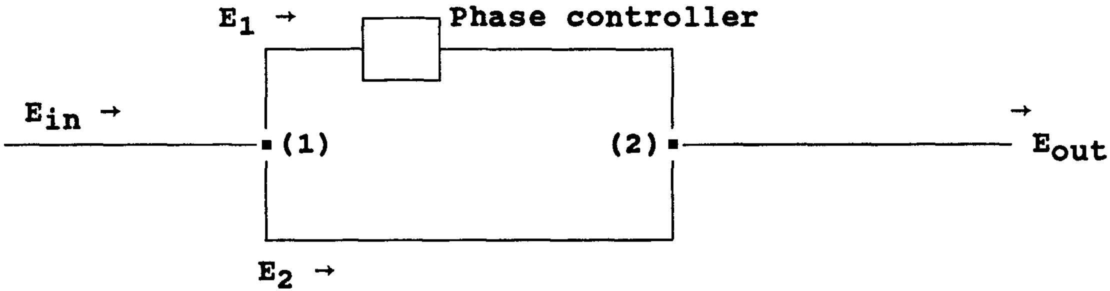

Fig 5: Basic model for a Mach-Zehnder interferometer

The circuit could be made either of rectangular or coaxial waveguides or a combination. The (1) and (2) points are either E-Plane tees or H-Plane tees in rectangular waveguides, or power combiner and splitter in coaxial waveguides. If properly designed and calibrated those devices split and add the power coming from E_{in}, and E_1 and E_2, respectively.

The intensity in the output as in (2.V.3) is function of the difference in the phases of the two arms $(\Phi_1 - \Phi_2)$.
Thus if Φ_1 changes, the output could be controlled by those increments in phase.

2.V.2 MICROWAVE MICHELSON INTERFEROMETER

The principle of operation is basically the same as the Mach-Zehnder, but the division and addition of the waves has a different configuration. A basic model of a Michelson interferometer is shown.

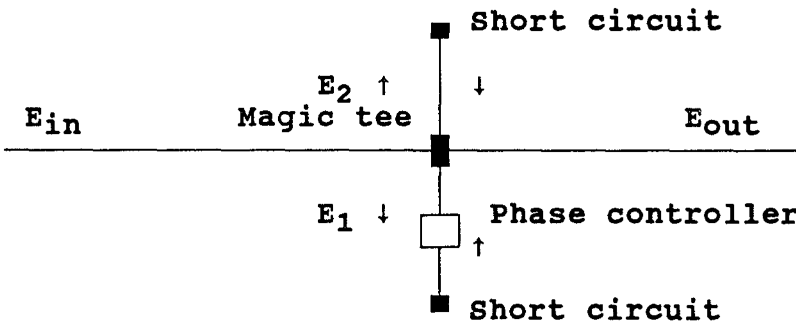

Fig 6: Basic model for a microwave Michelson Interferometer

The circuit is based on the magic tee in the center, which is a combination of the E-Plane and the H-plane tee. The input wave is fed into the magic tee through the H-arm. There it is divided equally between the collinear arms and

does not appear in the output port or E-arm. In the collinear arms, it propagates through until due to the short circuits, reflections are produced. Those reflected waves will be combined and fed into the E-port, producing E_{out} which again will follow equation (2.V.3) where the input wave equations (2.V.1) are the ones reflected in the short circuits. If a phase variation is produced in one arm, the output will be function of that phase change.

'2.VI HOMODYNE DETECTION PRINCIPLES' [2.15]

The homodyne detection principle involves mixing an unmodulated signal of frequency w to a modulated signal (also of frequency w but with sidebands) that corresponds with the information channel. Those two signals are summed through an envelope detecting device. The output is taken at the modulation frequency w_m

Since the mixing process is coherent, the system is of zero IF variety and the output displays the phase and amplitude information contained in the information channel.

The modulation process in the information channel produces sidebands of order $w \pm w_m$, $w \pm 2w_m$, etc. Higher harmonics than the modulation frequency w_m are of little consequence, since the detected fundamental modulation frequency w_m, can be narrowband filtered to obtain the necessary frequency and noise discrimination. The filtering is accomplished as an integral part of a narrowband amplifier and indicator such as a lock-in voltimeter or amplifier.

Assuming that $w_m << w$, both sidebands suffer the same attenuation and phase shift in passing through the information channel. Typical choices are 1 Khz, although higher frequncies avoid the 1/f detector noise.

The process of mixing the signals from the two channels can be analyzed as a simple envelope detection for high levels as well as low levels of reference signal. The signals in the reference channel carrier and in the modulated information channel are represented by

$$
\begin{aligned}
E_r &= A \exp(iwt) \\
E_i &= b(1 + m\cos w_m t)\exp(i(wt+\phi)) \qquad (2.VI.1)
\end{aligned}
$$

where A and b are the amplitudes of the reference and information signals, respectively, m is the amplitude modulation index, and ϕ is the RF phase angle

between the two signals. The common excitation factor exp(iwt) is supressed, and the resulting excitation phasor, corresponding to the sum $(E_r + E_i)$ will be designated as E_t

2.VI.1 AMPLITUDE MODULATION

2.VI.1.1 LOW LEVEL OR SQUARE LAW DETECTION: Double Side Band with Carrier (DSBWC) Amplitude Modulation.

Nearly all microwave detecting devices respond to the envelope of the signal. At low levels of A where the detector characteristic curve is square law, the output low frequency signal is proportional to the envelope of the input signal squared, i.e. $E_{in}^2 = (E_r + E_i)^2$. However, it can be shown that odd powers contribute no output at frequency w_m and higher orders. Even powers contribute terms at wm which are of the same form as those obtained from square law operation if $A >> b$. Without loss of generality, it is therefore sufficient to consider the device as a square law detector.

The law of cosines gives the square of the resultant phasor signal input to the detector

$$E_t^2 = A^2 + b^2(1 + m\cos w_m t)^2 + 2Ab(1 + m\cos w_m t)\cos\phi \quad (2.VI.1.1.1)$$

As E_t represents the envelope and the detector is square law, the last equation is proportional to the detector output. Considering only the wm terms,

$$E_{out} = K_1 Ab(b/A + \cos\phi)\cos w_m t \quad (2.VI.1.1.2)$$

where K_1 is the low level conversion constant. It is assumed that the mixer output adequately filters all RF terms generated. This is accomplished in the detector mount. The narrowband filter in the lock-in amplifier is in synch with the modulating frequency wm, and therefore eliminates the D.C. and $2w_m$ terms.

The low level conversion constant K_1 is largely determined by the quiescent operating point or DC terms generated from the equation of E_t^2. For amplitude measurements, it is essential that K_1 be constant over the entire dynamic range of b. This is possible if the operation is entirely within the square-law (parabolic) region or if b is sufficiently small compared to A. This is also

desirable when making amplitude and phase measurements at low levels, and for phase measurements at high levels of A.

VI.I.2 LOW LEVEL OR SQUARE LAW DETECTION: Double Side Band with Carrier Suppression (DSBSC) amplitude modulation.

The way to remove the restriction that $A>>b$ in the preciding paragraph is by partially suppressing the carrier in the information channel. Then the previous equations become

$$E_i = b(k_o + m\cos wmt)\exp i(wt+\phi) \quad 0<k_o\leq 1 \quad (2.VI.1.2.1)$$

where K_o is the carrier suppression factor. If $K_o=1$, the previously analyzed DSBWC case is obtained. Forming E_t^2 as before

$$E_t^2 = A^2 + b^2(k_o + m\cos w_m t)^2 + 2Ab(k_o + m\cos w_m t)\cos\phi$$

$$(2.VI.1.2.2)$$

the square law output then becomes

$$E_{out} = K_1 Abm(k_o b/A + \cos\phi)\cos w_m t \quad (2.VI.1.2.3)$$

Making k_o of the order of -45dB makes the first term in the previous equation negligible. Then the output at w_m is proportional to $b\cos\phi$, even if $b\equiv A$. Thus, suppressing the carrier in the information signal by an amount k_o has the net effect of increasing the upper end of the dynamic range by k_o This is true for amplitude and phase measurements using square law detection and is equally true for phase measurements using linear detection.

VI.1.3 HIGH LEVEL OR LINEAR DETECTION (DSB modulation)

In actual operation the response is directly proportional to the amplitude of the reference signal A, up to a certain point. Beyond this, the gain obtained by increasing A ceases. Operation is then in the linear portion of the dynamic characteristic rather than the square law portion. Considering only the DSBSC (or the DSBWC for $K_o=1$), for high level operation where A is large, the condition $A>>b$ is easily satisfied, and the output response for linear envelope detection can be obtained from Equ.(2.VI.1.2.3) by multiplying the negligibly small second term by $\cos 2\phi$, completing the square of

$$E_t \equiv A + b(k_o + m\cos w_m t)\cos\phi \quad (2.VI.1.3.1)$$

The output signal at w_m then is

$$E_{out} \equiv K_h bm\cos\phi \; \cos w_m t \qquad (2.VI.1.3.2)$$

which is directly proportional to the high level gain constant K_h (the slope of the characteristic curve), and $b\cos\phi$ which exhibits the phase and amplitude information, but not A.

In the case that $\phi = \pm \beta\pi$, Eqs. (2.VI.3.1. and 2) and are exact without requiring that $A >> b$. This means that the high level homodyne detection is extremely linear for amplitude measurements, and that the information signal b can be as large as the reference signal A with very small error.
However, for phase measurements at high levels, we still need $k_o b << A$ for DSB modulation. This is also required for both amplitude and phase modulation.

VI.1.4 PHASE MEASUREMENTS (DSB amplitude modulation)

From Eq. (2.VI.1.2.3) zeros will appear in the response at w_m when $\cos\phi = -k_o \; b/A$ for square law detection. Thus, if a phase-shifting device is provided in either the information or reference channels, the relative phase ϕ can be varied to locate these zeros. The zeros occur at

$$\phi = \pm[(2n+1)\pi/2 + (-1)^n \epsilon p] \qquad n = 0,1,2 \; .... \qquad (2.VI.1.4.1)$$

where

$$\epsilon = 1/\sin(k_o b/A) \qquad (2.VI.1.4.2)$$

is the phase error from some odd multiple of $\pm\pi/2$.

If the phase span between adjacent zeros is different from π, the sign and phase error ϵ_p can be determined. The difference between any two successive zeros is simply $\pi \pm 2\epsilon$. Another way of observing the error is by determining the difference in maxima as the phase is changed. The difference in dB of two adjacent maxima is

$$20 \log \left| \frac{K_o \; (b/A) \; - \; 1}{K_o \; (b/A) \; - \; 1} \right| \qquad (2.VI.1.4.3)$$

The maximum tolerable value of K_o b/A can be set as desired by adjusting the level setting attenuators in the reference and information channels when the test samplet is set for minimum attenuation.

Since the phase error is a function of both b and A, it is important to account for a change in b which occurs as the test sample is varied. Thus, a new ϵ_p should be computed or measured at each setting of the test sample.

2.VI.1.5 LOCK-IN AMPLIFIERS

The homodyne detected AF signal at wm is usually narrowband filtered to obtain the necessary noise and frequency discrimination. This filtering is accomplished as an integral part of a narrow band amplifier and indicator such a phase sensitive detector. The most useful phase sensitive detector in homodyne detection is the lock-in voltmeter (amplifier) because of its extremely high sensitivity and narrow bandwidth. It also accepts frequencies from d.c. to hundreds of KHzs.

The lock-in voltmeter operates in a coherent fashion, much in the same way as the microwave homodyne detection system. Thus, the total measurement system becomes doubly coherent for detection of the microwave information signal, and again for the measurement of the AF detected signal. Each detection operation respectively provides a characteristic $\cos\phi_{RF}$ and $\cos\Phi_{AF}$ output, ϕ_{RF} being the RF phase difference between the reference and information signals (w), and Φ_{AF} the phase difference between the detected AF modulated signal and the modulating signal reference (w_m). Thus, the response of the total system is proportional to

$$b\cos\phi_{RF}\ \cos\Phi_{AF}$$

The reference signal for the lock-in is taken from the modulating generator. Normally, the AF signal phase does not change in the process of measurement, so the phase of the AF modulating reference signal can be adjusted so that $\cos\Phi_{AF} = \pm 1$ and left at this setting for the measurements. This is accomplished by an AF phase shifter provided within the lock-in voltmeter. In this manner, the phase sensitive detector/amplifier becomes a very sensitive narrowband voltmeter. The effective bandwidth of the instrument could be also be changed. This, plus its coherent feature, provides an instrument with a very low noise figure,

and makes possible the detection of an AF signal which is buried in microwave mixer noise.

As a lock-in is phase sensitive, it senses the sign of its input. Consequently, its response follows a sinusoidal curve with positive and negative values rather than sensing just the magnitude (only positive). Zero crossings are observed rather than nulls.

Some lock-ins are also equipped to measure second harmonics of the modulating signal, using w_m as the reference.

2.VI.2 PHASE MODULATION

A symmetrical spectrum consisting of an infinite number of frequencies, spaced by multiples of w_m from the carrier, occurs when the phase of the information channel is modulated. The amplitude of all odd harmonics is proportional to $b\sin\phi$, and to $b\cos\theta$ for the even harmonics.

The advantage of phase modulation with respect to amplitude modulation is that no errors in phase or amplitude measurement are detected due to nonlinearities in the detector.

The disadvantage of phase modulation with respect to amplitude modulation is that is difficult to phase modulate the information channel without causing some amplitude modulation. The phase modulated information channel can be represented as

$$E_i = b \exp i\{wt + \phi + m_p \cos(w_m t)\} \quad (2.VI.2.1)$$

m_p: maximum modulation angle
b: amplitude in the information channel
w: carrier frequency
w_m: modulating frequency
ϕ: phase difference between the two channels

and the reference channel as

$$E_r = A \exp(iwt) \quad (2.VI.2.2) \quad \text{from } (2.VI.1)$$

A: amplitude in the reference channel

Mixing both signals in a square law mixer, the a.c. output is

$$E_{out} = K_1 A b \cos\{\phi + m_p \cos(w_m t)\} \quad (2.VI.2.3)$$

and transforming the cosine term into Bessel equations,

$$E_{out} = K_1 \; A \; b \; [J_o(m_p) \; \cos\phi \; - \; 2 \; J_1(m_p) \; \sin\phi \; \cos(w_m \; t) \; - \; 2 \; J_2(m_p) \; \cos\phi \; \cos(2 \; w_m \; t) \; + \; \ldots]$$

(2.VI.2.4)

The d.c. term can be discarded, then the output at w_m is basically at the first harmonic w_m

$$E_{out1} = K_1 \; A \; 2b \; J_1(m_p) \; \sin\phi \; \cos\; (w_m \; t) \quad (2.VI.2.5)$$

and at the second harmonic $2w_m$

$$E_{out2} = K_1 \; A \; b \; J_2(m_p) \; \cos\phi \; \cos(w_m \; t) \quad (2.VI.2.6)$$

In the w_m output, zeros occur at $\phi = \pm \pi$

and at $2w_m$, they occur at $\phi = \pm(2n + 1) \; \frac{1}{2}\pi$

2.VI.3 SIMULTANEOUS PHASE AND AMPLITUDE MODULATION

When both modulations occur at the same time at the same modulation frequency, the signals in the information and reference channels are expressed as

$$E_i = b[1 + m_1 \cos(w_m \; t + \Phi_1)] \; \exp \; i(w \; t + \phi + mp \; \cos w_m \; t)$$

(2.VI.3.1)

$$E_r = A \; \exp(iwt) \qquad \text{from (2.VI.1)}$$

Φ_1 : phase difference between amplitude and phase modulation

Adding and mixing both signals in a square law device, the output at the w_m frequency is

$$E_{out} = K_1 \; A \; b \; [m_1 \; J_o(m_p) \; (\cos\phi + \frac{b}{A \; J_o(m_p)}) \; \cos(w_m \; t + \Phi_1)$$

$$- \; 2 \; J_1(m_p) \; \sin\phi \; \cos\; (w_m \; t) \qquad (2.VI.3.1)$$

The two terms in the equation cancel for $\Phi_1 = 0$ and then,

$$m_1 \; J_o \; \cos\phi = 2 \; J_1 \; \sin\phi. \qquad (2.VI.3.2)$$

If this doesn't happen, then there are no zeros and only extrema will occur when

$$\tan 2\phi = \frac{4m_1\ J_o\ J_1\ \cos\Phi_1}{(2\ J_1)^2\ -\ (m_1\ J_o)^2} \qquad (2.VI.3.3)$$

All the maximas are equal and the distance between a maxima and a minima is $\frac{1}{2}\pi$ radians as ϕ is varied.

Other cases that could happen are when either phase and amplitude modulation is much more significant than the other. Consider when:

A. Phase modulation is smaller. $(2\ J1 \ll m1\ Jo)$

In this case the extrema are shifted backward (clockwise) from the position where phase modulation does not occur. For example:

- For no PM, zeros occur for $2\phi = 2(n+1)\pi$, and maxima occur for $2\phi = 2n\pi$
- With some PM, minima occur when

$$2\phi \approx (2n+1)\pi - \frac{4\ J_1\ \cos\ \Phi_1}{m_1\ J_o} \qquad (2.VI.3.4)$$

and maxima occur when

$$\phi \approx 2n\pi - \frac{4\ J_1\ \cos\ \Phi_1}{m_1\ J_o} \qquad (2.VI.3.5)$$

This would show in the graph of phase variation as a slightly shift (clock wise) in the extrema.

B. Amplitude modulation is smaller. $(2\ J_1 \gg m_1\ J_o)$

- When there is no AM, zeros occur at $2\phi = 2n\pi$, and maxima occur at $2\phi = (2n+1)\pi$
- If there is some AM, the extrema are shifted forward (counterclockwise) so that zeros occur at

$$2\phi \approx 2n\pi + \frac{m_1\ J_o\ \cos\Phi_1}{J_1} \qquad (2.VI.3.6)$$

and maxima occur when

$$\phi \approx (2n+1)\pi + \frac{m_1\ J_o\ \cos\Phi_1}{J_1} \qquad (2.VI.3.7)$$

3. MATERIALS AND EXPERIMENTAL METHODS

3.1 SUBSTRATE FABRICATION

The substrate's embedding selection was based on the need for a transparent material that allowed the maximum transmission and minimum absorption of light and could be mixed in its liquid state with clusters of semiconductor materials, which in its solid state would form a homogeneous paste. The embedding chosen was methyl methacrylate from Polyscience Inc.

The steps to fabricate the substrate are described bellow:

3.1.1 INHIBITOR REMOVAL

The first step was to remove the amount of methyl ether of hydroquinone (MEHQ) that is added to the methyl metacrylate monomer to prevent polymerization during shipment and storage [3.1]. The inhibitor imparts a slight color to the finished embedment that is not suitable for the experiment, since it reduces the transmission. The removal was done by passing the inhibited monomer downward through a column packed with De-hibit 100 resin. This macroreticular resin absorbs the MEHQ. First the resin was cleaned. For that, the resin was pretreated by passing it through a column of methanol then rinsed with deionized water and passed again through another column of methanol. The monomer was then passed down through the column with the clean resin at a very slow rate. Then, the monomer was used promptly to avoid excessive atmospheric contact since oxygen also acts as an inhibitor.

3.1.2 CATALYST SELECTION AND POLYMERIZATION

Polymerization was accomplished by using heat in combination with small amounts of a soluble organic catalyst, Azobisisobutyronitrile. The amount of catalyst added was about 0.1% by weight of unhibited monomer. The catalyst was added at room temperature and was dissolved by stirring it rapidly with a magnetic bar on a heat plate.

A clear casting syrup (monomer-polymer solution) was prepared by heating about 25 milliliters at 70°C on a hot plate with continuous stirring. Because the polymerization reaction is highly exothermic, constant watching was

required to avoid fast polymerization in the preparation container. At the moment that the first bubbles from boiling were seen, the container was cooled off in a bigger container of cold water and stirred again to avoid polymerization in the bottom of the solution. After it cooled off, it was returned to the hot plate at 70 °C, and the process was repeated until the syrup formed. After that, it was cooled off again in cold water to let all the air out of the solution and avoid possible bubbles.

3.1.3 ADDITION OF SEMICONDUCTOR CLUSTERS

In the case of the addition of semiconductor clusters, the process was the same as before, except that when the solution had the appearance of slurry, the clusters were added. This was followed by a very fast stirring. The process afterwards required a faster stirring than previously without the clusters.

The clusters of CdS consisted of a fine powder of different sizes. Observed under the microscope, the ratio of the smallest with respect to the biggest was about one to ten. The purity of the material was unknown. The silicon was obtained from a Si-SiO_2 wafer. The crystalline structure was (1,1,1,). The amount of the p-doped Silicon was unknown. The first step was the removal of the SiO_2 upper layer. For that the wafer was dipped into a 10% HF solution in distilled water for 5 minutes. Then, after drying in the oven, it was "smashed" until it became a fine powder. Observation under the microscope gave an estimate of the ratio between the smaller and the biggest clusters of about 1 to 20.

The Gallium Arsenide was from Johnson Mattey Catalog Company, product number 88458 with a purity (metal basis) of 99.9999%. The product comes in small cubes and it had to be smashed until a fine powder was obtained. Observation under the microscope gave an estimate of the ratio between the smallest and the biggest clusters of about 1 to 20. The proportions used were 2 gr. of Cds in 18 ml. of PMMA, and 1 gr. of GaAs or Si in 18 ml. of PMMA.

3.1.4 MOLDING THE MONOMER.

The amount of clusters was enough to saturate the solution, and a thin layer of clusters (even with fast stirring) were deposited on the bottom of the preparation container at the end of the process. At this point, the slurry solution was poured into the molding, and closed carefully so as not to trap bubbles.

The molds selected were made from Corning microscope glass, since glass offers good smoothness and transparency. The structure of the molding is shown in Figure 7.

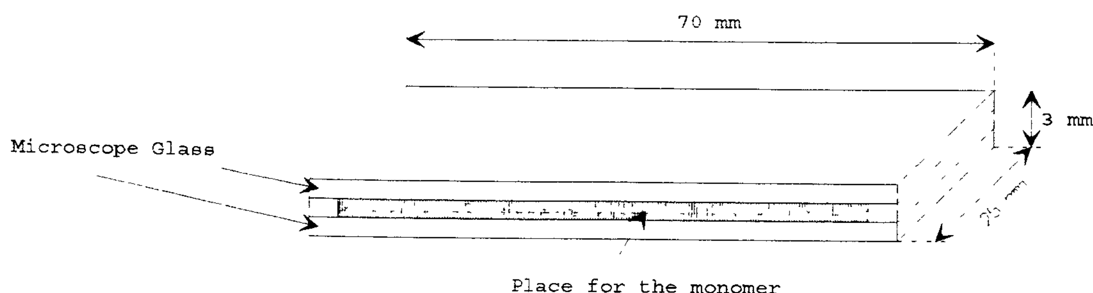

Fig 7: Molding for the substrate polymerization

To avoid any inhomogeneous adherence of the monomer to the glass, the microscope slides were cleaned in an ultrasonic oven and rinsed with distilled water, acetone and methanol, and finally dried with paper tissues.

The molded monomer was enclosed with aluminum paper to exclude oxygen and placed in an oven at 60°C. After 10 minutes the molds were turned face down to prevent heavy clusters from depositing on the bottom and to have a more homogeneous layering. After 24 hours the solution was totally polymerized. To extract the substrate from the molding, the polymer that was around the edges of the glass was sanded in a rotary sanding machine. After that, the substrate was extracted carefully with a knife.

Looking into the microscope, it was observed that the heavy and biggest particles of semiconductor were located more in the lower half of the substrate increasing the concentration towards the bottom. This happened especially in the substrates of GaAs and Si, where the difference in sizes of the clusters were bigger and the bigger particles where heavyer. We can consider that the differences in concentration between clusters in the top and those in the bottom of the substrate were about double in GaAs and Si samples and a small difference in the CdS sample.

3.2 MICROSTRIP FABRICATION.

The microstrip consisted of a thin conducting strip of copper placed above the dielectric material (in this case the substrate was PMMA with clusters of GaAs, Si or CdS
embedded on it), which was supported on the bottom by a conducting plate of copper.

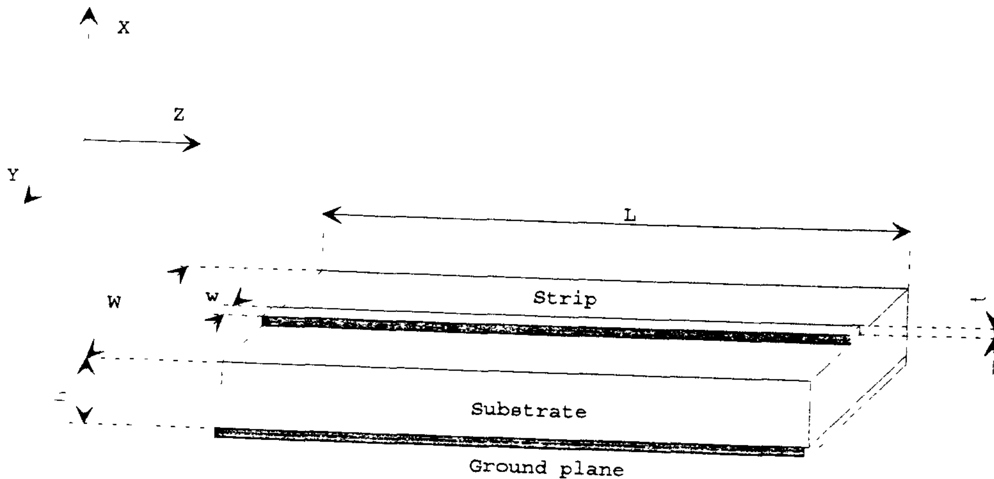

Fig 8: Quantitative dimensions and structure of the microstrip

Electroplating was used to obtain the conducting surfaces of copper, top and bottom. The electrodeposition process consisted of carrying electric current across an electrolyte while a substance was deposited at one of the electrodes.

The electrolyte was an acid copper sulfate bath. The two essential constituents were copper sulfate dissolved in sulfuric acid and distilled water. The salt furnished the metal ions; the acid served to reduce the resistivity, decrease the metal-ion concentration, increase the anode corrosion, and prevent precipitation of basic cupric salts [3.2].

The proportions used were in the proportion of 250 g/l of Copper sulfate to 75 g/l of Sulfuric Acid [3.3]. Considerable agitation was required to bring about solution. The electroplating was done at room temperature in a glass tank. The current density applied was less than 50 A. per square foot (in this case smaller than 0.1 A.). The initial deposition was done at low current, (about 0.02 A.) to avoid damage to the thin electrodes film. As the film thickened, the current was

increased by small steps until 0.1 A. The whole process lasted about twenty minutes. A mild agitation, produced with a stirring bar on a hot plate, was applied to increase the plating rate.

The anode consisted of copper sheets placed as in Figure 9.

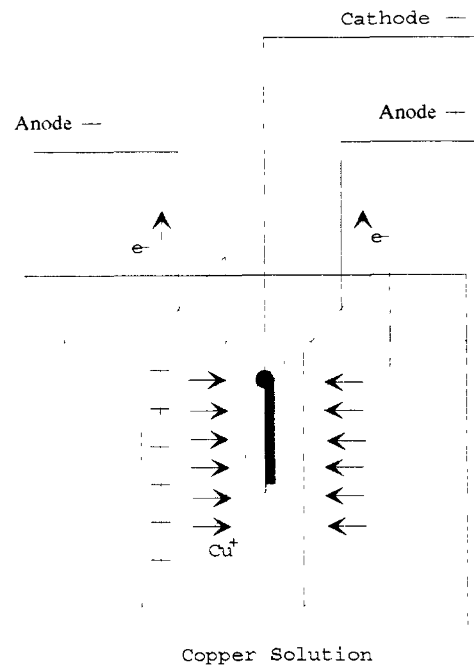

Fig 9: Setup used for electroplating the microstrip

The electricity was carried across the electrolyte by the charged ions of Cu^+ and products of the electrolysis appeared in the electrodes (in this case the PMMA substrate). See fig 9. After that, the microstrip was rinsed with distilled water and dried with paper tissues.

The substrate of PMMA was converted into an electrode by making conductive the surfaces that were intended to be coated with copper in the microstrip. For that, a very thin coating of copper or aluminum was deposited by vacuum evaporation. The vacuum machine used was a Denton Vacuum, DV-502. Both surfaces of the substrate were rinsed with distilled water, petroleum ether, and methanol, and dried with paper tissue. The bottom surface of the substrate was deposited with copper from direct exposure to the evaporating metal. For

the top surface, a mask was built from microscope slides, masking the exact dimensions of the microstrip (see figure 10).

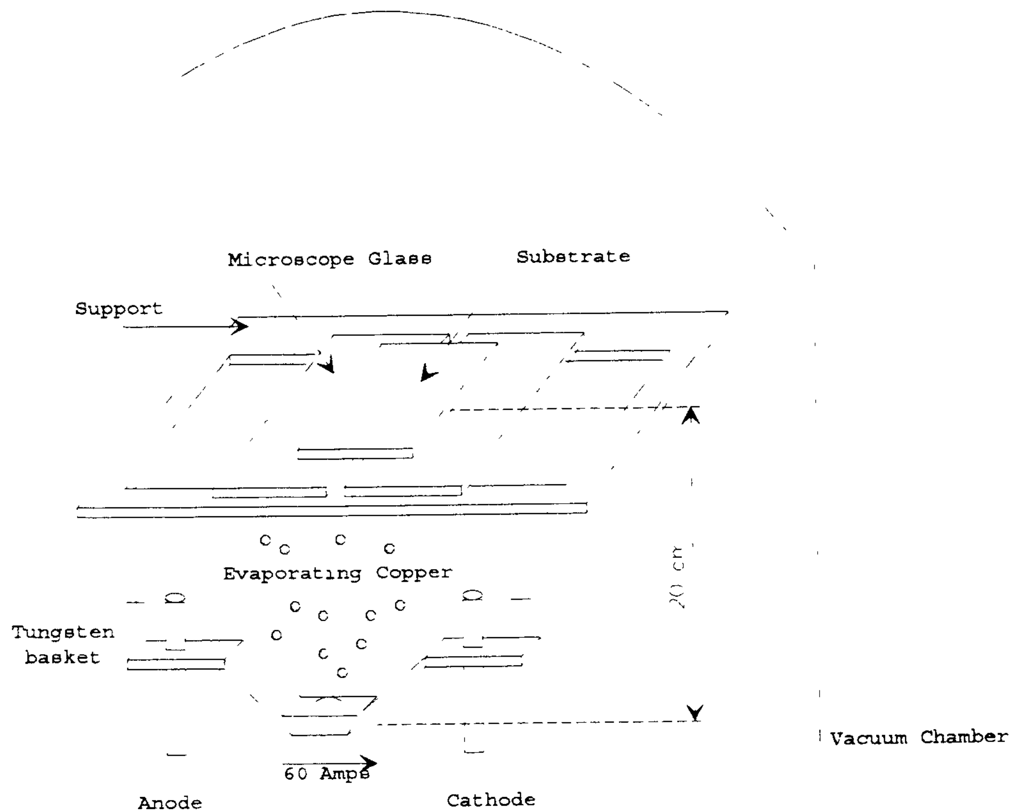

Fig 10: Formation of the conductive coatings in the microstrip by copper evaporation

The bottom coductive surface was obtained by turning the hole support, then copper was deposited from direct exposure to the evaporating copper source.

To start evaporation, first pressure of about 50 millitorrs was created in the vacuum chamber using the rotary pump. At that point, the rotary pump was connected in series with the diffusion pump, after having closed the valve to the chamber from the rotary pump. When 50 mtorrs were reached again in the whole system, (chamber and connection between the rotary and diffusion pump), the valve between the diffusion pump and the chamber was opened, bringing the

gauge was turned on. That brought the vacuum up to 10 E-5 Torrs. At that point, current was applied to the copper source.

The copper was placed around a tungsten basket and connected to the electrodes (see fig. 10). Evaporation started a few minutes after a current of 55 A. was applied. The fusion point of copper is much lower than the fussion point of tungsten, so even at very high temperatures the deposition was 99.9% copper. To obtain thicker deposition, the current was turned off to cool down the substrate for fifteen minutes. Then the current was applied again, increasing up to 55 A. This process was repeated until a visible coating was seen.

Nevertheless, this conductive coating was not thick enough to transport the current required for the microwave circuit. At microwaves frequencies, the current flows through the thin layer on the outside surface of the microstrip conductor. With no significant magnetic losses ($\mu = \mu o$) and with the conductivity $\sigma >> w\epsilon$, the skin depth is defined as [3.4]

$$\delta = \left| \frac{2}{w\mu\sigma} \right|^{1/2} \quad \text{m.}$$

where the frequency w is 10 Ghz, the permeability μ_o in vacuum is $4\pi \cdot 10^{-7}$ H/m and the copper conductivity σ is $18 \cdot 10E^{7}$ S/m. Those values lead to a value for a skin depth of $\delta = 1.212$ μm. On the other hand, the thickness obtained only from evaporation was far too low for the skin depth needed since

Thickness = length / (conductivity • Resistance • width)

and the resistance measured in the conductive strip was about 10 ohms, then applying the above formula for the microstrip parameters obtained, the thickness is

$$T = 2.6 \cdot 10^{-3} \text{ [m]} / (65 \cdot 10^{6} \text{ [1/ohm} \cdot \text{m]} \cdot 10 \text{ [ohms]} \cdot 1.9 \cdot 10\text{-}3 \text{[m]})$$
$$= 0.021 \ \mu\text{m.}$$

What is about 50 times smaller than the needed.

To solve this problem and also to avoid the possibility of too easily removing the conducting continuity of the film by accidental scratching, the film thickness and durability was enhanced by electroplating as described previously.

The considerations for the design are based in the fabrication of microstrips with ideal 50 Ohms characteristic impedance. The considerations are based in the equations shown in section 2.IV.1.1 and the calculations shown in section 4.3. The following table describes the actual dimensions and concentration of dielectric for all the fabricated microstrips:

TABLE 1. Actual dimensions of the fabricated microstrip

Microstrip Number	Undoped		CdS		GaAs		Si	
	I	II	I	II	I	II	I	II
Strip (Dimensions in mm.)								
Width(w)	2	2.4	1.9	1.3	2.3	1.8	1.1	2.8
Length(l)	59	50	54	50	64	62	64	69
Thickness(t)	0.05	0.05	0.05	0.05	0.05	0.05	0.05	0.05
Substrate (Dimensions in mm.)								
Width(W)	24	25	24	25	25	25	25	25
Length(L)	60	60	56	61	65	63	64	69
Thickness(T)	1	1	1	1	1	1	1	1
Concentration of dielectric								
(gr/ml of PMMA)	0	0	0.1	0.1	0.05	0.05	0.05	0.1

The experiments were realized for all the microstrips. However to avoid repeatitive data, only for the undopped PMMA-I, the CdS-I, the GaAs-I and both Si-I and Si-II will be the data obtained shown. The reason for showing two Si samples is because the results obtained for Si showed no response to the light and more repeatability was required to confirm the zero response.

3.3 ABSORPTION OF CdS, GaAS AND Si

The experimental setup to measure the absorption of the three materials used is shown in figure 11.

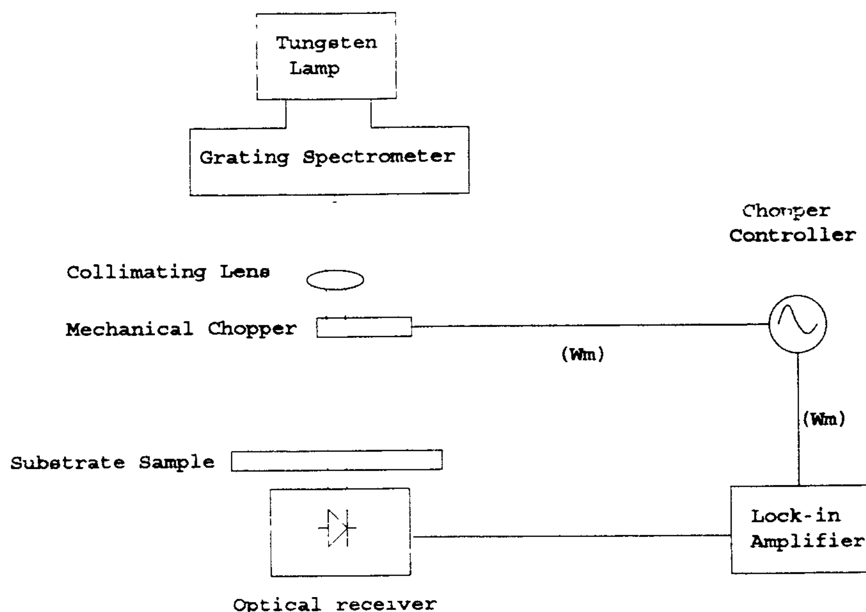

Fig 11: Setup used to measure the absorption of the different substrates

The wavelength selection in the Grating-Spectrometer, (SPEX- 1681, 022m), was varied from the ranges where absorption was expected (see fig. 1).

The tungsten lamp provided the whole visible, near and far infrared spectrum needed for the absorption of the dielectrics while in use. The grating spectrometer has a grating that by diffraction and interference selects, depending on the angle of incidence of the light to the grating, the wavelengths from near visible UV to 1100 nm. After 800nm the spectrometer starts diffracting the second order harmonic as well. To avoid the longer wavelengths also being diffracted, a 840 nm high-pass optical filter was added to the system.

The mechanical chopper and the lock-in amplifier (Stanford Research Sytems SR-510) acted as a band pass filter for the frequency selected in the chopper controller (200 Hz). This provided a filtering of the noise signal of all other

light sources in the room, since the lock-in only detects signals that have the same frequency that the one that is lock in, in this case was 200 Hz. The beam coming out of the spectrometer was focused by both an objective and a collimating lens, and launched to the optical receiver.

To measure the transmission absorption of the different samples, first the undoped PMMA sample was placed as close as possible to the photodiode. The system was maximized in the locking amplifier and in the beam focusing to improve the signal detection. Data was obtained for the entire frequency range in the spectrometer at 10 nm. intervals. Then, the undoped sample was replaced with the different samples of doped PMMA with CdS, GaAs and Si. The signal was maximized again for each sample, and the sweeping was reduced to the expected wavelength region of absorption for each semiconductor. Readings were taken and plotted as the dB attenuated in comparison with the PMMA readings for each wavelength.

3.4 MEASUREMENT OF THE RELATIVE PERMITTIVITY AND PERMEABILITY

The method used was taken from the Hewlett-Packard manual "Measurements of the permittivity and permeability with the HP-8515A Network analyzer" [3.5]. This method is suited for measurements of $\epsilon_r', \epsilon_r'', \mu_r', \mu_r''$ of solid materials with metallic and dielectric characteristics.

To measure these parameters, it was necessary to fabricate separate samples of PMMA embedded with each of the semiconductor clusters of Cds, GaAs and Si. First, the thin slurry of embedded monomer with the dielectric clusters as described in 3.I.1. was obtained, then the embedded monomer was poured into a thin cylindrical glass container and placed in the oven to polymerize. After 24 hours the polymer was extracted and machined with a precision driller and a precision sander to make the sample as flat and smooth as possible so that good mating contact could be achieved. Two different cylinder samples for every doped polymer were obtained with the following dimensions:

Inner radius: 3.04 mm , outer radius: 7 mm. length:10, 8 mm.

The samples obtained were slided into the HP-sample holder, which consisted of a 50 Ω, 7 mm coaxial beadles air line. The sample replaced the air at one end of the air line. A schematic of the setup is shown in fig 12.

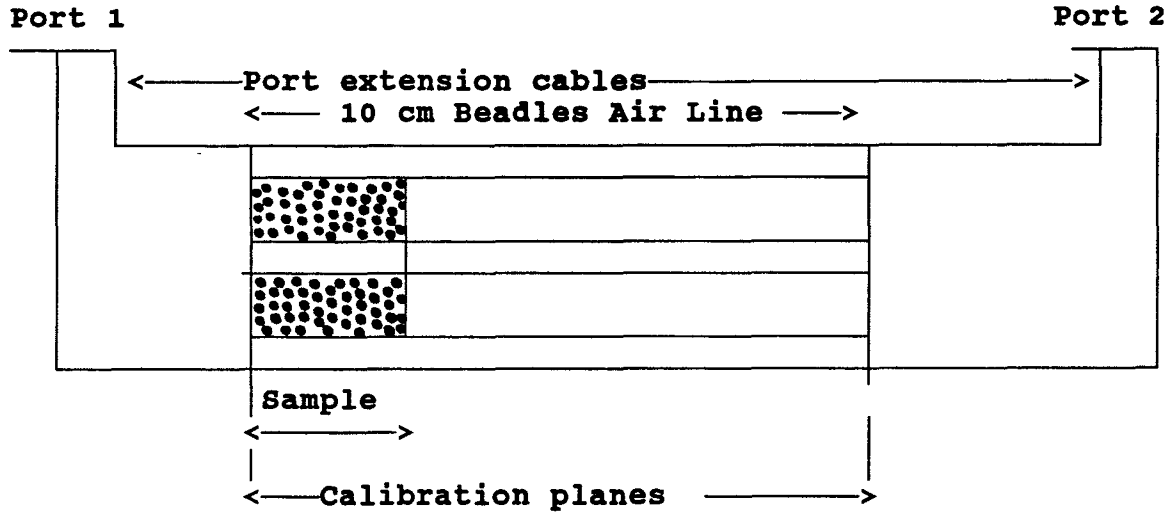

Fig 12: Coaxial Measurement setup

The system used to perform the experiment consisted of the HP-8510A network analyzer, the HP-8340A synthesized sweeper and the S-parameter test set. Measurement calibration was performed using the standards in the HP 8505A 7 mm. calibration kit at the planes of the input and output of the beadles sample holder. Full two-port calibration was performed to achieve more accuracy. The values of S11, and S12 were then obtained using the sweep mode with 201 frequency points and a averaging factor of 10.

3.5 MICROSTRIP LAUNCHING CHARACTERIZATION

SMA connectors were chosen as the microstrip launchers since they cover the X-Band wave spectrum. The launcher was the SMA-microstrip launcher from Omni-Spectra.

To hold the launcher, a jig was fabricated as show in Figure 13.

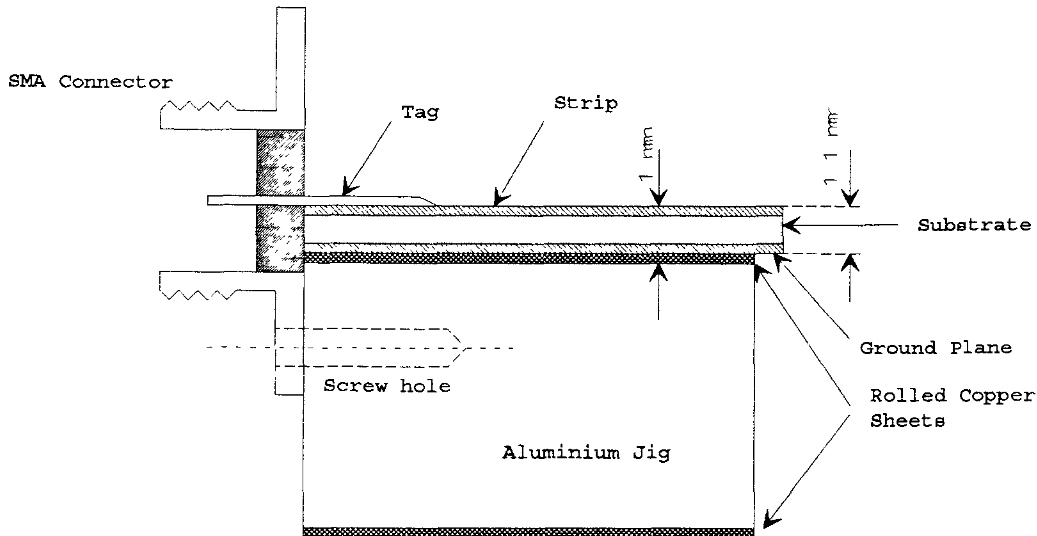

Fig 13: Coaxial to microstrip launcher transition (left portion)

A different jig for each of the microstip launchers (microstrip's input and output) was machined for the purpose of easily removing the microstrip from the jigs, and to have the capability of handling different microstrip lengths. For that, two aluminium blocks with two calibrated screw holes (for tightly screwing the launchers into the blocks) each, were selected. The distance between the tag of the launcher and the top of the jig was 1.1 mm.. An extra 0.1 mm over the thicknesss of the microstrip was allowed in order to place a rolled copper sheet 0.03 mm thick, making two turns around the aluminum block. The copper sheets acted as a spring, pushing the microstrip against the tag of the launcher and also making a double contact with the aluminum jig and the ground of the microstrip. Resistivity measurements were made between the grounds of the two SMA lauchers (input and output of the microstrip) with the microstrip in place and showed insignificant impedance, which demonstrated that good contact was achieved.

3.6 MICROSTRIP DC MEASUREMENTS

To confirm that the doping in the substrates was not too high and showed conductivity, DC measurements were carried out. The measurements were done under the same environmental conditions in which the substrates were going to be., i.e. under light and with RF going through the microstrip. The HP-3465A digital voltmeter with a range up to 20 mega-ohms was used. The probes were placed in the ground plane and in the strip of the microstrip. The impedance measured for all the microstrips in all the conditions was out of the range of the voltimeter, or bigger than 20 megaOhms.

3.7 MICROSTRIP S-PARAMETER MEASUREMENTS

As stated in section 2.IV.3, the reflection and transmission coefficients could be extracted from the s-parameters. The measurements were made with the HP-8341B network analyzer, which has a spectral bandwidth from 300 Mhz to 3 Ghz, the HP-85046A S-parameter test set and a HP-plotter. Since high accuracy and repeatability are required for the measurements, the full 2-port calibration with smoothing and averaging, and the step sweep mode at 201 frequency points were used. The calibration was done at the input and output planes of the microstrip with a SMA standard calibration kit. The setups used are as shown in Figure 14.

The s-parameters were measured with and without incident light. Two sources of light were used, a blue light laser of approximately 5 mW maximun power and 442 nm. wavelength, and a halogen focused white source with a dimmer to control its intensity. Measurements of the phase and linear amplitude were taken for the reflection and transmission parameters, S11 and S21. The blue light laser was used in the CdS measurements, since blue light is in the spectral absorption spectrum of the CdS. The white light was used for all the dielectrics, CdS, GaAs and Si. Also measurements were taken at the maximum and minimum intensities offered by the dimmer of the white light, whose maximum intensity was roughly twice its minimum intensity. The normalized spectrum of the white light was obtained using the setup in Fig. 15 The results obtained are shown in Fig. 21.

The measurements were carried out using the same setup for absorption but replacing the tungsten light built in in the spectrometer with the halogen lamp that was used in the experiments. A filter was placed for readings of wavelengths higher than 820 nm. to avoid second order harmonic difraction. The wavelength

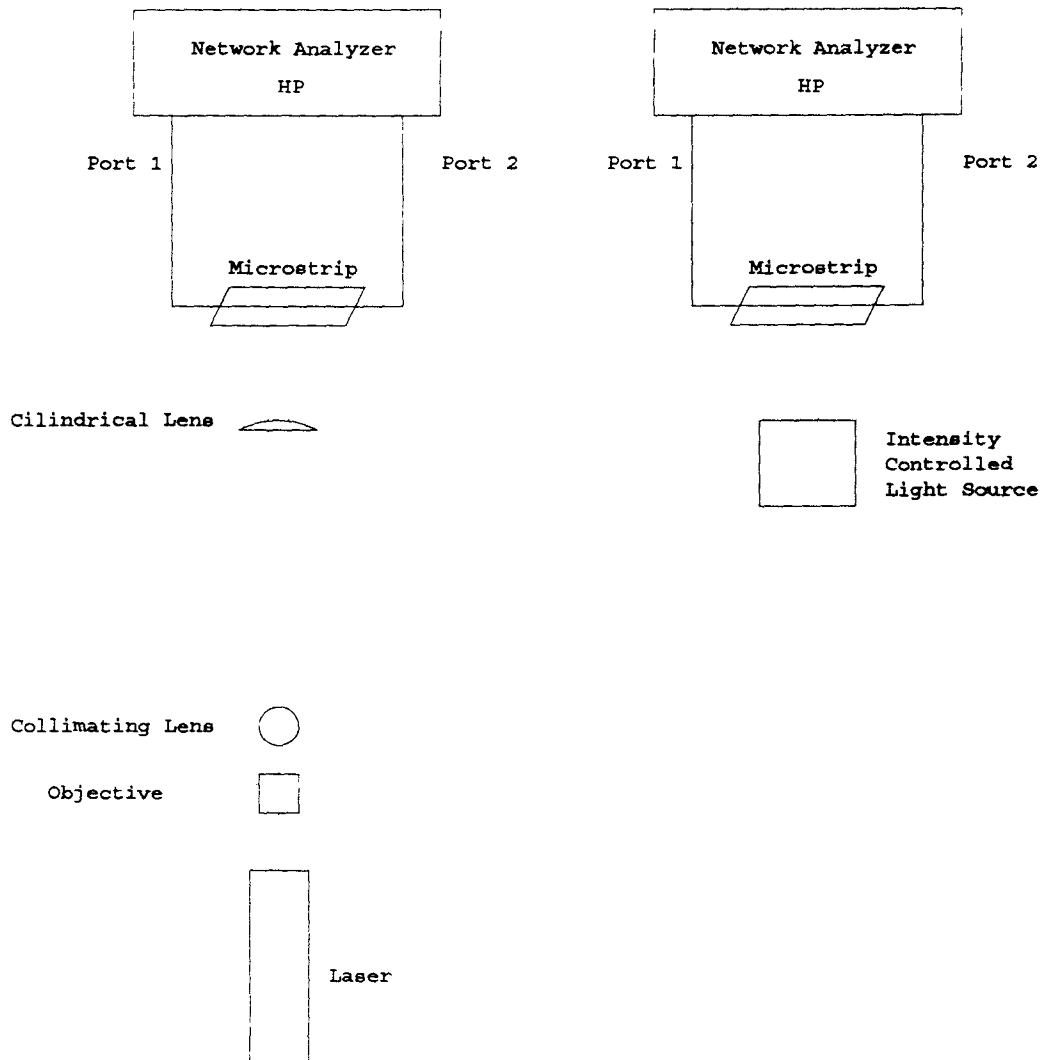

FIG. 14. Systems to determine the variation of the S-parameters when light is applied to the microstrip.

response was normalized with the responsivity curve of the receiver, obtained from the data sheet of the manufacturer (EG & G Photon Devices UV-series).

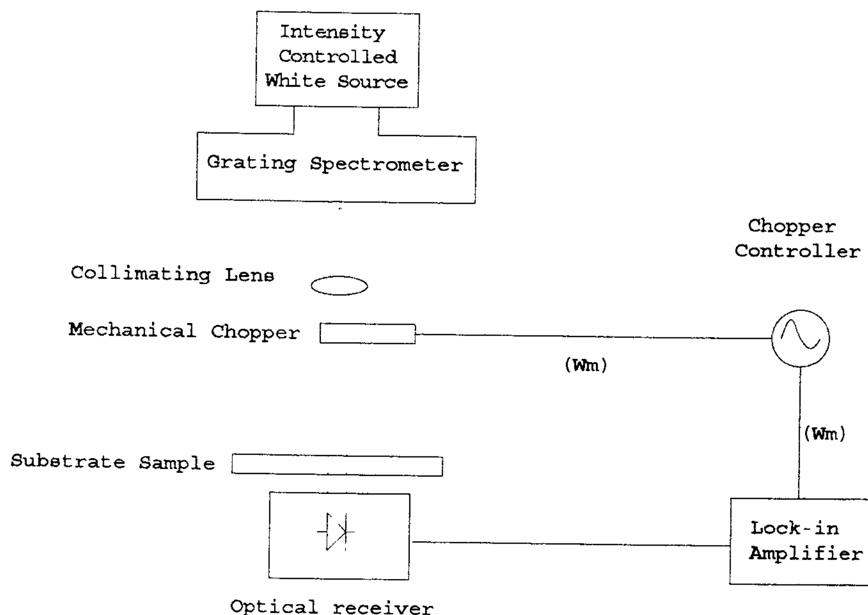

Fig 15: System used to measure the spectrum of the white light source

Since the network analyzer's measurements become more precise as the frequency sweeping bandwidth becomes smaller, a sweeping bandwidth between 2.999 and 3 Ghz was chosen. Since the microstrip was going to be used in the X-band range of frequencies, the election of the frequency for the measurements at the network analyzer was the highest available, 3 Ghz. At the bandwidth chosen, the system was calibrated and then the amplitude and phase of the S-parameters were measured .

The plots obtained for Cds, GaAs, Si, and undoped microstrips are displayed in Figures 23, 24, and 25. Also shown are the variations in phase and linear magnitude when the different light sources were applied.

To observe if there were any nonlinearities at the frequency chosen for the measurements, data was also taken at a frequency sweeping from 1 to 3 Ghz. The plots obtained are displayed in Fig. 27.

To verify that, at the bandwidth chosen, the sign of the variation of the phase and linear magnitude was not in any resonance point or a non-linear point, several plots were taken zooming a specific point and observing the sign of the variation. The series of plots are shown in Fig. 26.

3.8 HOMODYNE DETECTION MEASUREMENTS

Another system to determine the changes in phase and amplitude in the transmission of a wave propagating through the fabricated microstrips, was based on the interference principle described in sections 2.V and 2.VI.

3.8.1 MACH-ZEHNDER AND MICHELSON INTERFEROMETERS

The first setup is shown in Fig 16. It is based on the Mach-Zehnder interferometer described in 2.V.1. The CW sources used were the synthesized sweeper (HP-8341B), and the signal generator (Anritsu-M67245), both showing similar performance and stability. The experiments using the synthesized sweeper were performed at a frequency of 10 Ghz and an output power of 16.4 dBs. The Anritsu signal generator was used at 10.6 Ghz (the lowest frequency available on it) and 15 dBs output power (maximum available). The carrier frequency chosen was 10 Ghz, since the rectangular waveguide components (Isolator, waveguides, phase shifter, and amplitude controller) had a higher measured transmittivity of power at that frequency. The maximum transmissivity of those components was at 10 Ghz and the cutoff frequencies at 7 and 13 Ghz. At 10.6 GHz the power transmitted was one Db down from the transmitted power at 10 Ghz. A X-Band Isolator was placed after the source to prevent reflections. The isolator was connected to a waveguide tee H-plane (shunt tee). There, the wave split equally into the other two ports in phase and in magnitude [3.6] . The tee showed good matching, since the powers at the outputs were identical. One of the arms had a phase shifter (0° to 360°) and an amplitude controller (0 to 50 Dbs attenuation) in series, both in the X-band. This arm was the reference channel, since it carried the unmodulated signal that was going to interfere with the modulated carrier. The other arm, or the information channel, consisted of an amplitude controller (0 to 50 Dbs attenuation) in series with the microstrip. Both arms were assembled into a coaxial-SMA power spplitter-combiner, model HP-11667B of bandwidth from DC to 26.5 Ghz. The power combiner featured a matched input impedance in the two input arms, converging into a virtual ground. The SWR was 1.1 , what produced minimum reflections. The output was extracted from the virtual ground. The combined signals were driven to the RF sensing unit made by Weinschel Engineering with a bandwidth of 0.01 to 18 Ghz. There the signal was divided by a power divider; one arm went to a power sensor

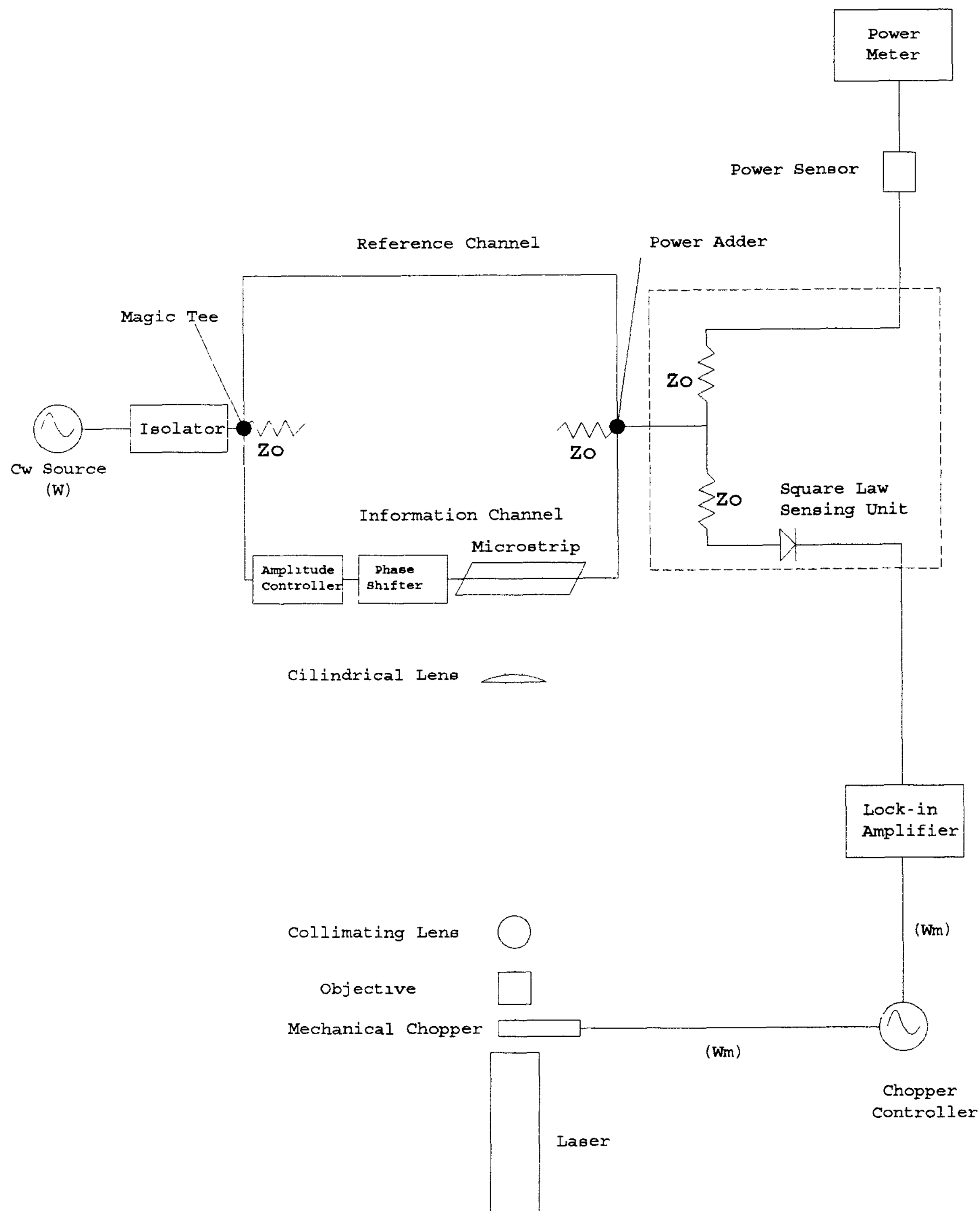

FIG. 16. Basic homodyne system to detect amplitude and phase modulation caused by a blue light laser modulated by a mechanical chopper.

and from there to a power meter (Boonton PM-4200RF). The other arm was driven to a square law detector. From the square law detector in the RF sensing unit the signal was driven to the lock-in amplifier.

The lock-in amplifier was synchronized to the same modulating frequency as the mechanical chopper that was cutting the light either from the white source or from the laser. The light sources used were the same as in the network analyzer.

The laser was driven into the microstrip by focusing the beam either through an objective and collimating it into the cylindrical lenses and from there to the microstrip, or directly through the cylindrical lenses into the microstrip.
In both cases, the illuminated area on the microstrip was 1.5 to 2 cm. thick, and covered the whole length of the microstrip. Since the density of field lines is bigger under the surface of the microstrip [3.7], more effect could be achieved if light is incident in that region.

The thickness of the copper strip was about 1.2 μm. and, as shown in fig 17, [3.8], at that thickness no light is transmitted to the substrate.

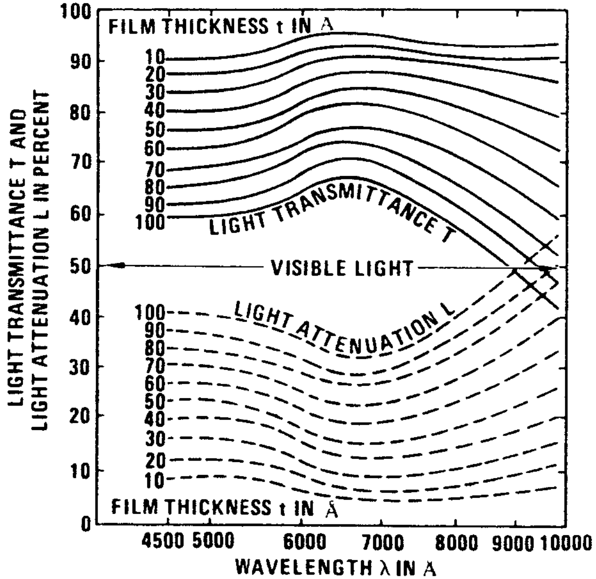

Fig 17: Light transmittance(T) and light attenuation loss (L) of copper film versus wavelength with film thickness t as parameter

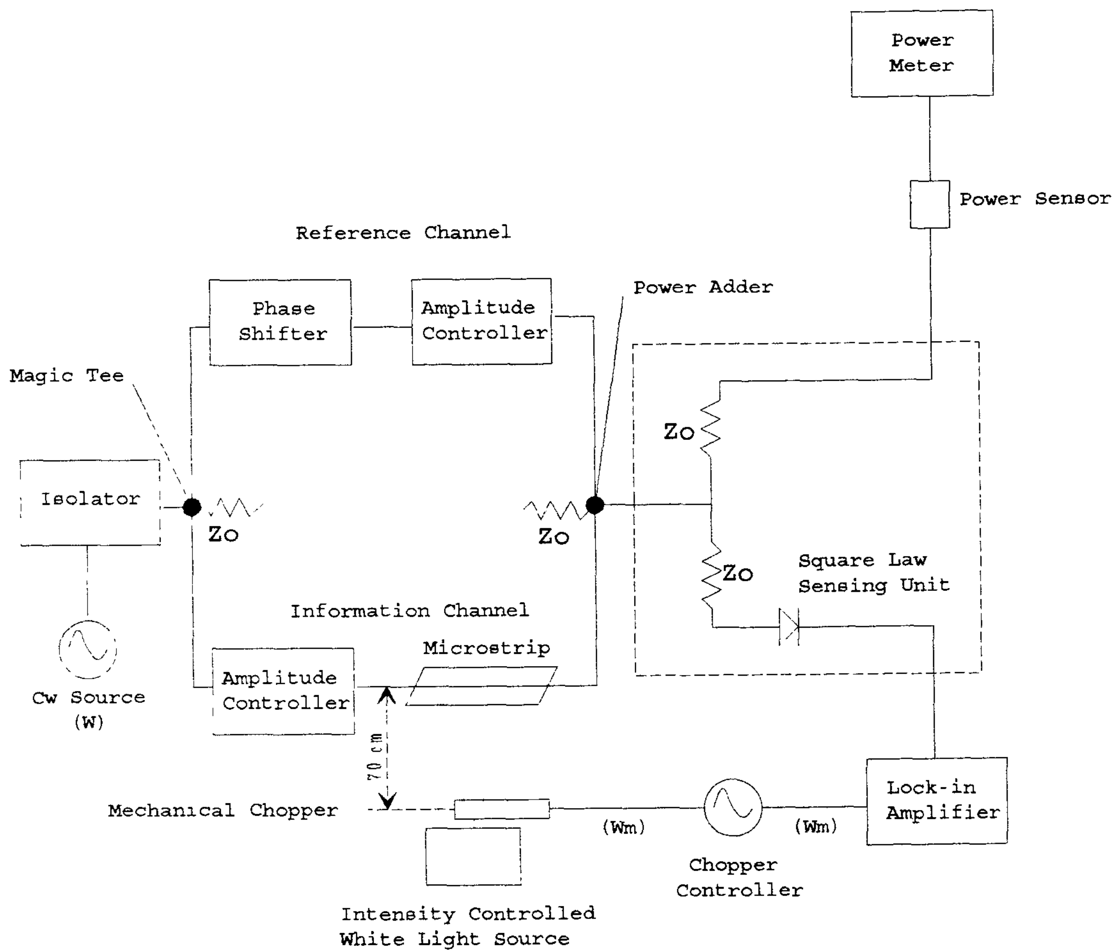

FIG. 18. Basic homodyne system to detect amplitude and phase modulation caused by a white light source.

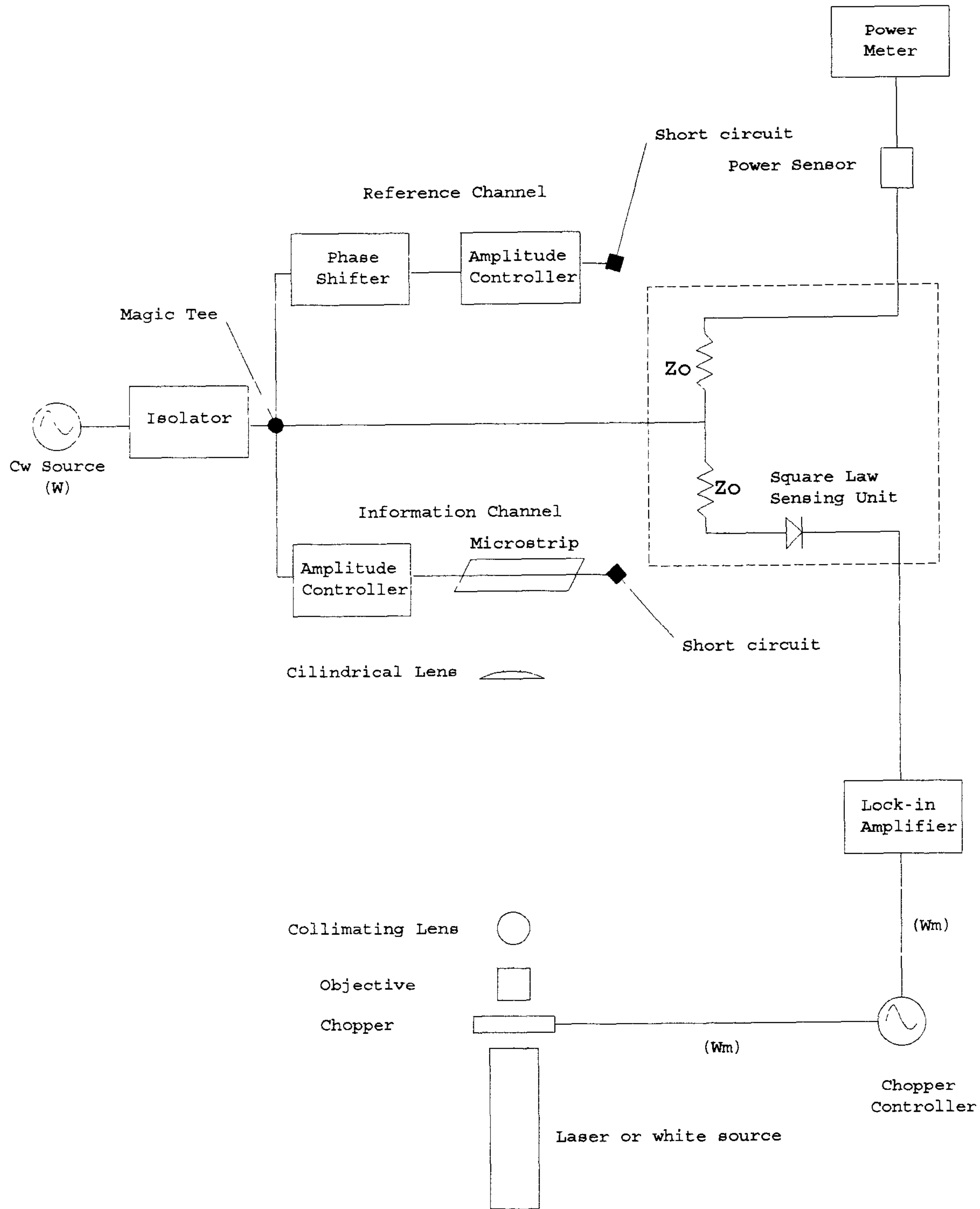

FIG. 19. Alternative Michelson interferometer to detect amplitude and phase modulation caused either by a white light or blue light laser.

To get more light under the strip of copper, the light was launched at a 45° degree angle from the plane of the microstrip with the help of a big reflecting mirror.

For the laser setup the copper was placed at the output of the laser. However, for the white light source used in the setup shown in figure 18, since its beam diverges rapidly, the source was placed as close as possible to the microstrip to get the most energy from the light. The problem was that the mechanical rotation of the chopper could interfere with the line forces of the microstrip, and the microstrip could act as an antenna and pick up the signal comming from the chopper, since it was at the same frequency as the band pass in the lock-in. To avoid that, the light was turned off and the minimum distance observed at which the microstrip didn't pick up any signal was 70 cm. Since the aperture output of the white light had the same size as the holes in the mechanical chopper, it was necessary for the light to be placed as close as possible to the rotating chopper.

The light incident in the microstrip had an elliptical shape that covered the whole surface. As in the laser, the light was launched at a 45 ½angle to the plane of the microstrip.

The Michelson interferometer setup is displayed in Figure 19. A magic tee was used to split the wave into the reference and the information channels. At the end of the channels were placed two short-circuits. For the reference channel, since it is a rectangular waveguide, a sheet of copper was tightly clapped to the end. For the information channel, a standard SMA short-circuit was placed at one end of the microstrip.

The configuration of the rest of the circuit was the same used for the Mach-Zehnder interferometer. The different microstrips fabricated were placed in the circuit and the following measurements were performed:

A. The response of the detection as the phase in the phase-shifter was increased by steps of 10 degrees from 0° to 720°. This experiment shows the repeatitivity of the measurement throughout two periods. The system settings were: Output from the source: 15dBs, Carrier frequency: 10.6 Ghz, Modulating frequency: 50 Hz, Attenuators settings: 0 Dbs. This was performed for the undoped substrates and for the different doped microstips substrates.

B. For the same settings as in A, the same experiment was performed, although only through one period. In this, case the attenuation in the information

channel was of 10 Dbs. This experiment shows the variation in the amplitude and phase errors with an attenuated signal in the information channel.

C. To observe if the measurements were in the linear region instead of in the square law region, the response of the system to increments in the attenuation in the reference channel was tested.

D. The modulating frequency was increased to 200 Hz. This experiment shows the variation of the detection for different modulation frequencies.

E. The frequency response was studied up to the maximum available speed of the chopper, 400 Hz.

F. The response of the power detected as the phase was varied.

G. The difference between the power detected in the power meter when the light was and was not incident into the microstrip for every phase shifted

H. The difference of detection in the system using the white light or the blue light from the laser.

I. The comparison of the detection using either the Mach-Zehnder or using the Michelson interferometer is shown for the lock-in measurements for two periods, the frequency response, and for attenuation in the information channel.

4. RESULTS

4.1 ABSORPTION IN THE CdS, Si AND GaAs DOPED SUBSTRATES.

The results obtained from the absorption experiments described in section 3.3 are shown in Figs. 20 for CdS, GaAs and Si. Fig 20 shows strong power absorption of the CdS embedded substrate at 510 nm as was expected from Fig.1. For wavelengths shorter than 510 nm the absorption decreases. This matches the theory since the wavelength peak response for CdS is at 500 nm and the cutoff frequency (50% value) is at 510 nm [4.4]. Therefore, it was expected that for the light sources used, the blue light laser at 442 nm. and the white light laser source whose spectrum is shown in Fig. 21, the CdS will absorb energy. Some of that energy, as described in section 2.1, will generate electron-hole pairs and some will be dissipated as heat.

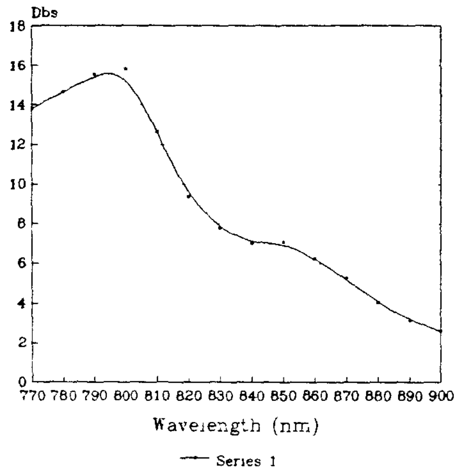

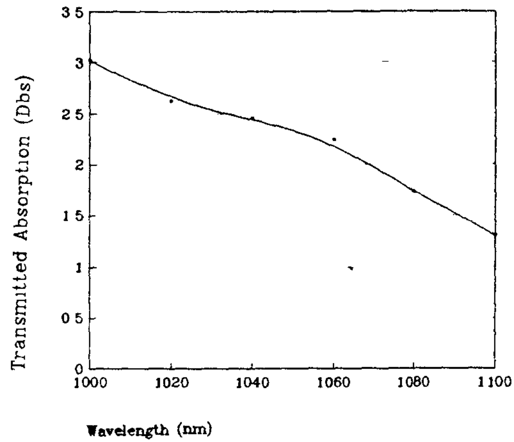

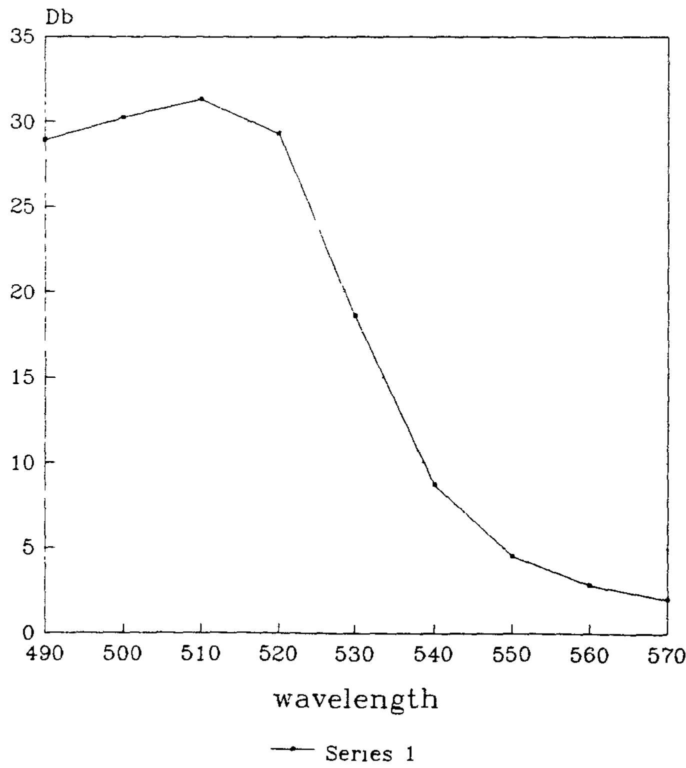

FIG. 20. Absorption of CdS, GaAs, and Si substrates

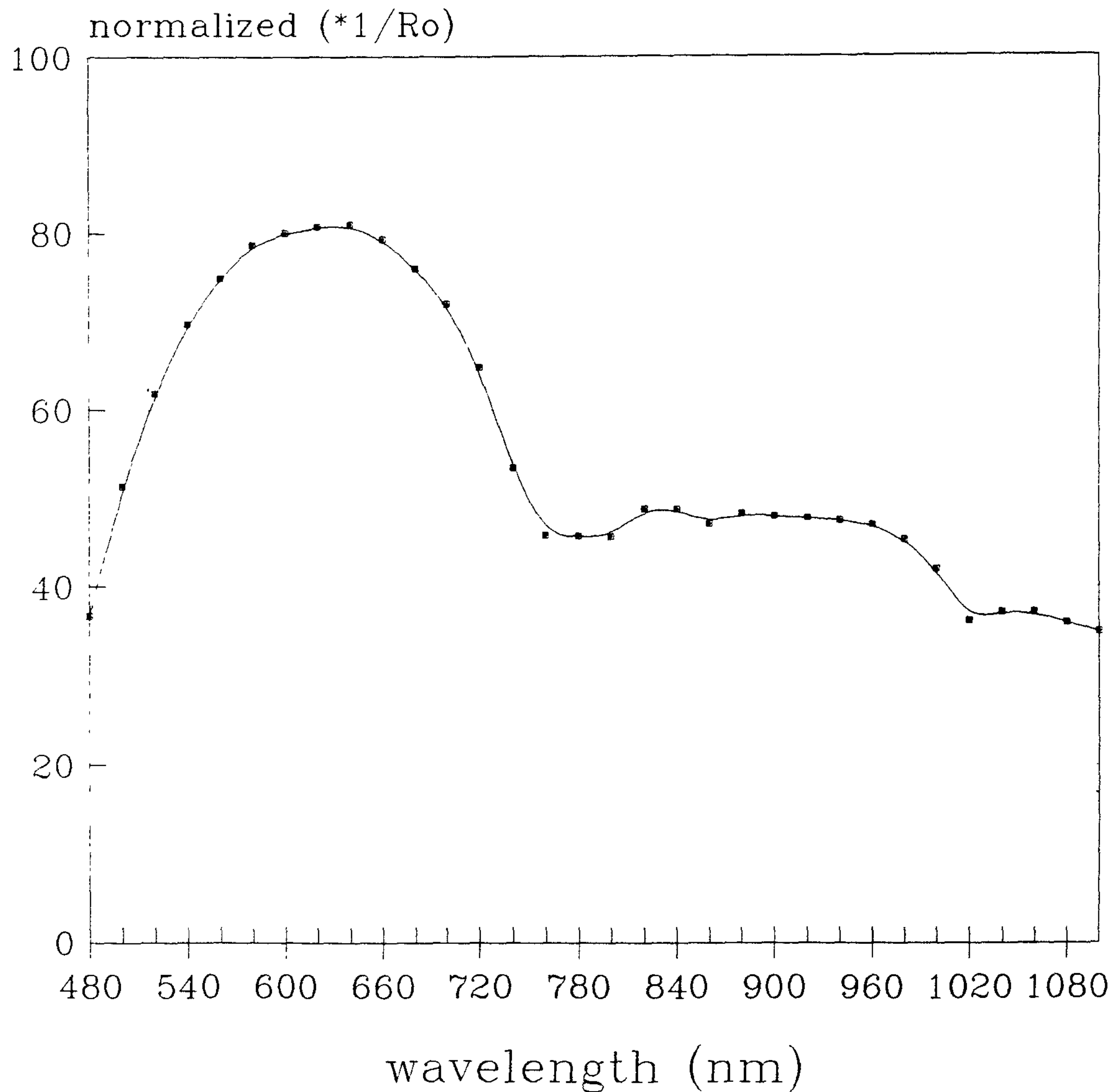

FIG. 21. Spectrum of the white light source

For GaAs, the range of wavelengths that was expected to be absorbed was between 640 and 870 nm, with 890 nm the cutoff wavelength and the wavelength of peak response at 800nm. [4.5] for the exact energy bandgap.

For Si, the absorption range as shown in Figure 1 is from UV wavelengths up to 1,100 nm. The wavelength required for the exact bandgap energy is around 1060 nm.

4.2 SUBSTRATE PERMITTIVITY AND PERMEABILITY RESULTS

The S11 and S21 parameters for undoped PMMA and that doped with Si, CdS and GaAs materials were obtained from the experiments described in section 3.4.

The boundary conditions obtained from the air line filled with the dielectric material placed in the network analyzer could be explained by looking to Fig 22.

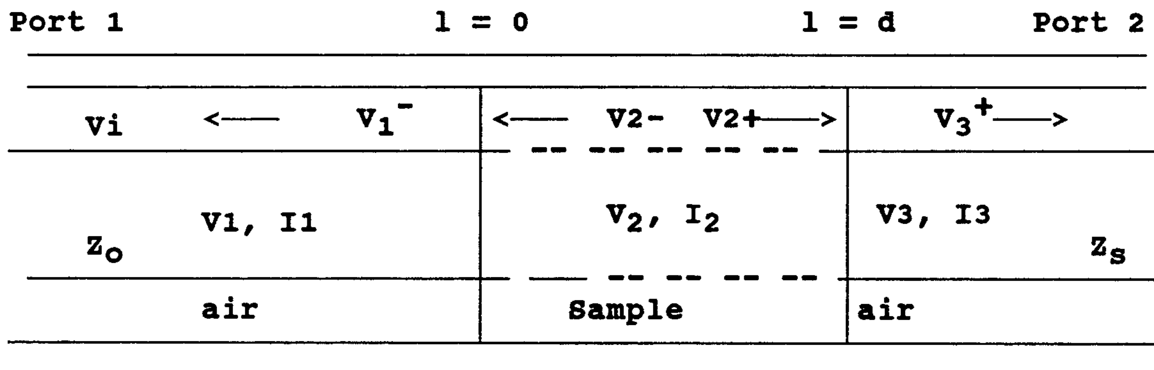

Fig 22: Boundary conditions

By solving the boundary conditions of the problem at l = 0 and l = d, of:

$V_1 = V_2$ at $l = 0$
$I_1 = I_2$ at $l = 0$
$V_2 = V_3$ at $l = d$
$I_2 = I_3$ at $l = d$

the following relations between the S-parameters and the reflection and transmission coefficients are deduced:

$$S_{11}(w) = \frac{(1 - T^2)\,\Gamma}{1 - T^2\Gamma^2}$$

$$S_{21}(w) = \frac{(1 - \Gamma^2)\,T}{1 - T^2\Gamma^2} \qquad (4.2.1)$$

Γ : Reflection coeff. when $l = \infty$, between Z_o and Z_s
T : Transmission coeff. when $l = d$

or

$$\Gamma = K \pm (K^2 - 1)^{1/2}, \qquad (4.2.2)$$

where

$$K = \frac{S_{11}^2 - S_{21}^2 + 1}{2S_{11}} \qquad (4.2.3)$$

$$T = \frac{S_{11} + S_{21} - \Gamma}{1 - (S_{11} + S_{21})\Gamma} \qquad (4.2.4)$$

The reflection coefficient is defined as

$$\Gamma = \frac{Z_s - Z_o}{Z_s + Z_o} = \frac{\sqrt{(\mu r/\epsilon r)} - 1}{\sqrt{(\mu_r/\epsilon_r)} + 1} \qquad (4.2.5)$$

and the transmission coefficient can be written as

$$T = \exp\ (-j(w/c_o)\sqrt{(\mu_r/\epsilon_r)}d \qquad (4.2.6)$$

From (4.2.5) and (4.2.6), the variables x and y are defined as

$$x = \frac{\mu_r}{\epsilon r} = \left[\frac{1 + \Gamma}{1 - \Gamma}\right]^2 \qquad (4.2.7)$$

$$y = \mu_r \cdot \epsilon_r = -\ [c_o/w \cdot d]^2 \cdot [\ln(1/T)]^2 \qquad (4.2.8)$$

Then,

$$\mu_r = (x \cdot y)^{1/2}$$
$$\epsilon_r = (x/y)^{1/2}$$

4.3 MICROSTRIP DESIGN CONSIDERATION RESULTS

At the time of the design of the microstrips, the relative permittivity of the dielectrics was unknown. The objective of the design was to obtain a 50 ohm characteristic impedance. The estimate for the design was a function of the

proportions of dielectric used in the fabrication, since the theoretical relative permittivity of the dielectrics used is known.

PMMA [4.1]: 2.22, Si: 11.9, GaAs: 13.1, CdS: 5.4 [F/cm] [4.2].

The proportions of PMMA with respect to the semiconductor were similar (18 ml. of PMMA for 1 gram of semiconductor for GaAs and Si, and 2 grams for CdS). From those proportions, an approximate relative permittivity was estimated for the doped substrates of

CdS: 2.55, GaAs: 2.8, Si: 2.75. [F/cm]

Using those values in equations (2.IV.1.1.3)
and its modification for $\epsilon r < 16$ [r 4.3]

$$\frac{w}{h} = \frac{8}{\exp(A) - 2\exp(-A)} \qquad (4.3.1)$$

$$\text{where} \quad A = \frac{Zo\sqrt{(2(\epsilon r + 1))}}{119.9} + \frac{(\epsilon r - 1)}{2(\epsilon r + 1)}\left[0.46 + \frac{0.242}{\epsilon r}\right]$$

we obtained a width w for the microstrip for low frequencies of:

PMMA: 2.49 , CdS: 2.45, Si:2.42, GaAS:2.39 [mm.]

For the static effective permittivity applying equation (2.IV.1.1.4) it was obtained:

PMMA: 2.167, CdS: 2.376, Si: 2.5295, GaAs: 2.5835 [F/cm]

The effective permittivity at 10 Ghz, calculated from (2.IV.2.2) and (2.IV.2.3) is:

PMMA: 2.16687, CdS: 2.3659, Si:2.5294, GaAs: 2.5834 [F/cm]

The ideal characteristic impedance of 50 ohms considered in the design, would have changed, considering equation (2.IV.2.4), from its static evaluations to the followimg values at 10 Ghz

Z_o(PMMA): 50.18, Z_o (CdS): 50.16, Z_o (Si): 50.15 Z_o (GaAs): 50.14 [ohms]

Since the dimmensions obtained for the microstrip (see table 1.) are not exactly the same as the ones recommended for the design, the formulas used for the theoretical matched microstrip give the following values for the static and dynamic characteristic impedance and permittivities.
The static effective permittivity using (2.IV.1.1.5) is :

PMMA: 1.84, CdS: 2.067, GaAs: 2.3, Si: 2.21 [F/cm]

The static characteristic impedance using (2.IV.1.1.4) is:

PMMA: 65.477, CdS: 61.8, GaAs: 54.54, Si: 48.52 [Ohms]

At 10 Ghz the dynamic effective permittivity using (2.IV.2.2) is

PMMA: 1.798, CdS: 2.034, GaAs: 2.291, Si: 2.198 [Ohms]

The Zo(10Ghz) using Eq. (2.IV.2.5) is:

PMMA: 66.237, CdS: 62.29, GaAs: 54.64, Si: 48.65 [Ohms]

At 3 Ghz the dynamic permittivity using (2.IV2.2.) is

PMMA: 1.83, CdS: 2.057, GaAs: 2.298, Si: 2.207 [F/cm]

The Z_o (3 Ghz), using (2.IV.2.5) is:

PMMA: 66.41, CdS: 61.85, GaAs: 54.58, Si: 48.55 [Ohms]

The difference between the parameters obtained from the different microstrips shows a close approximation for GaAs and Si to the ideal 50 ohm

impedance. The theoretical difference between the values obtained at 3 Ghz and 10 Ghz shows little variations, so we can assume that values obtained in the network analyzer at 3 Ghz could be approximated with a small coefficient to the values obtained at 10 Ghz.

The expected reflection coefficients for the different microstrips are calculated from the equation (2.4.4.1.2) and (2.4.4.1.1) Since the microstrip will be placed in a 50 ohm matched impedances throughout the circuit in the interferometer, and the measurements in the network analyzer consider a 50 ohm load impedance after the calibration planes of the microstrip, Z_L will be considered as a 50 ohm load. The following table shows the values of Z_o, Z_{in} and S_{11} for all the microstrips at a frequency of 3 Ghz:

TABLE 2. Values of Zo, Zin and S11 expected from the design considerations for all the microstrips.

Substrate	length (mm)	Z_{oeff}(10 Ghz) (ohms)	Z_{in} (ohms)	S_{11}
PMMA	59	66.41	50.166+j2.52	0.001+j0.001
CdS	52	61.85	50.116+j1.75	0.0015+j0.0175
Si	69	48.65	49.964-j0.30	-0.0003-j0.003
GaAs	63	54.58	50.087+j0.91	0.0001+j0.009

4.3.1. NETWORK ANALYZER RESULTS

The plots obtained for the linear magnitude and phase of the S11 and S21 parameters at 2.999 - 3 Ghz for all the microstrips are shown in figures 23, in polar or Smith chart representation, showing the total values for all the samples. Figures 24 shows the variation of the S11 parameter in phase and in linear magnitude for CdS and GaAs as light was applied. Figures 25 a and b shows the variation of the S22 parameters in phase and in linear magnitude for CdS and GaAs as light was applied (the 442 nm. laser and the white light). Figure 26 shows the phase variation for all the microstrips as the frequency is swept

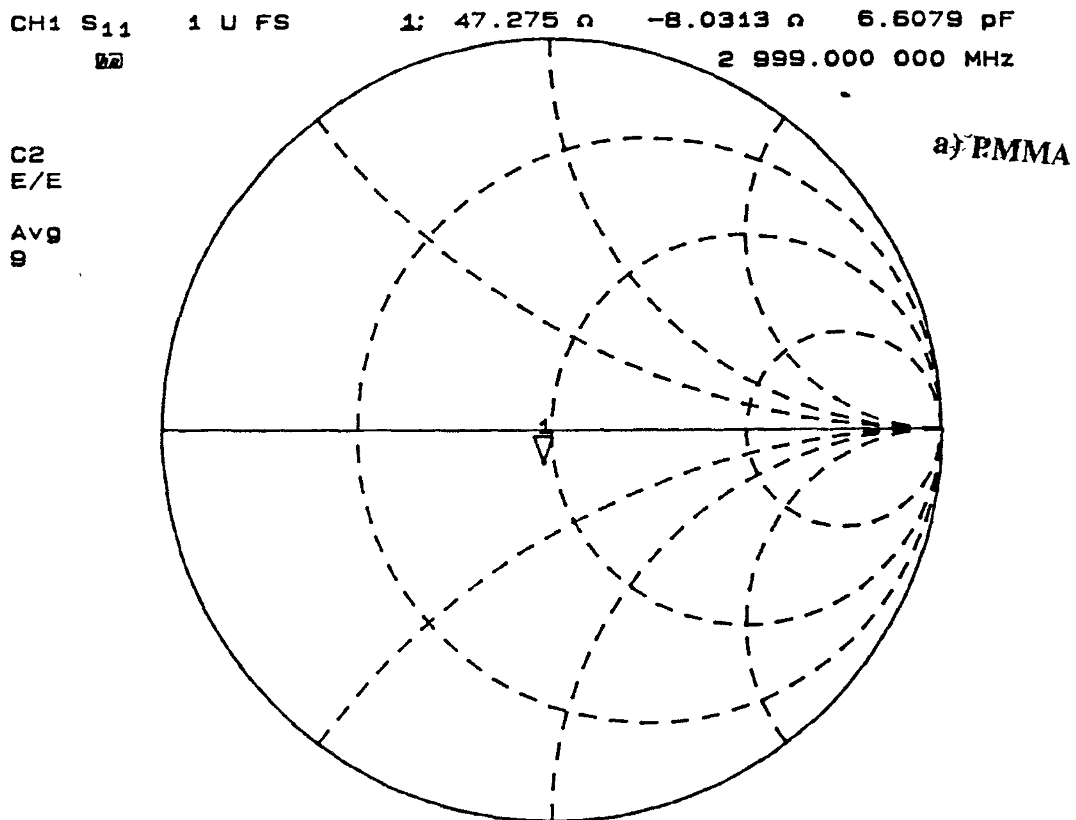

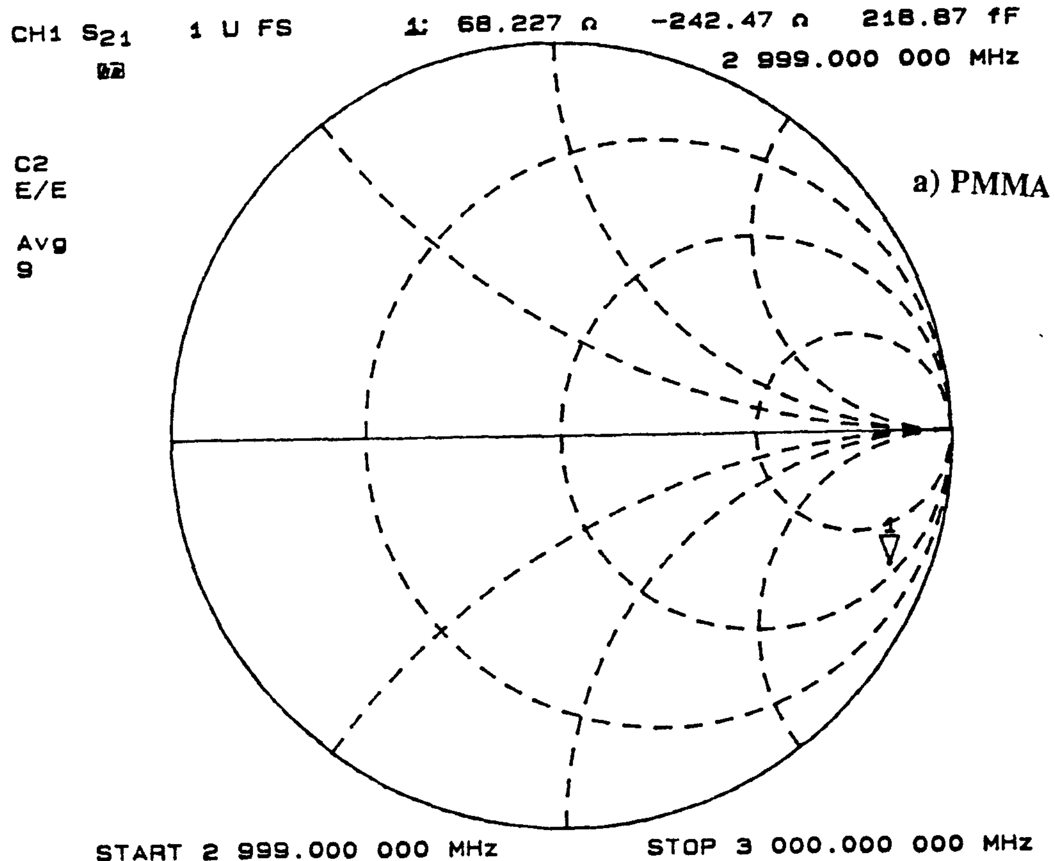

FIG. 23. S11(2.99-3 Ghz) and S22 (2.99-3 Ghz) values of the a)PMMA, b)CdS, C)Si1, d)Si2, e)GaAs in polar or Smith chart representation

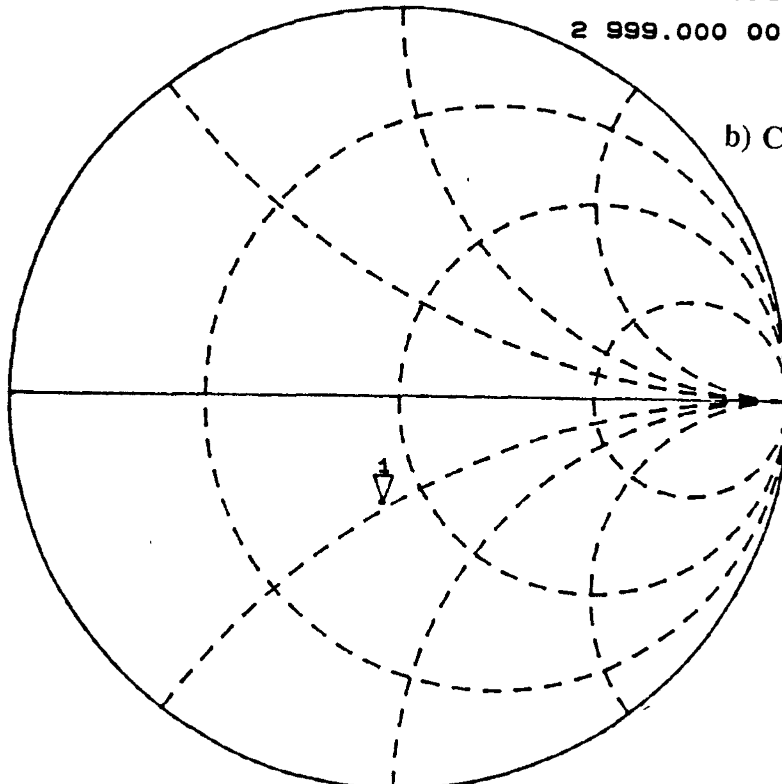

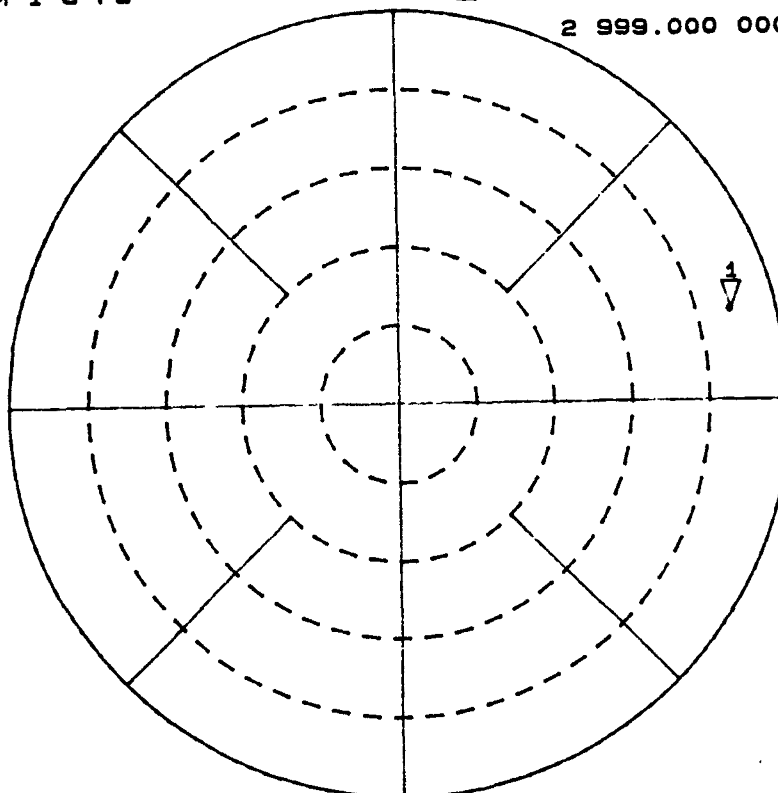

Figure 23 (Continuation)

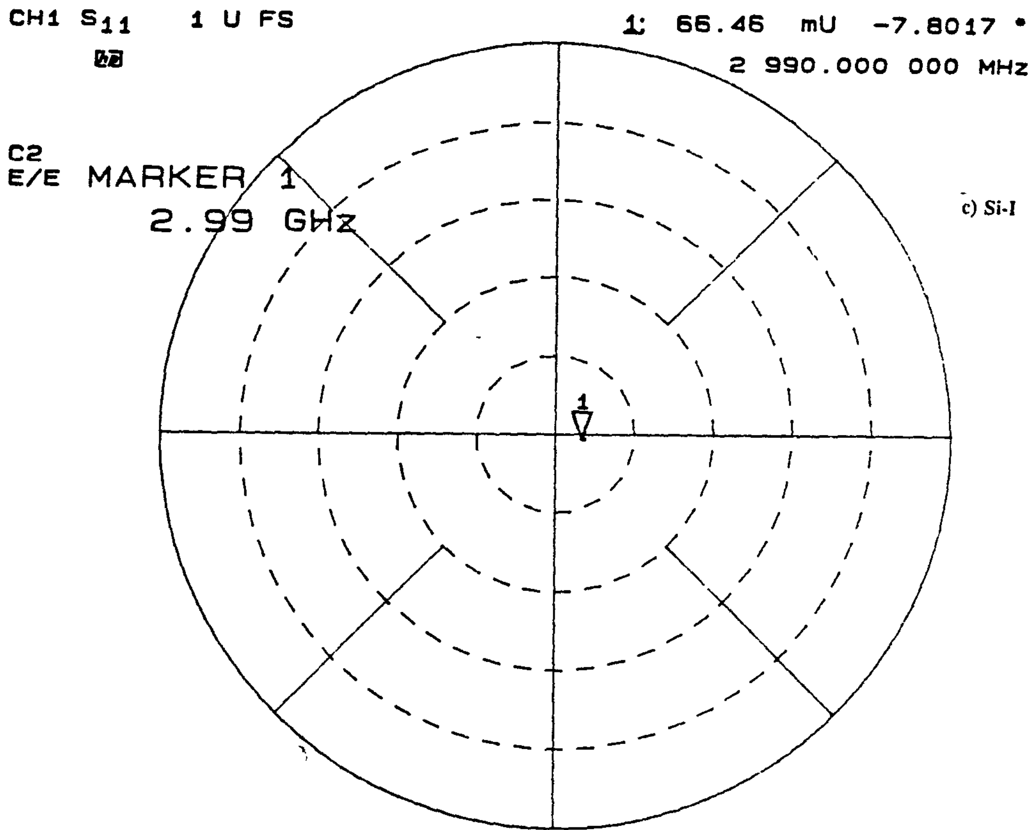

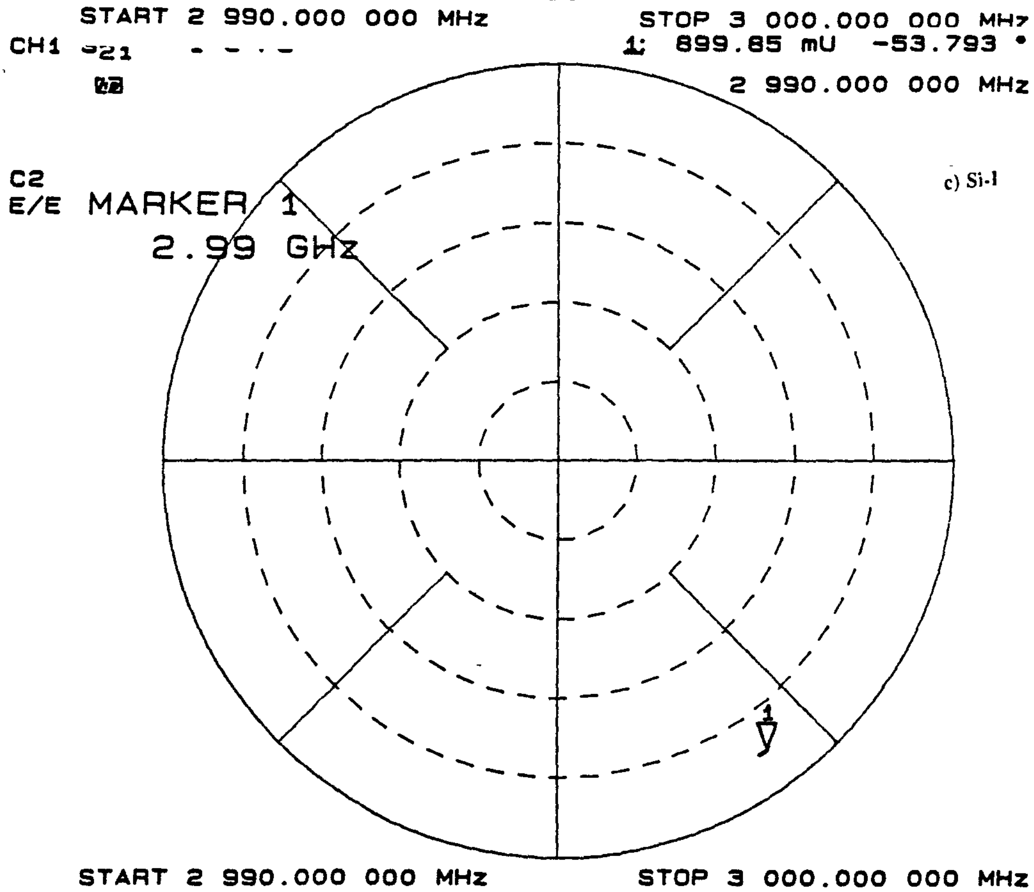

Figure 23 (Continuation)

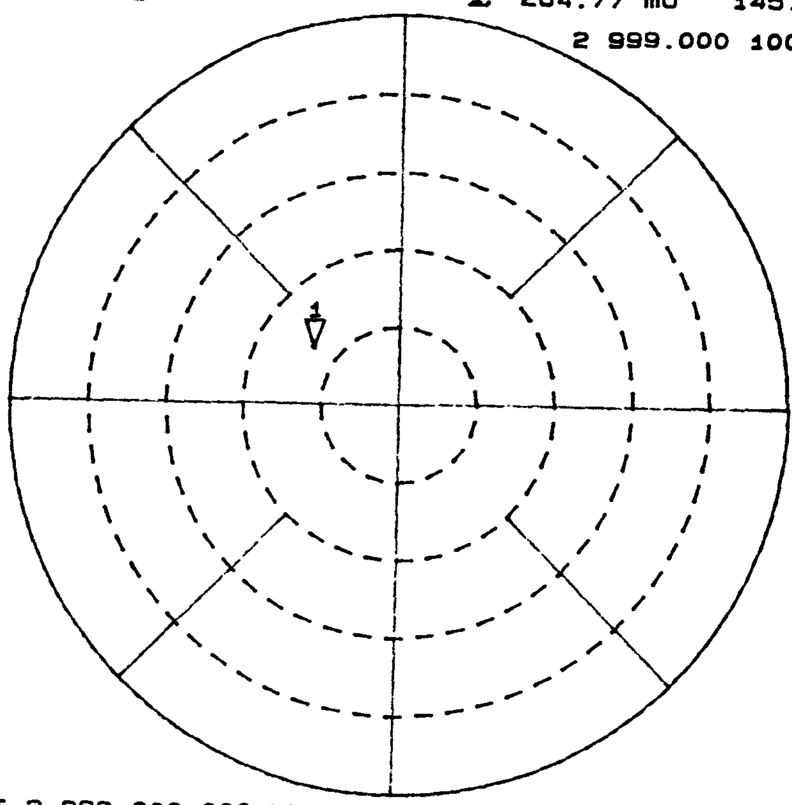

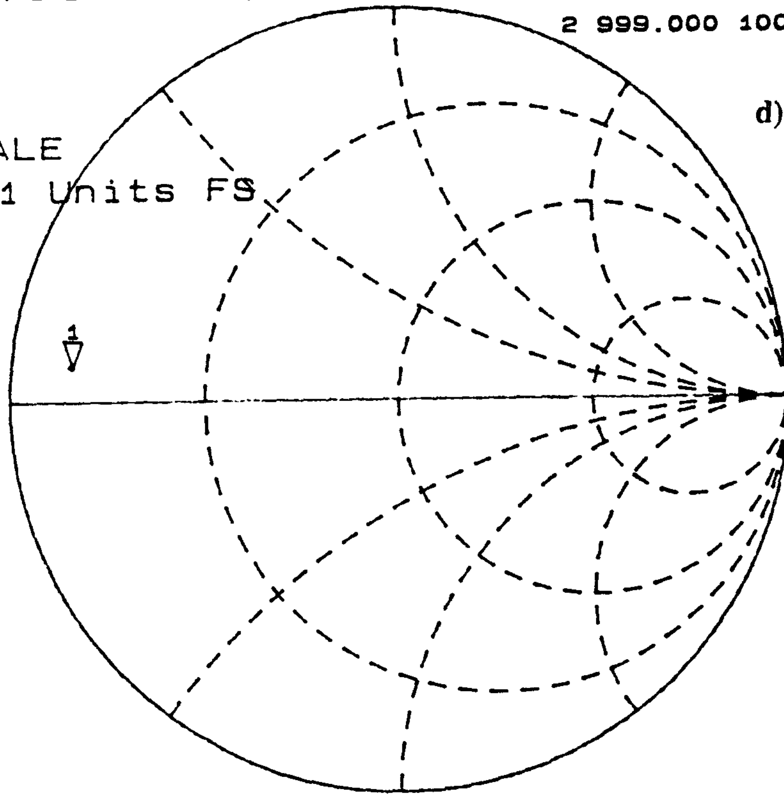

Figure 23 (Continuation)

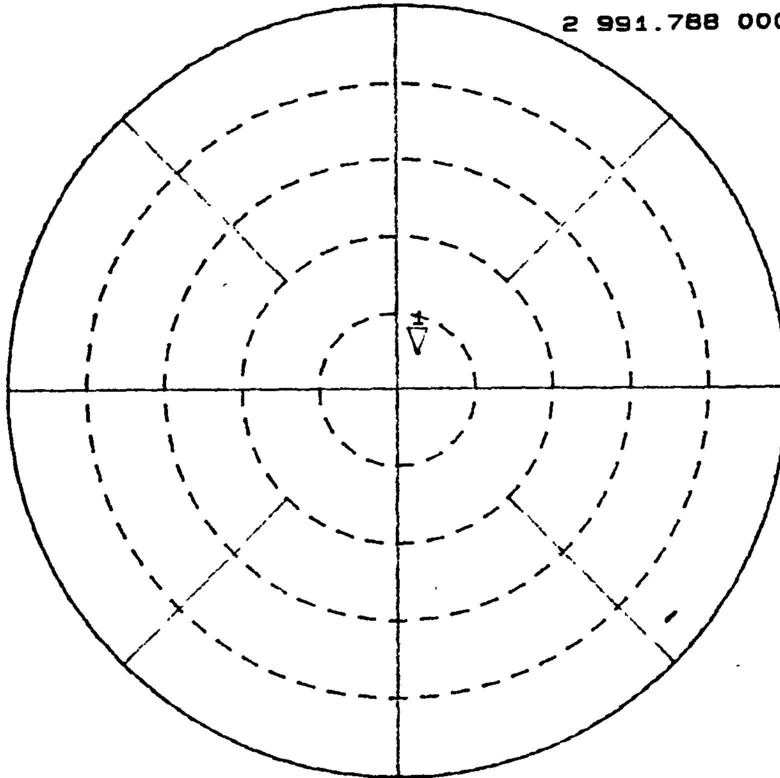

e) GaAs

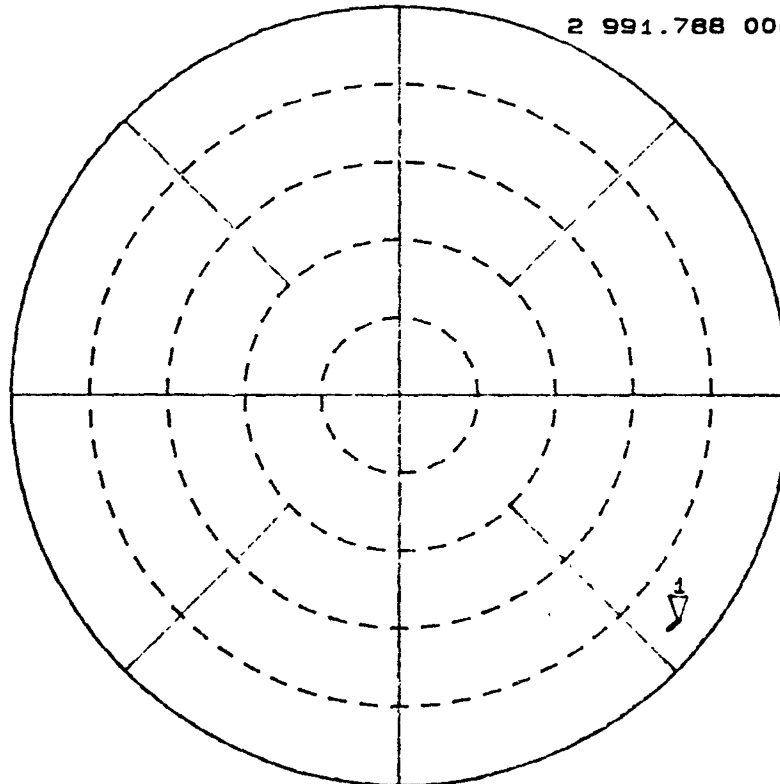

e) GaAs

Figure 23 (Continuation)

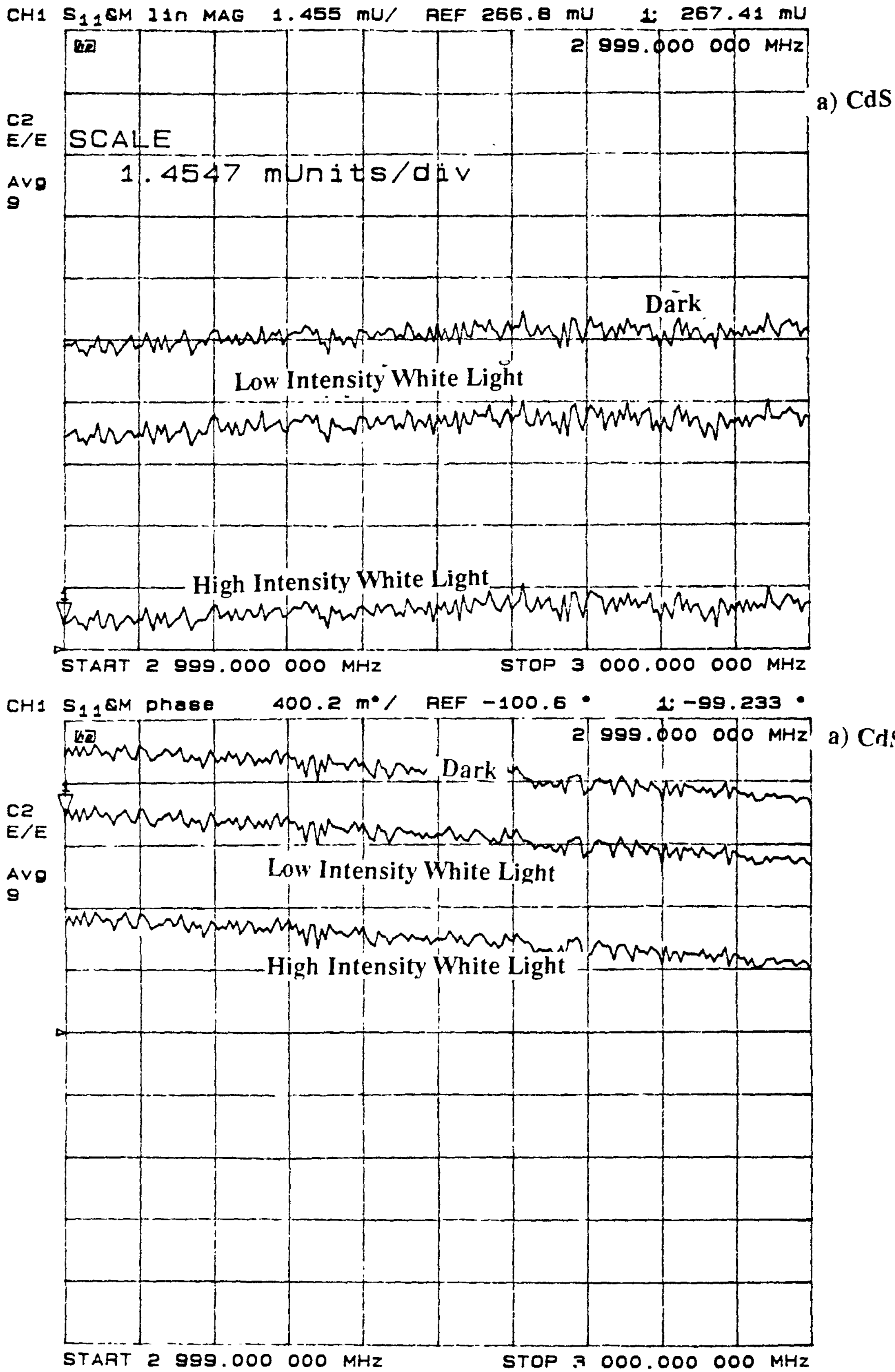

FIG. 24. Variation of the phase and linear magnitud of the S11(2.99-3 Ghz) parameter as the a)CdS and b)GaAs microstrips are illuminated

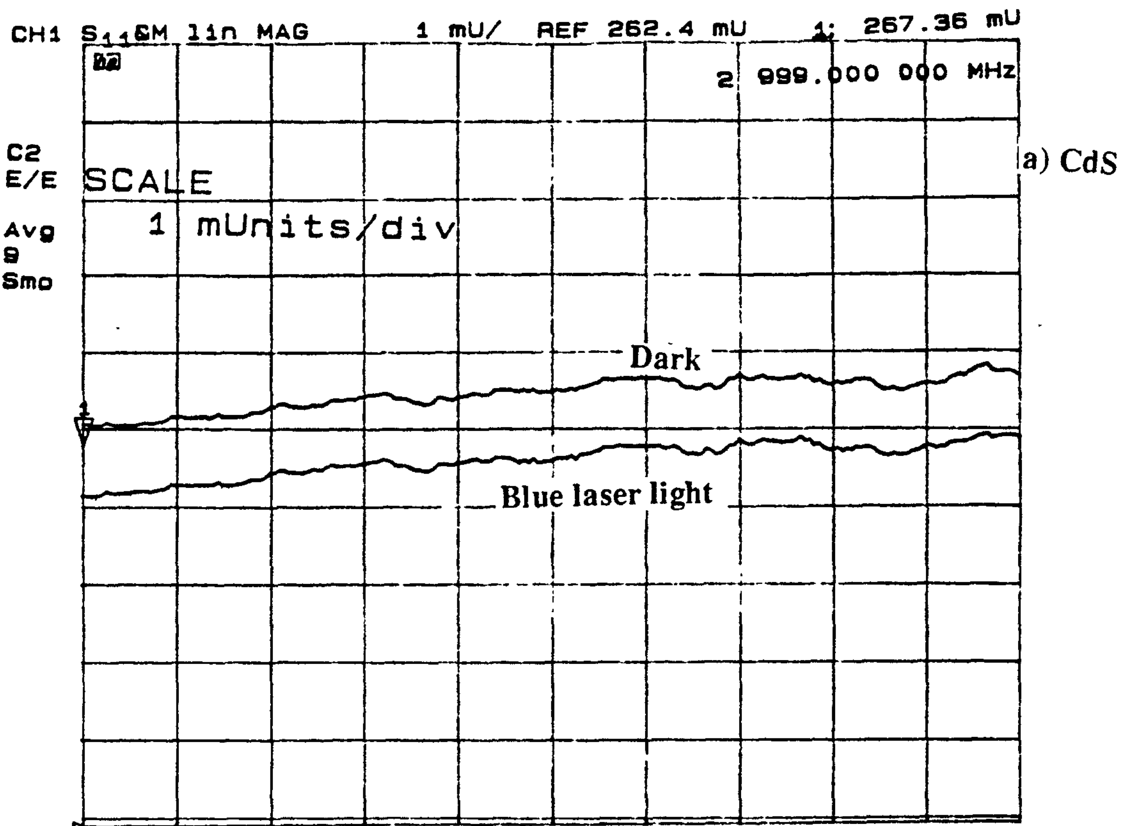

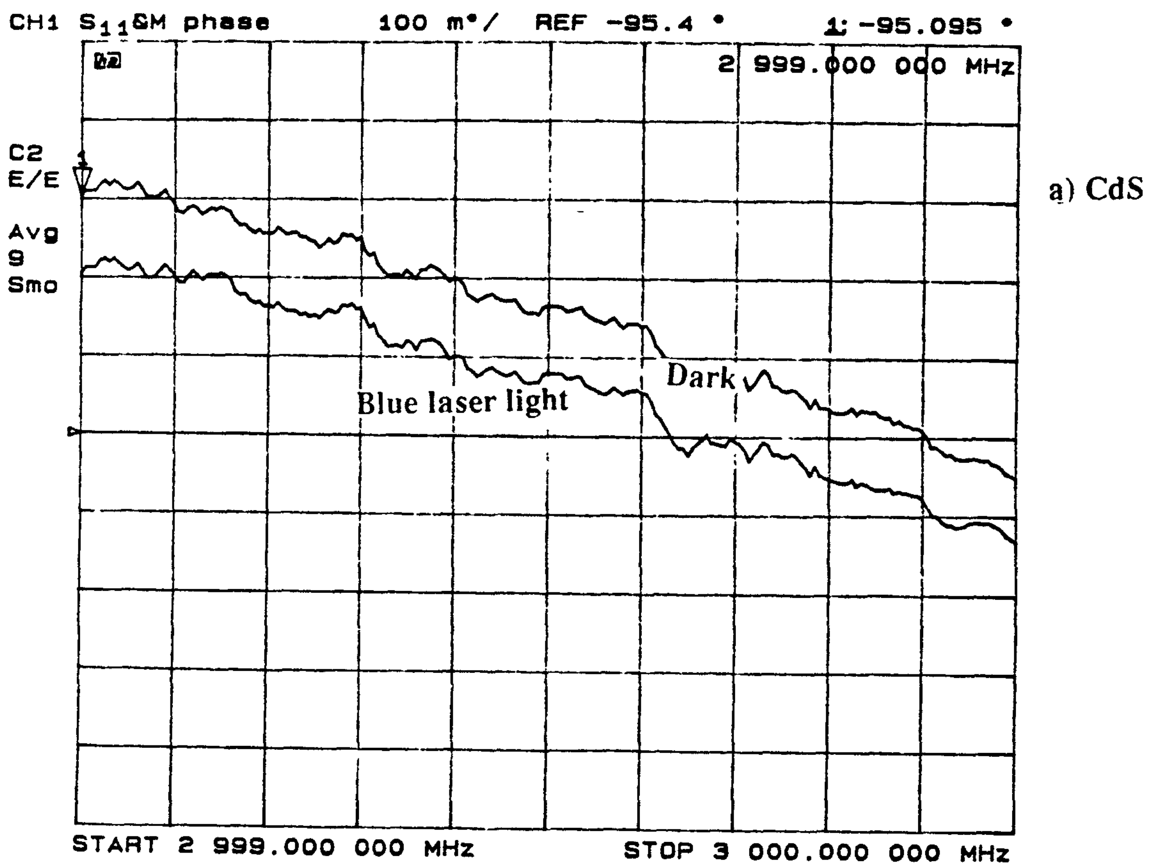

Figure 24 (Continuation)

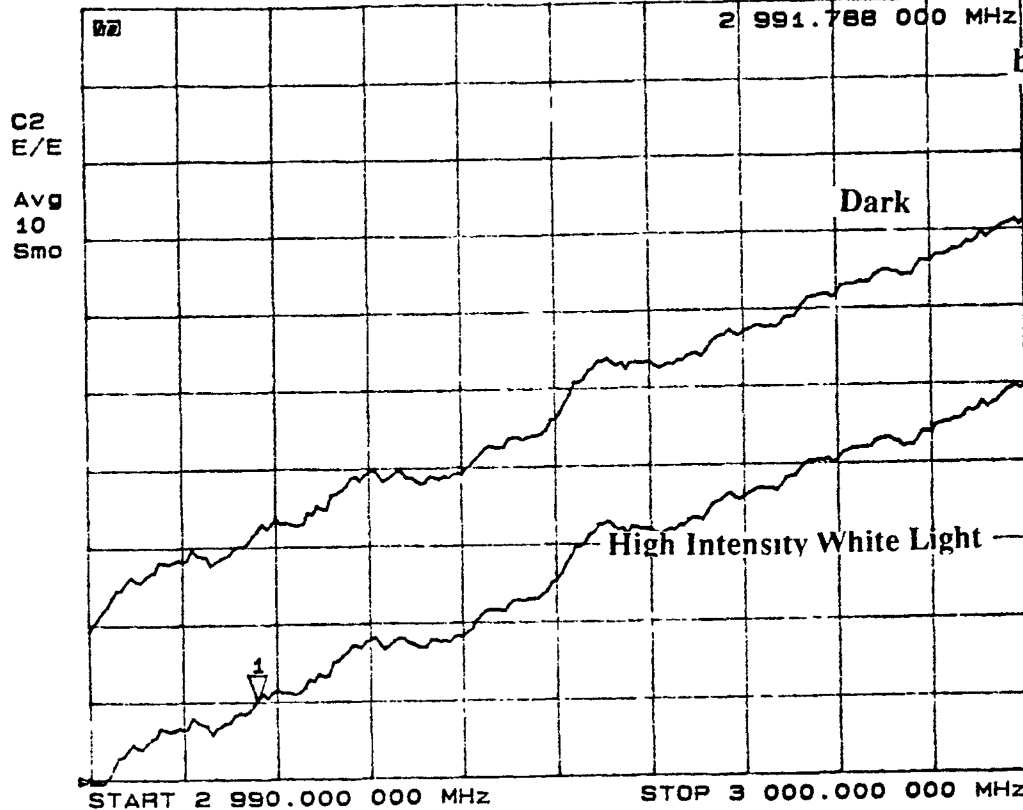

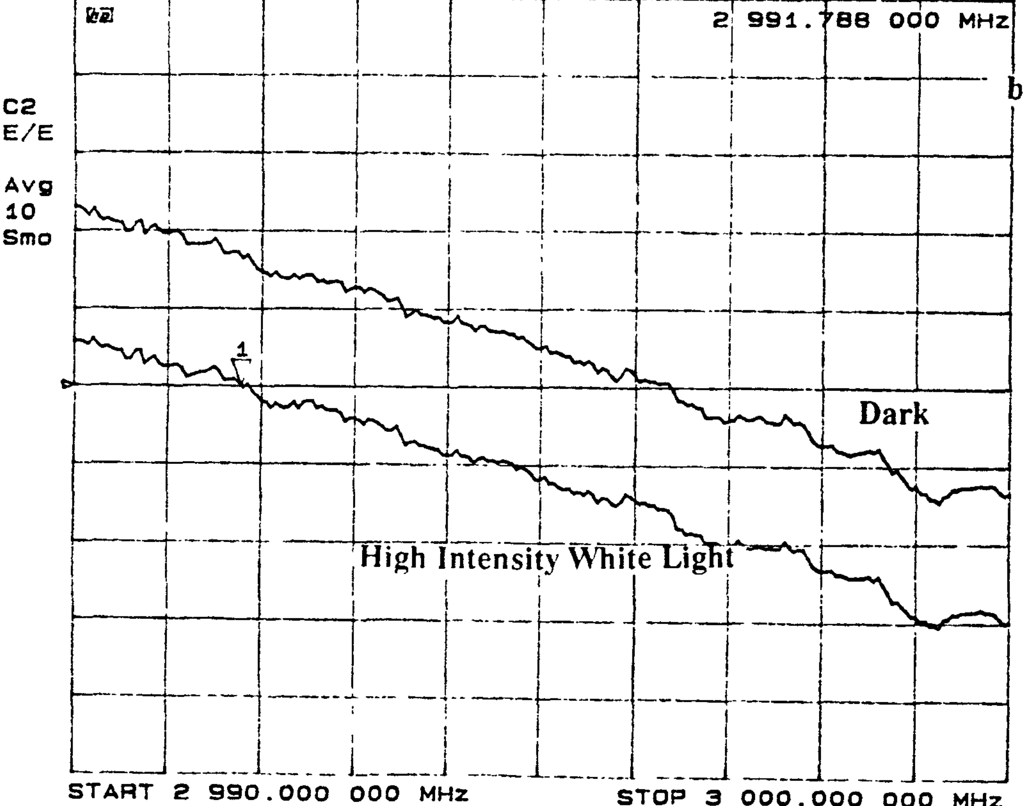

Figure 24 (Continuation)

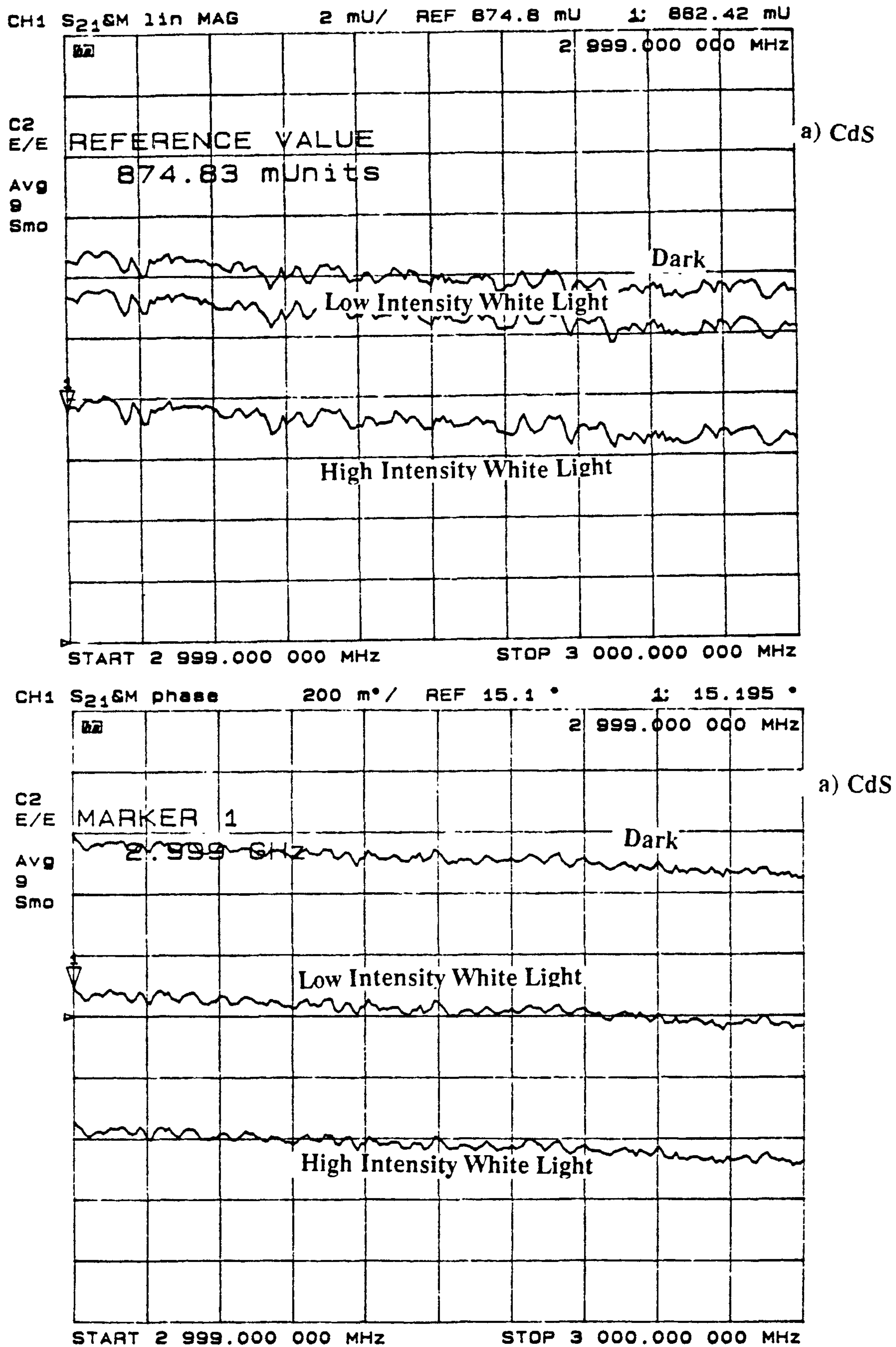

FIG. 25. Variation of the phase and linear magnitud of the S21(2.99-3 Ghz) parameter as the a)CdS and b)GaAs microstrips are illuminated

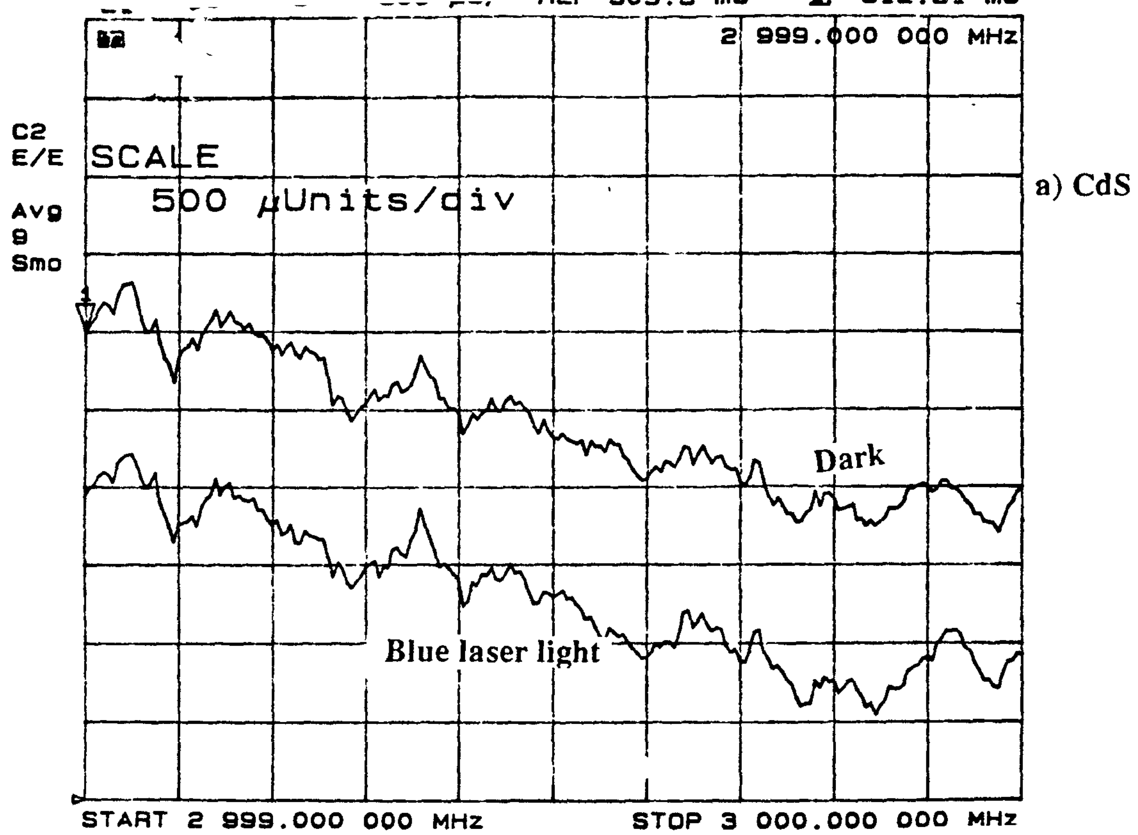

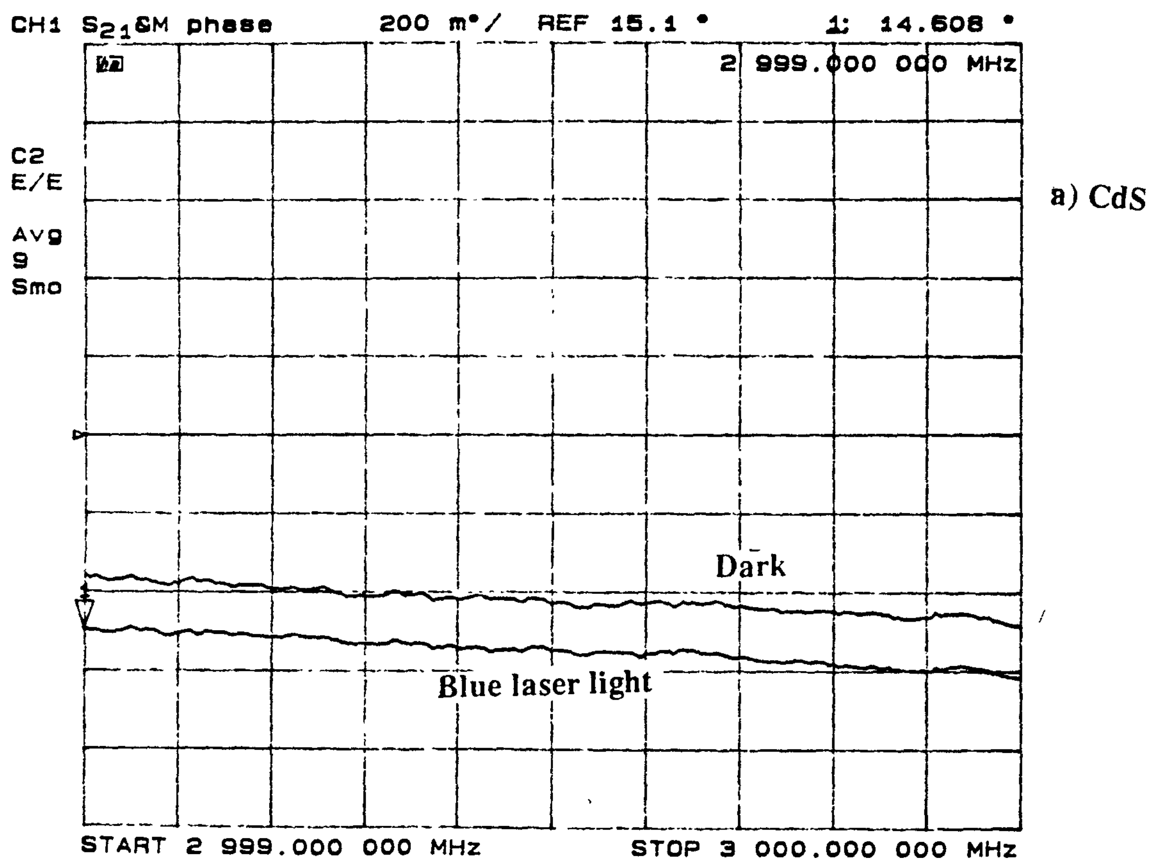

Figure 25 (Continuation)

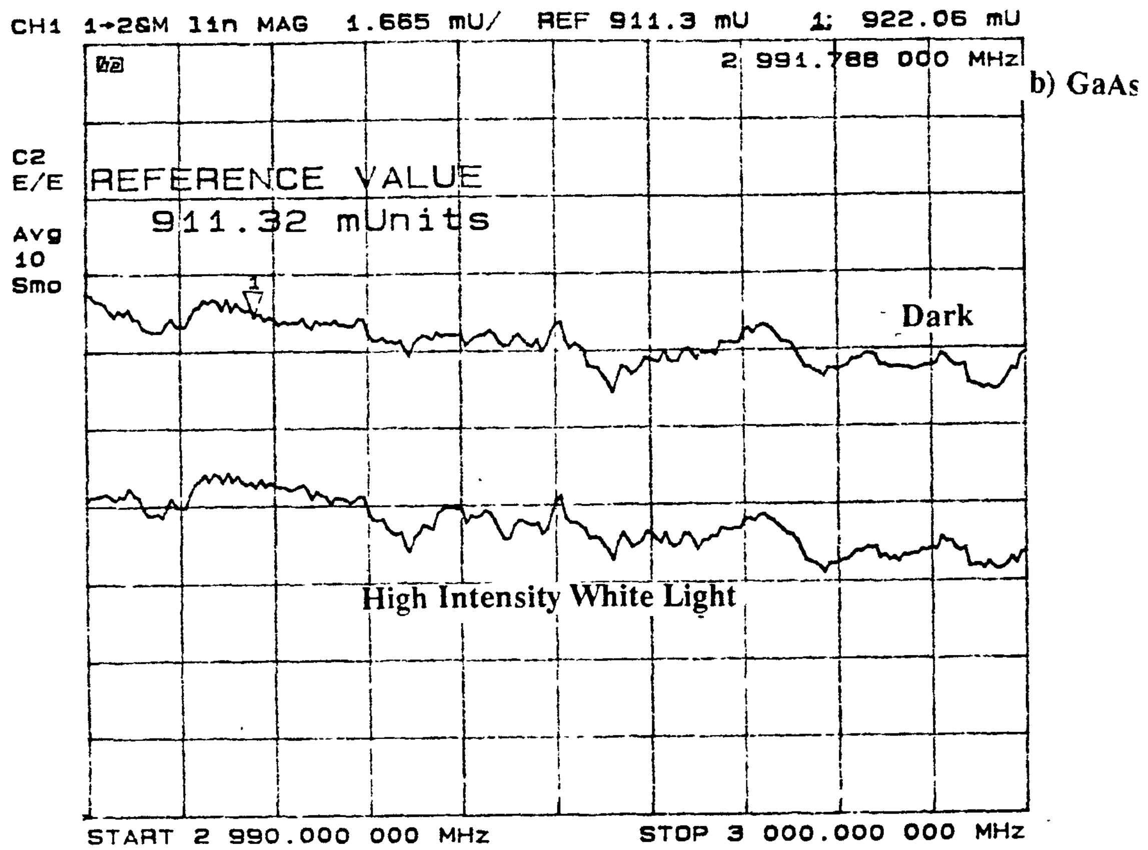

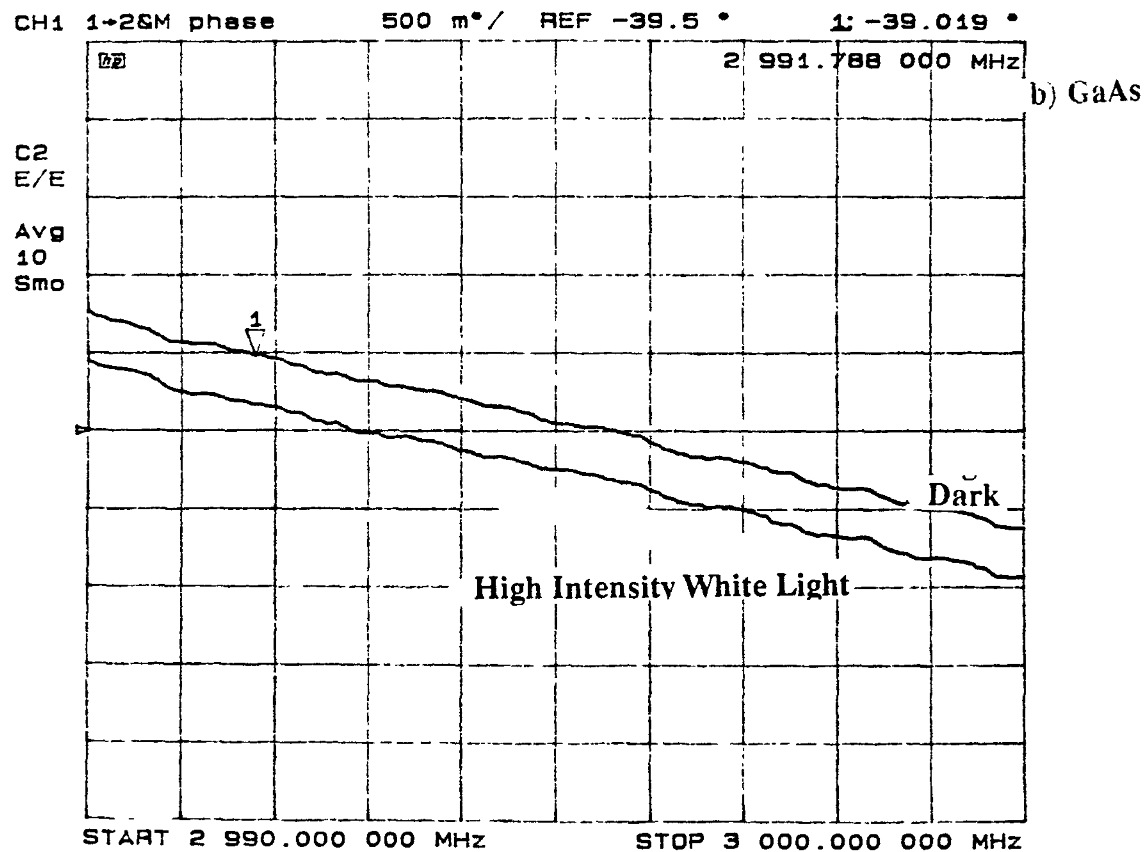

Figure 25 (Continuation)

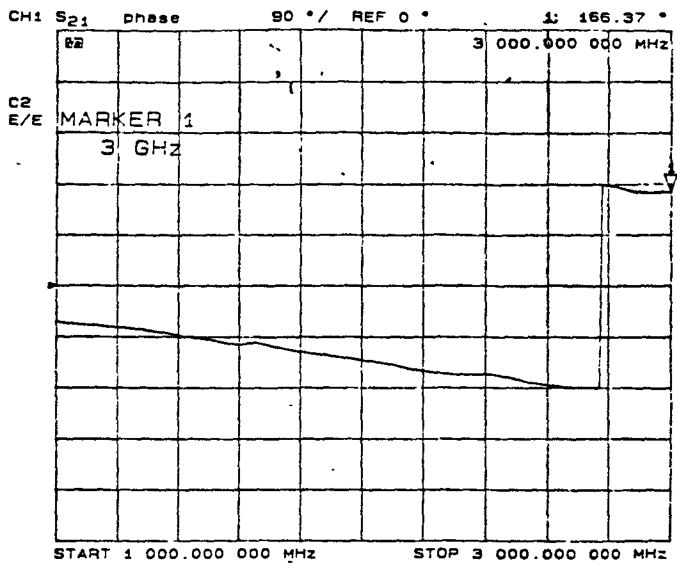

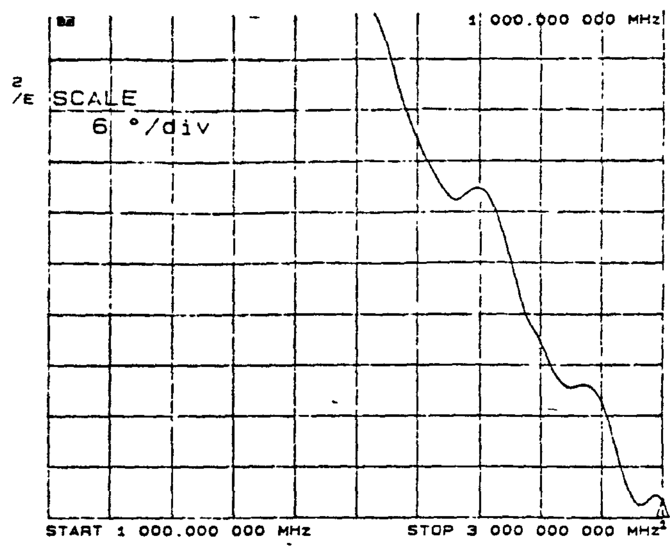

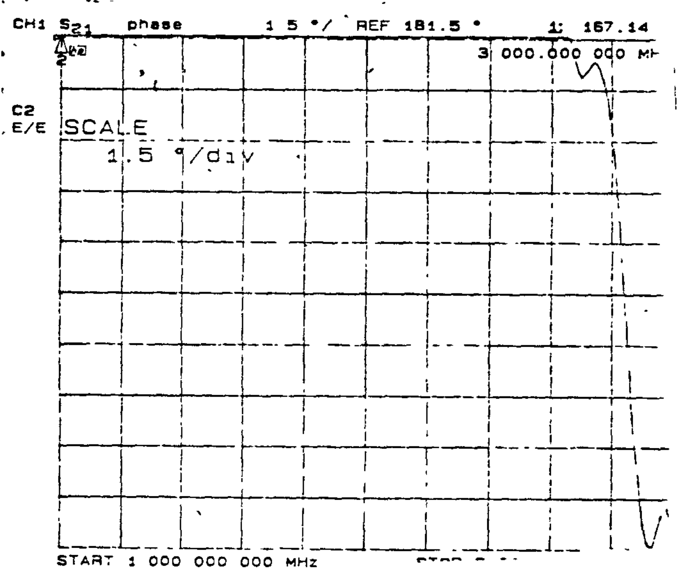

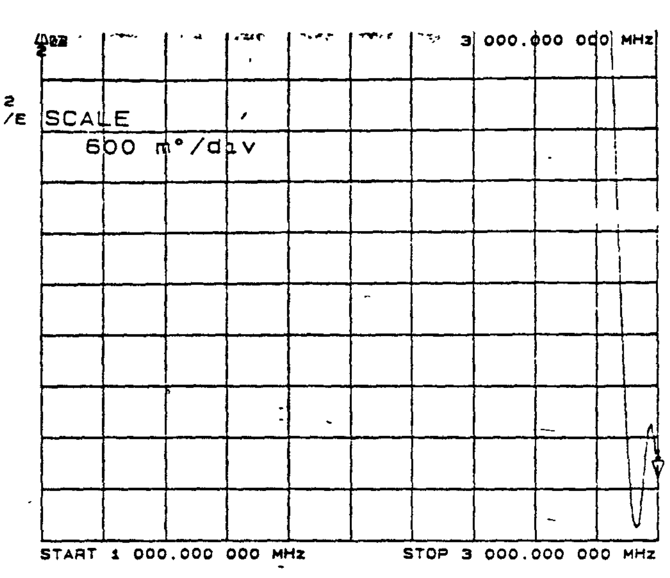

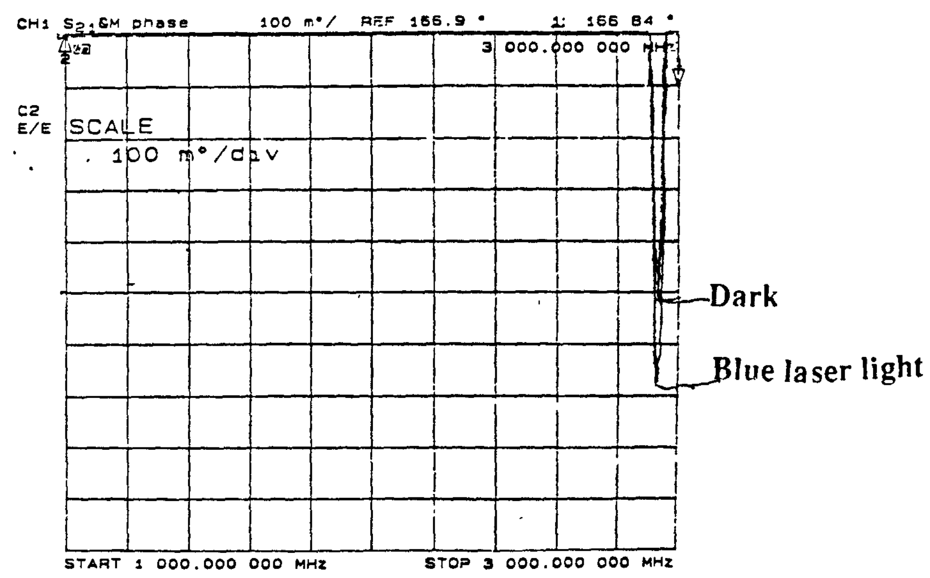

FIG. 26. Zooming of the the phase response to observe the sign of the variation in a long range sweeping

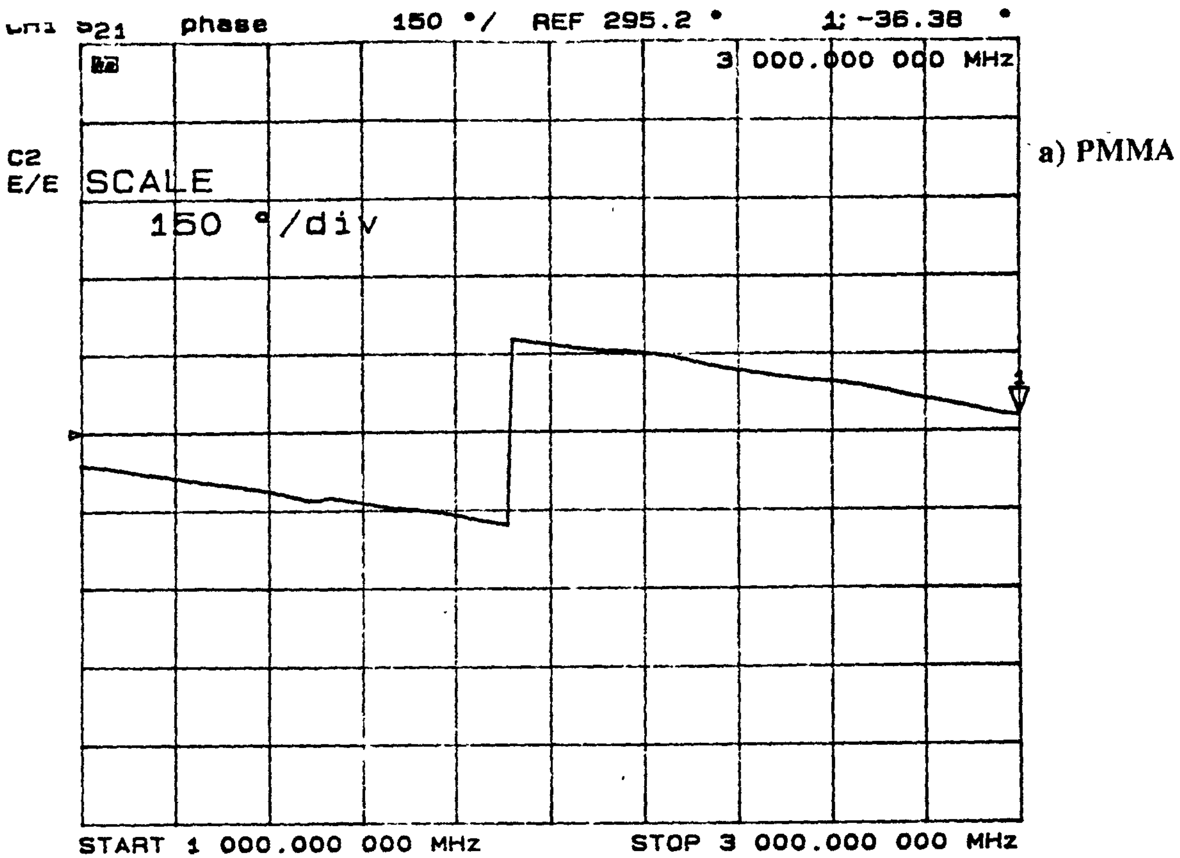

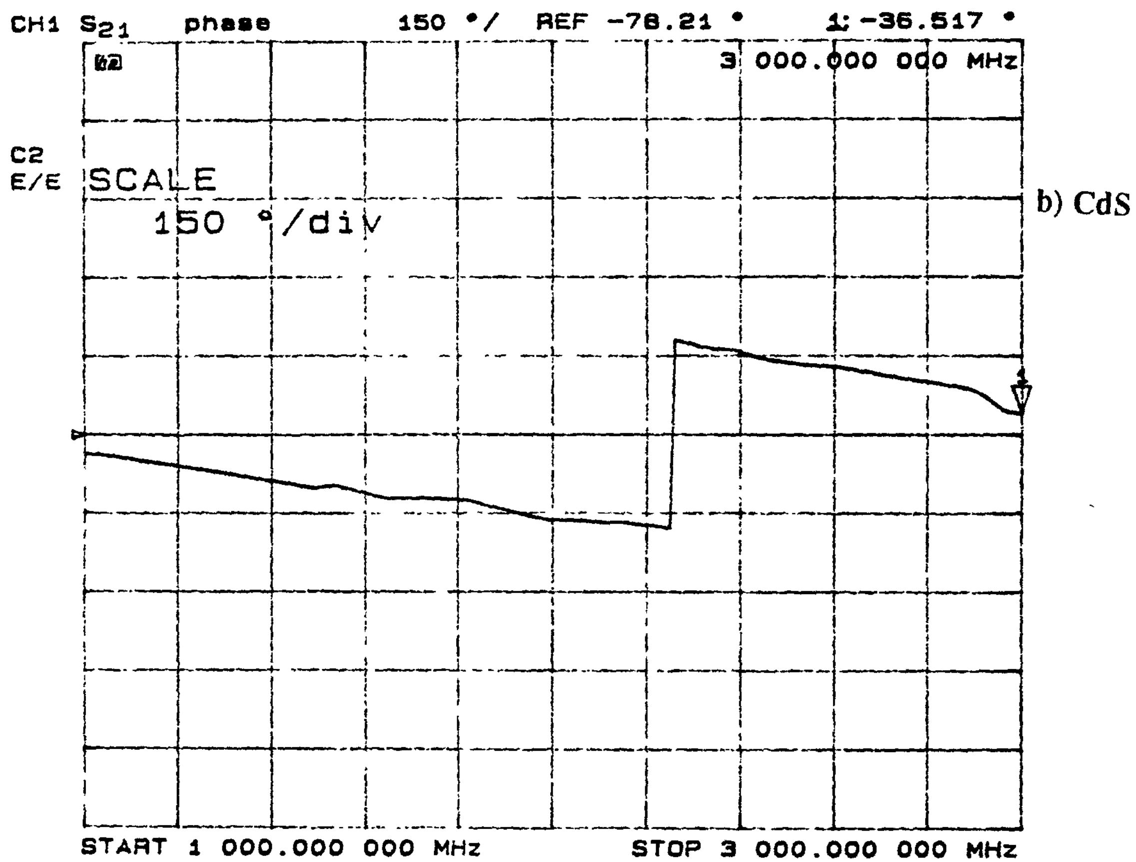

FIG. 27. Phase response over the sweeping between 1 and 3 Ghz.

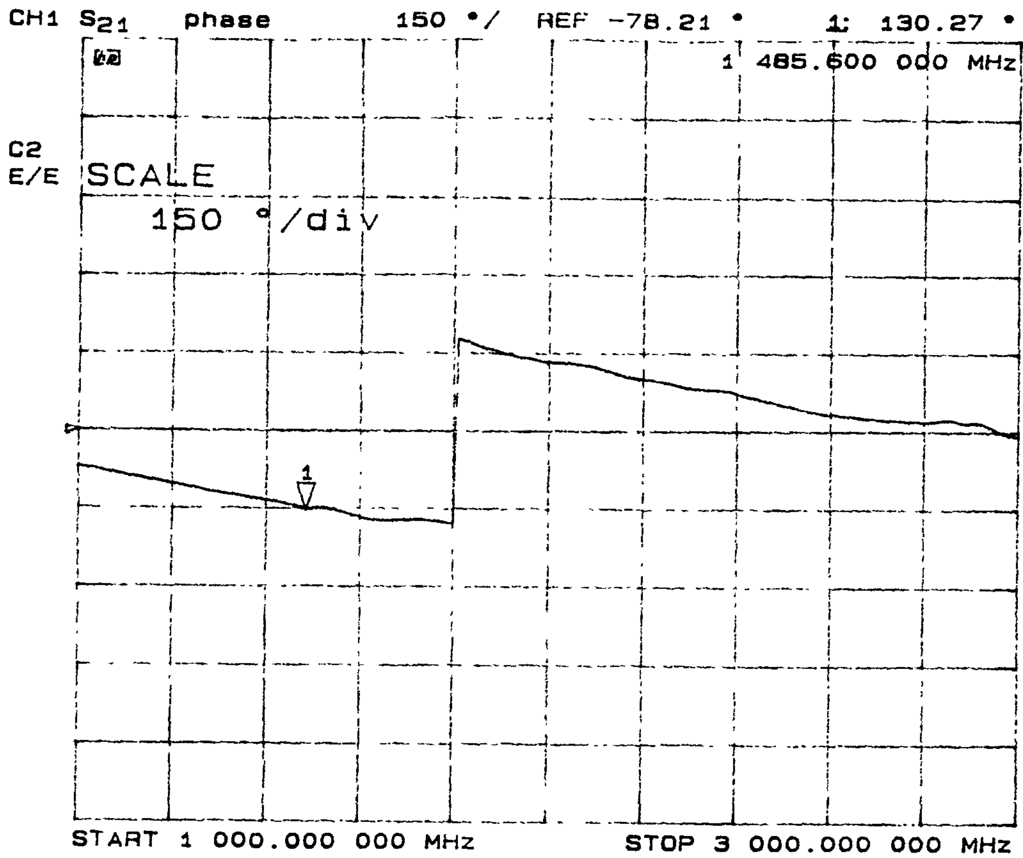

c) Si-I

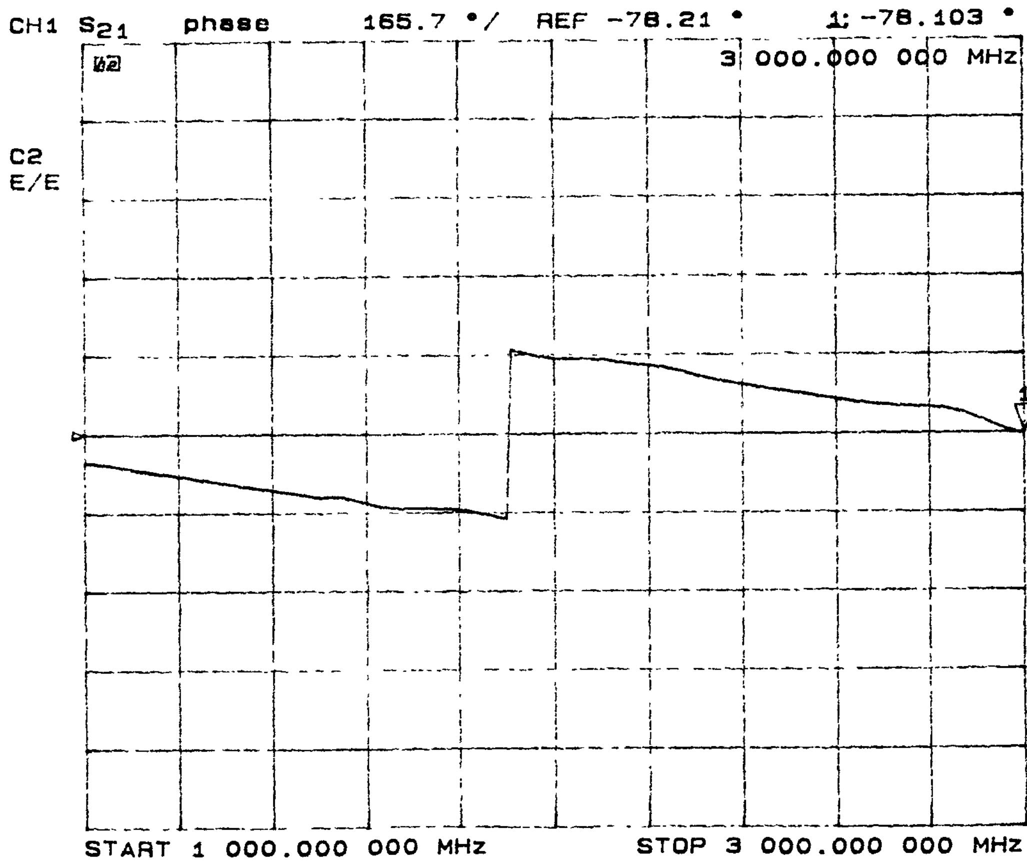

e) GaAs

Figure continuation

from 1 to 3 Ghz for all the samples. Figure 27 shows the zooming of the sweeping of the phase response from 1 to 3 GHz. Table 3 shows the absolute values of the S-Parameters for all the microstrip and Table 4 shows their variation from darkness to illumination.

TABLE 3: S-Parameters for all the microstrip, measured in the network analyzer at 3 Ghz in darkness.

	$S_{11(magn.)}$	$S_{11(phase)}$	$S_{21(magn.)}$	$S_{21(phase)}$
CdS	.267	-95.1°	.885	15.1°
GaAs	.106	60°	.911	-39.5°
Si,(I)	.066	-7.8°	.899	-53.8°
Si(II)	.264	145.52°	.832	110°
PMMA	.081	-109.94°	.899	-22.4°

TABLE 4: S-parameters variation from dark to the illumination condition, measured in the network analyzer, (all values are negative).

Variation of	$S_{11(mg.)}$	$S_{11(ph.)}$	$S_{21(mg.)}$	$S_{21(ph.)}$
CdS (blue l.)	.8 mu	.1°	.9	.15°
CdS (white l.)	6.54 mu	1.1°	5 mu	1°
GaAs(White l.)	2 mu.	0.9°	4.5 mu	0.7°
Si (White l.)	0	0	0	0
PMMA(White l.)	0	0	0	0

If we compare the absolute value of the S-Parameters obtained by the network analyzer shown in table 3 with the values expected from the design considerations in table 2., there are some discrepancies. The reasons for these differences are explained in Section 5.1

The values obtained for the S_{11} and S_{21} indicate that there will be standing waves in the line, with the maximum standing wave ratio for the CdS on the order of 1.7.

Nevertheless, the values obtained for the variation of the phase and linear magnitude of the s-parameters when light was applied indicate the phase and amplitude modulation index for the interferometer.

The table and the plots indicate the performance of all the microstrips. For CdS and GaAs changes of phase and magnitude for all the s-parameters were observed. For Si no permanent changes were observed. However, there was an instantaneous variation of the linear magnitude (about 0.1-0.2 milliunits) at the first sweeping of the network analyzer, and the value came back to its original position at the second sweeping, (sweeping speed of twenty milliseconds). This fast perturbation could be due to the warming of the copper strip from the radiation of light, since the same phenomenon was observed with the undoped microstrip substrate.

4.4 HOMODYNE DETECTION RESULTS (LOCK-IN MEASUREMENTS)

4.4.1 PHASE RESPONSE OF THE GaAs, Si AND CdS SAMPLES

The square law detection response as a function of phase for the Mach-Zehnder interferometer described in Figure 18 for the CdS and GaAs samples is shown in Fig. 28. The phase shifting device provides the variation in phase to locate the zeros and the maximum and minimum values of the detection. For the Si sample no signal was detected as expected from the measurements in the network analyzer. Looking to the response of the CdS and GaAs samples in Figure 25, we observe the repeatability of the detection over two periods. The maximum and minimum points and the crossings are well defined. Also shown are the phase and amplitude errors of the detection. The plots in Fig. 28 are similar to the DSBWC amplitude detection with amplitude and phase errors plus the deviation from a perfect sinusoidal signal and a shift of the extrema. The reason for all of this effects is the addition to the aplitud modulation of some

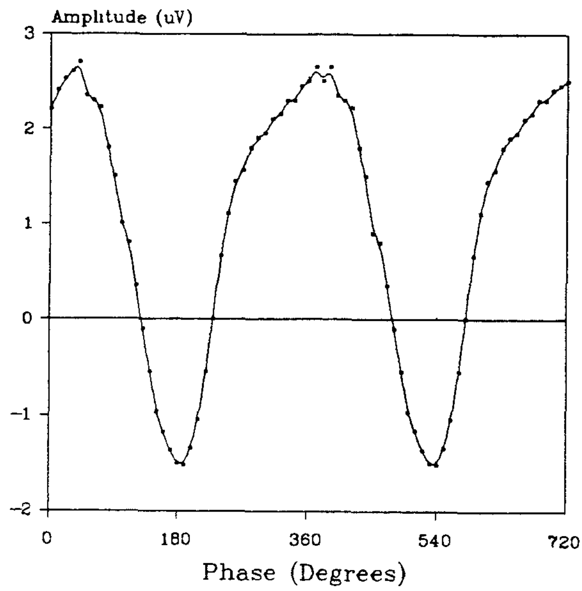

Figure

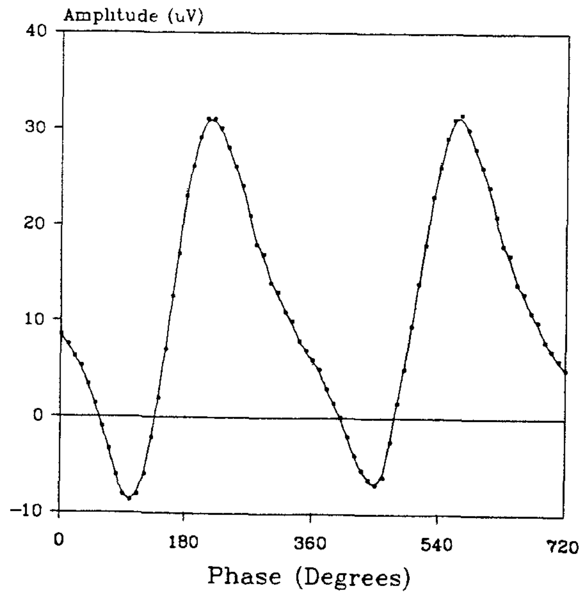

FIG. 28. Homodyne detection response function of the phase shifted in the Mach-Zehnder interferometer for CdS and GaAs

phase modulation as described in equations (2.VI.3.1) to (2.VI.3.7). The difference between the GaAs and CdS samples is also noticeable. While the CdS shows a wider positive amplitude, the GaAS shows narrower peaks. The amplitude error is defined in (2.VI.1.4.2) as the difference in absolute value between the maximum positive and negative detected amplitudes, and is a function of the ratio between the amplitude of the reference channel and the amplitude in the information channel [4.6]. The amplitude error could be calculated by the normalized subtraction of the negative amplitude from the positive amplitude. The results obtained for CdS and GaAs are:

Amp. error for CdS: (2.75 - 1.6) [nV]/ (2.75 + 1.6) [nV] = 0.265

Amp. error for GaAs: (32 - 8.5) [nV]/ (32 + 8.5) [nV] = 0.58

On the other hand, the detection phase error is defined as the phase difference between the zero crossing point in a detection curve with equal positive and negative amplitudes and the actual zero crossing. This error is proportional to the inverse of the sine of the ratio between the amplitudes of the reference and the information channels.

Phase error for CdS: $\phi(2.75 - 1.6/2) - \phi(0) = 30°$

Phase error for GaAs: $\phi(32 - 8.5) - \phi(0) = 60°$

4.4.2 DETECTION WITH PARTIAL SUPPRESSION OF THE CARRIER IN THE INFORMATION CHANNEL

If the carrier in the information channel is attenuated by 10 dBs as in Figure 29, the effects are obvious. Since the phase and amplitude errors are function of the ratio between the amplitude of the carriers of the information channel over the reference channel, the attenuation of the information channel carrier will reduce the ratio and therefore the errors. As illustrated from the data obtained for CdS and GaAs, the GaAs sample in particular shows close to no error in phase and in amplitude, with crossings at 90 degrees and close positive and negative amplitudes. For the CdS the error was improved but still shows a appreciable error, which could be corrected by increasing the attenuation in the information channel. Also, in those two plots it can be seen that the amplitude obtained for the

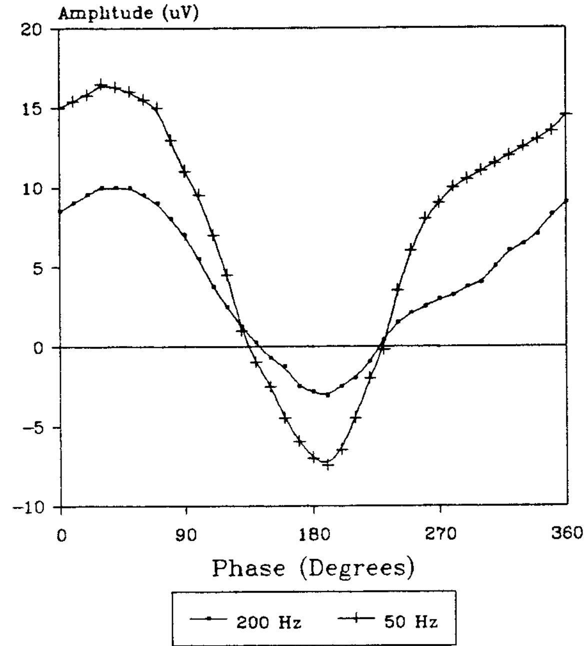

Figure

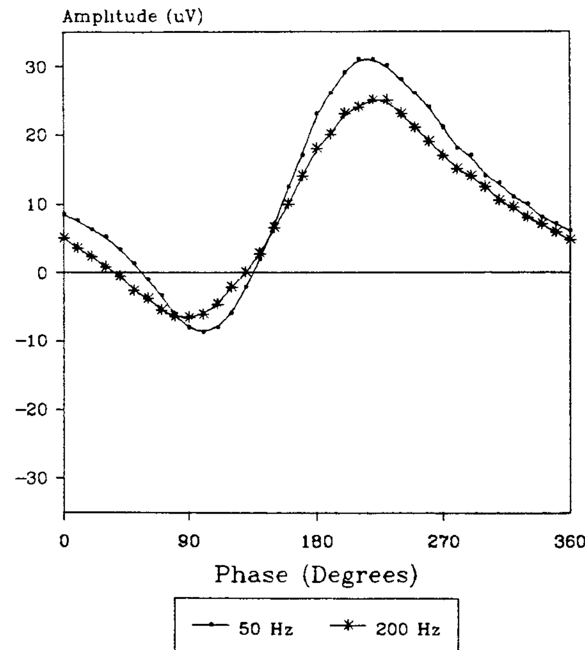

FIG. 29. Detection with partial supppression of the carrier in the information channel

GaAs is close to twice the amplitude obtained for the CdS (for the same variables in the system) . Observe also that the signal decreased proportionally more in the GaAs than in the CdS when the attenuation was applied.

4.4.3 RESPONSE FOR THE DIFFERENT LIGHT SOURCES

A blue light laser was also used in the system for the CdS substrate. The results are shown in Figure 30 and compared with the results for the white light source. The figures show similar position crossings and maxima and minima. This means that the amplitude and phase errors are a function of the ratio between the carriers of the two branches in the interferometer, since the errors also improve linearly for the two sources as the information channel is attenuated. The difference between the two plots is the difference in amplitude obtained, since the plot for the white source has a much bigger amplitude than the plot for the blue light laser. This confirms the results obtained in the network analyzer where the white light produced considerably bigger changes in phase and amplitude of the S-Parameters. At the moment of the experiment, no lasers were available in the absorption spectrum of the GaAs, therefore no comparison could be made with the data obtained with the white source.

4.4.4 GaAs AND Si SAMPLES MODULATING FREQUENCY RESPONSE

The plots obtained for the modulating frequency response of the CdS and GaAs substrates are shown in Figure 31. Also shown are the response of the system to a modulating frequency of 50 Hz and 200 Hz for CdS and GaAs in Figure 32.

The frequency response of the system was controlled for the generation and recombination time of the semiconductor used. After the electron-holes were created by the optical excitation, if the light is turned off during half of the cycle of the modulating frequency ($T/2 = \pi/wm$), the semiconductor will try to restore the equilibrium of the carriers by non radiative recombination. Since GaAs and CdS are direct bandgap semiconductors, when excess carriers are introduced by the radiation, the electrons and holes will recombine directly since no additional crystal momentum is required or the transition across the bangap. The response time , extracted from [4.8], for the detection of light in GaAs and CdS detectors gives a response time for CdS of 0.53 seconds, and for GaAs of less than 10^{-6} seconds. These numbers are just for those particular samples.

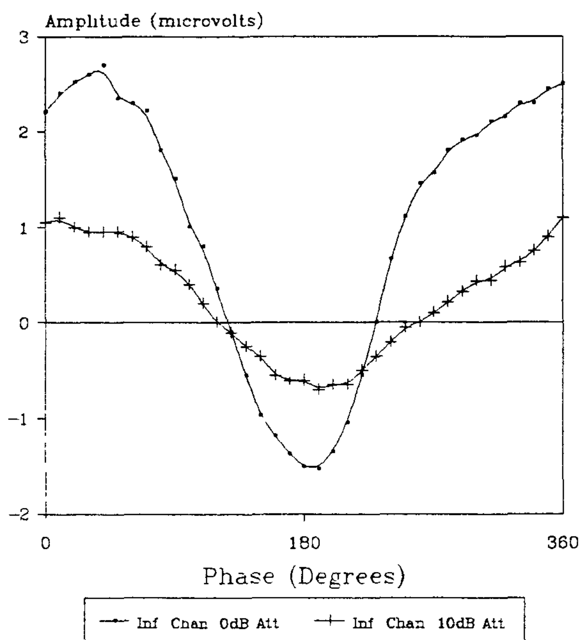

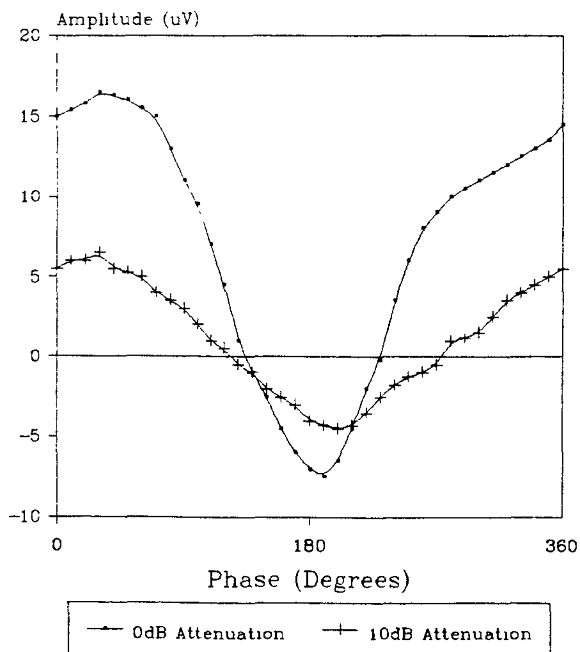

FIG. 30. Diference in detection for the white light source and for the blue light laser in the CdS sample

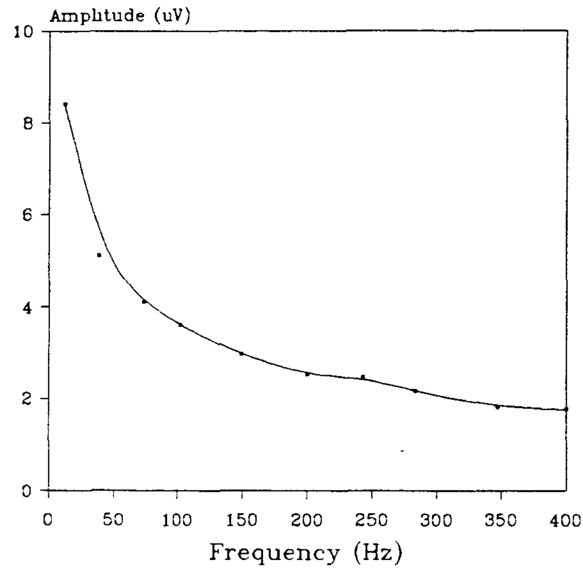

Figure

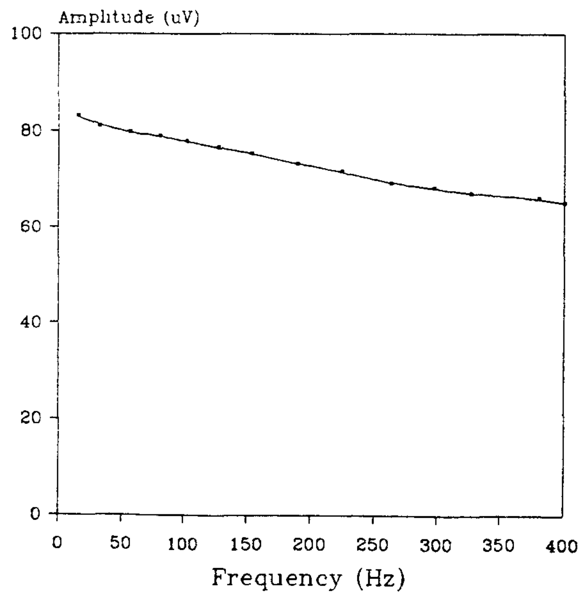

FIG. 31. Frequency response for the CdS and GaAs samples

Square Law Detection (White Light)
Frequency Comparison (CdS)

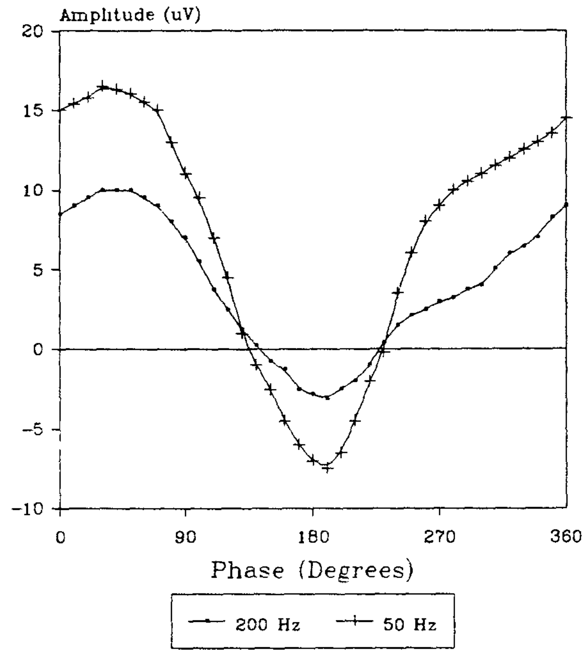

Square Law Detection, Function of Phase
Frequency Comparison (White Light)(GaAs)

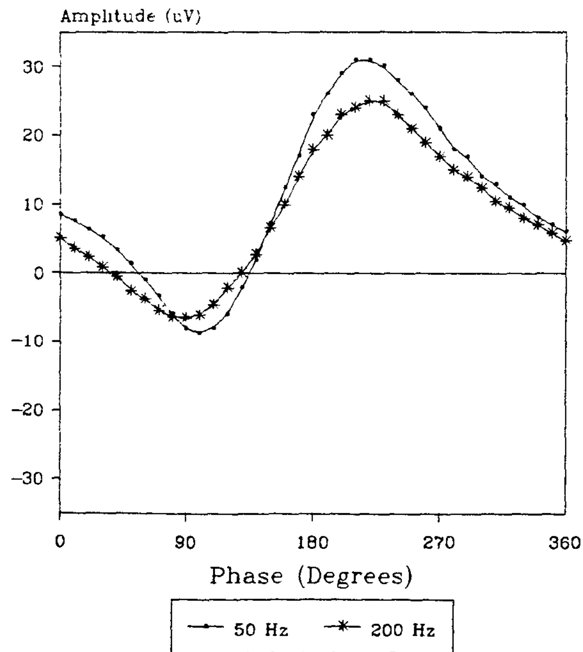

FIG. 32. Difference in detection for 50 and 200 Hz

However, the life time of the carriers is strogly sample dependent (by orders of magnitud). Nevertheless, Figure 35 indicates that the lifetime of the CdS carriers are much longer than the lifetime of the GaAs carriers as seen by the fast decreasing response for CdS and the slower slope in the curve of frequency response for the GaAs.

Curves in Figure 32 shows also the attenuation of the detection for increasing frequencies. However the position of the crossings and the maximum and minimum values don't change, only a decrease in the amplitude is observed. The small difference in the crossing is believed to be due to a small difference maximizing the signal in the lock-in amplifier. Also noticed is that the signal detected had less noise the higher modulating frequency since noise spectrum from the detector has a sizeable 1/f component [4.10]

4.4.5 RESPONSE OF THE DETECTION FUNCTION OF THE AMPLITUDE OF THE REFERENCE CHANNEL.

The response of the homodyne detection system is proportional to the amplitude of the reference signal up to a point. Beyond that point, the gain achieved by increasing the amplitude of the reference channel A ceases [4.11], and the detection is in the linear region. The results obtained from increasing the attenuation in the reference channel are shown in Figure 33. The information channel power was held constant at 0 db attenuation, while the reference channel signal was attenuated from zero to 50 dBs. The phase in the phase shifter and the detection angle in the lock-in were were both maximized to give the highest output.

4.4.6 DETECTION AT DIFFERENT CARRIER FREQUENCIES

The detection function of the carrier frequencies of 10 Ghz and 10.2 GHz is shown in Figure 34. Observing the curve, one sees a shift in the phase front of about 60 degrees. This is due to the change in the length of the wavelength, what will produce that the interference occurs at a different phase front.

Square Law Detection (Blue Laser)(CdS)
Reference Channel Attenuation Response

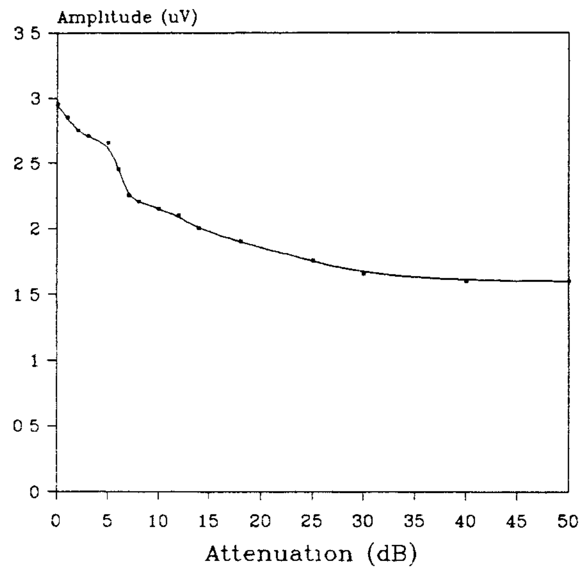

Figure

Square Law Detection (White Light)(GaAs)
Reference Channel Attenuation Response

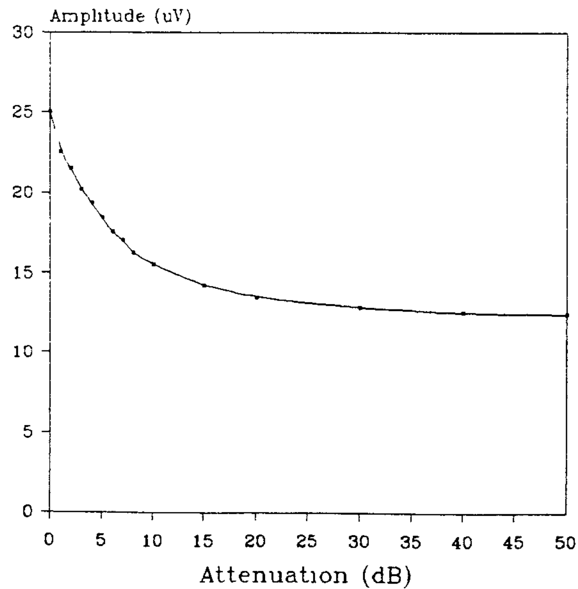

FIG. 33. Response of the system to attenuation in the reference channel

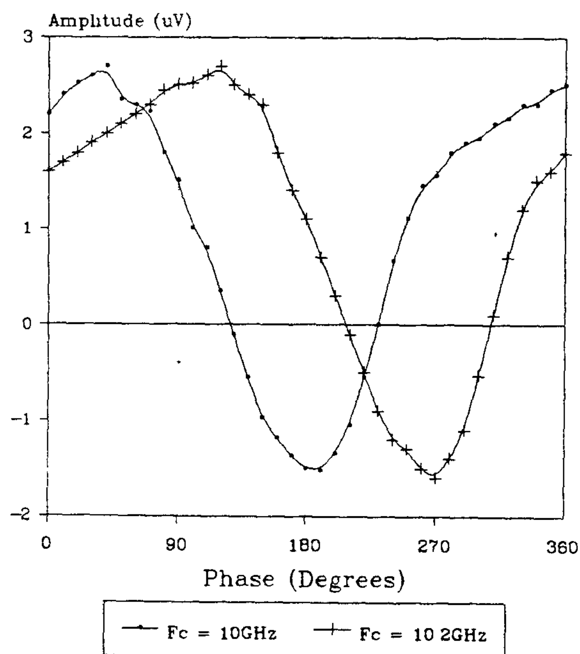

FIG. 34. Difference in the response for 10 a ıd 10.2 Ghz carrier fequencies.

4.4.7 MICHELSON INTERFEROMETER DETECTION

4.4.7.1 PHASE MEASUREMENTS WITH THE LOCK-IN AMPLIFIER

The plots illustrating the difference between Michelson and Mach-Zehnder detection are illustrated in Figure 35 for GaAs over two periods. We can observe the difference in the number of crossings for both systems

Figure 36 shows the response for the Michelson and Mach-Zehnder detection for the CdS sample as well as the variation in detection as the information channel was attenuated.

Figure 37 shows the frequency response for the CdS sample in the Mach-Zehnder interferometer under the blue light and in the Michelson under the white light. One can observe the similar decay curve. Figure 38 shows the frequency response of the GaAs sample and the difference in detection at 50 and 200 Hz.

The main advantage of the Michelson system over the Mach-Zehnder is that the reference signal A passes twice over the phase shifter. Then, when trying to find the maximum signal by adjusting the phase angle ($\cos 2\phi = \pm 1$) or the crossing ($\cos 2\phi = 0$), the values of 2ϕ will be :

for the crossings $2\phi = \pm(2n+1)\pi/2$
for the maximum $2\phi = \pm\ 2n\ \pi/2$

On the other hand, for the Mach-Zender those values were reached for ϕ. Thus, the change in the phase shifter setting in the Michelson is the same as the change of phase of the field. In contrast for the Mach-Zehnder the change in the phase shifted was half the phase of the field, and the phase shifter must have a range which is twice as large to measure the same variation in the phase of the field [4.11].

For the Michelson interferometer system, the phase shifter must have a minimum of 90° of differential phase shift to locate at least one zero or one maximum over the adjustable range of the phase of the shifter.

Square Law Detection, Function of Phase
Homodyne Detection (White Light) (GaAs)

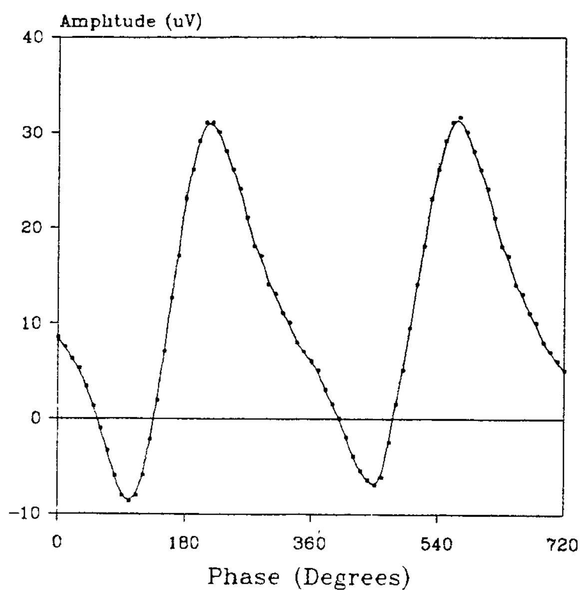

Figure

Square Law Detection (White Light)
Michelson Interferometer (GaAs)

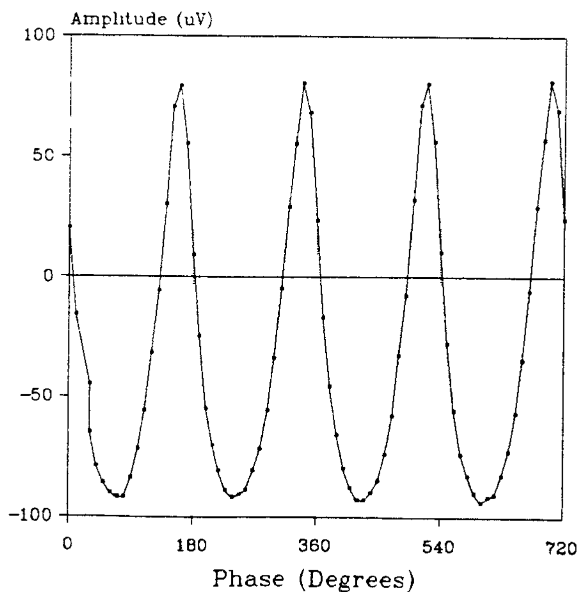

FIG. 35. Difference in the response for the Michelson and Mach-Zenhder homodyne detection systems

Square Law Detection (White Light)
Michelson Interferometer (CdS)

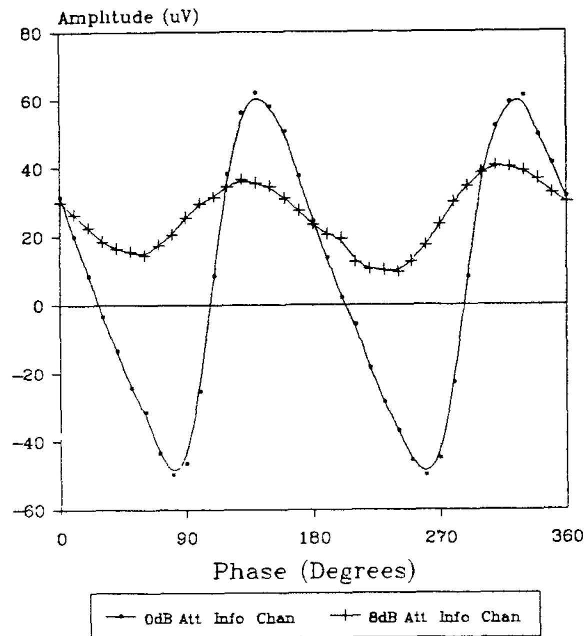

Figure

Square Law Detection (White Light)(CdS)
Information Channel Attenuation Response

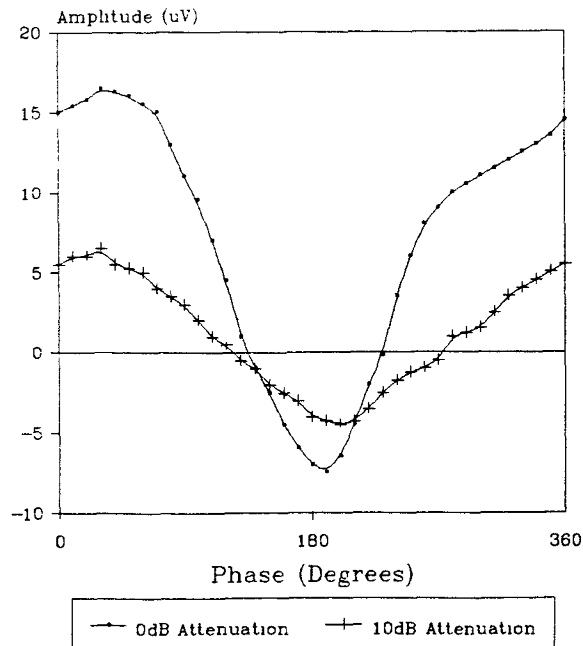

FIG. 36. Response of the Michelson homodyne detection for CdS and GaAs as a function of the attenuation of the information channel

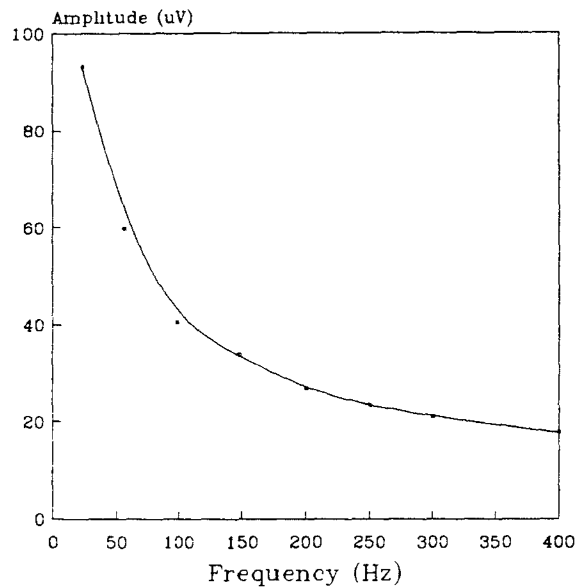

Figure

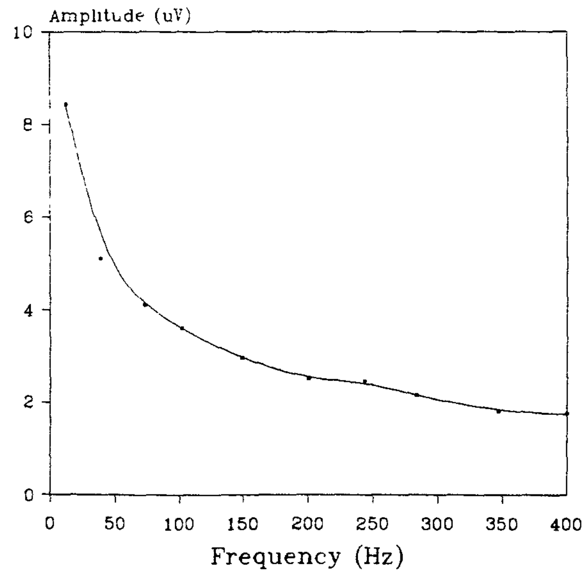

FIG. 37. Difference between the frequency response of the Michelson and Mach-Zehnder interferometers for the CdS sample

Square Law Detection, Function of Phase
Frequency Comparison (White Light)(GaAs)

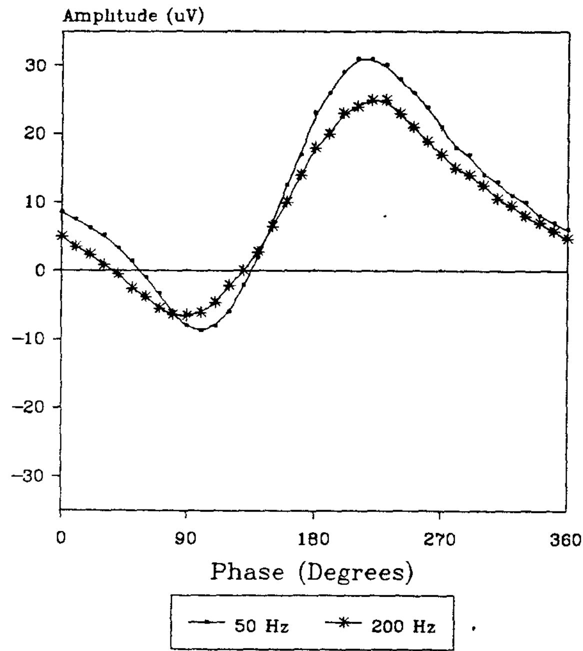

Frequency Response
Michelson Interferometer (GaAs)

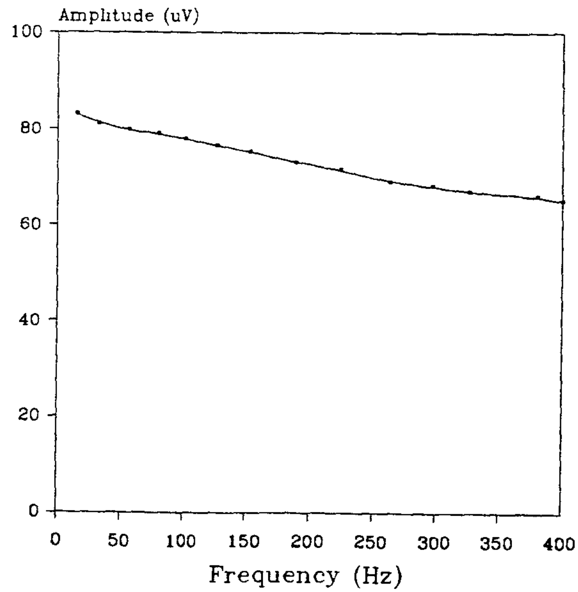

FIG. 38. Frequency response of the GaAs sample in the Michelson interferometer, and variation of the amplitude detection for 50 and 200 Hz

4.4.7.2 PHASE MEASUREMENTS IN THE POWER METER

Figure 39 shows the power detected by the power meter for the GaAs and CdS samples as a function of phase shifted, in comparison with the data obtained in the lock-in amplifier. The readings in the power meter and in the lock-in were done at the same time and at the same position of the phase shifter.

The mixer featured power splitting as shown in figures 16, 18 and 19 where power could be detected before the square law detection. The power attenuation between the input to the output power of the mixer was 9 Dbs, hence the low levels of powers obtained in comparison with the power in the generator.

Another experiment was performed by taking the reading in the power meter under illumination of the sample and then blocking the light and observe the difference in the readings. The readings were performed throught the range of the phase shifter. The results are shown in Figure 40. One can observe the matching in the crossings and in the maxima of the curve with the lock-in amplifier detection curve.

Power Detection (White Light)
Michelson Interferometer (CdS)

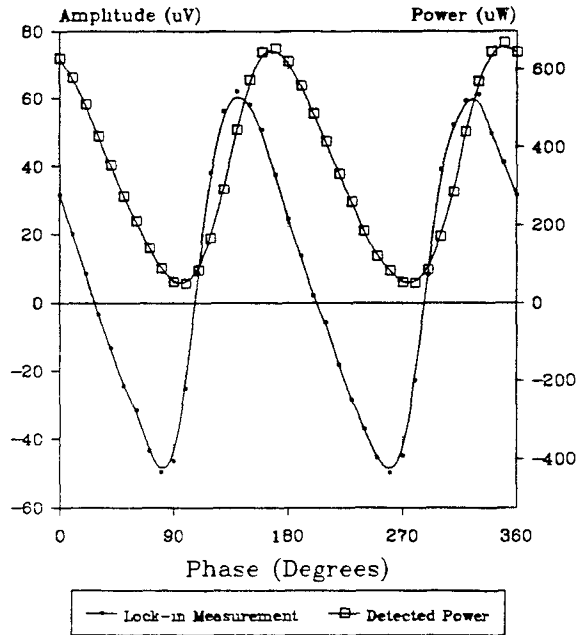

Figure

Michelson Detection
GaAs, Lock-in - Power

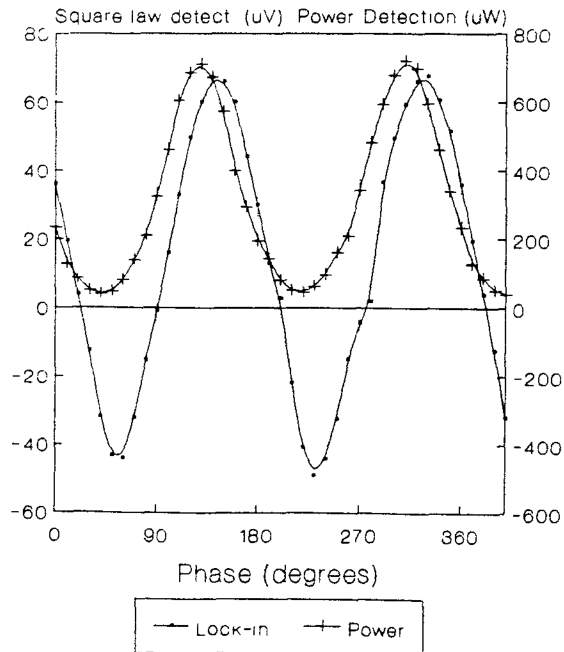

FIG. 39. Phase measurements in the power meter for the CdS and GaAs samples

Michelson Detection
GaAs, Lock-in - Differential Power

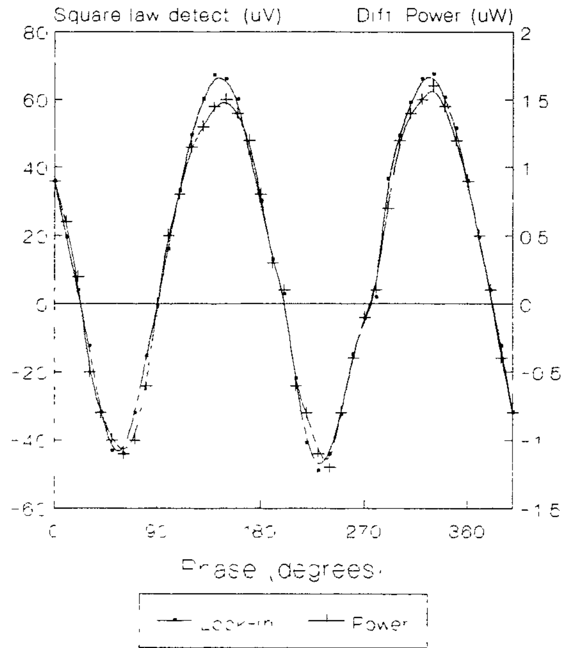

Square Law Detection (White Light)
Michelson Interferometer (CdS)

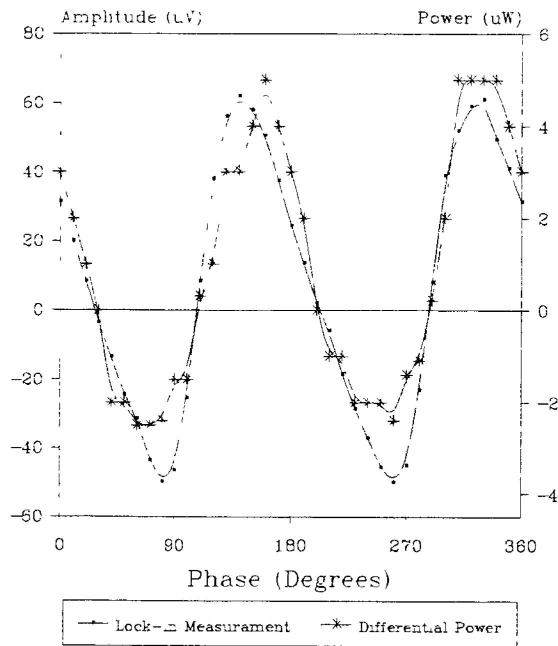

FIG. 40. Phase measurements of the difference between the power obtained with and without illumination of the sample.

5. DISCUSSION

5.1 SUBSTRATE AND MICROSTRIP CONSIDERATIONS

As stated in section 2.III, embedded elements in the artificial dielectric become conductive when light is applied. The permittivity of the artificial dielectric increases when an electric field is applied. This is due to the creation of dipoles in the clusters induced by the applied microwave signal which oppose the applied field. The same is true of the permeability, where the induced magnetic field will oppose the normal component of the applied field, since the propagating field in the microstrip is quasi-TEM mode as demostrated in section 2.IV.1. Therefore, the index of refraction, which is directly proportional to the relative permittivity and permeability (Eq. 2.III.2), will change.

When light is not incident on the dielectric, the dipoles are smaller, therefore the index of refraction will be lower since there are no induced fields opposing the microwave signal. This was seen in the experiments carried out in the network analyzer where the linear magnitude and the phase of the transmission coefficients for the CdS and GaAs samples decreased with the incident light.

The amount of change in the index of refraction could not be calculated accurately but an estimate by comparing the three dielectrics could be made. The CdS sample has about double the weight of clusters that the GaAs and Si samples have, and the size of the clusters is on average about one half the size of the GaAs and Si samples. Therefore, the number of clusters in the CdS sample is greater than in the GaAs and Si samples (See section 3.1.3). The bigger proportion and the smaller size of the CdS clusters produce more active dipoles, since light does not need to penetrate as deeply as in the bigger clusters. Thus, conductivity in the CdS clusters will be achieved more easily. As a result, the CdS sample was expected to have more variation in the index of refraction when light is applied than the Si and the GaAs samples. The artificial dielectrics formed the substrate of microstrips as shown in section 3.2. The relative permittivity of the microstrip substrate is one of the factors to consider in the design of the microstrip. Since the relative permittivity of the different samples was unknown, the design of a microstrip with an ideal 50 Ohm impedance was approximated by averaging the permittivities of the different substrates in relation to their concentration in PMMA.

Results that differed from the ideal considerations (section 4.3) were obtained from the measurements in the network analyzer, as described in section 4.3.1, and Figures 23. This be due to the following reasons:

- The permittivity suggested for the various substrates is different
- Errors in the calibration and in the plane transportation in the network analyzer
- The jig fixture wasn't making perfect contact, and inductions were obtained.
- The copper strip and the ground of the microstrip were not perfectly continuous throughout, also producing discontinuity losses and reflections.
- Imperfect contact was achieved between the tag of the launcher and the strip producing inductive capacitances.

The values obtained for the S_{11} and S_{21} indicate that there are standing waves in the line, with a maximum standing wave ratio for the CdS on the order of 1.7.

Nevertheless, the values obtained for the variation of the phase and linear magnitude of the s-parameters when light was applied indicate the phase and amplitude modulation index for the interferometer.

From table 4 we conclude the following:

- No changes were produced by the Si-doped microstrip, since Si-n doped has an excess of negative carriers, so the few electron-hole pairs created from the light are an insignificant proportion of the negative carriers already in the dielectric. Thus, the variation of characteristics of the Si substrate will be undetectable.
- The variation of the S-parameters when light is applied is proportional to the amount of the light intensity in the absorption wavelength region of the substrate. Thus, for CdS the variation of the S-parameters with the laser is smaller than with the white light source. This is because the white light source has more light intensity and covers the peak absorption wavelength of the GaAs at 510 nm., while the blue laser is only at 470 nm. Also, as shown in the plots in Figures 24, the lower light intensity from the white source produces less effect than the higher intensity for both GaAS and CdS.
- Both phase and amplitude of the S-parameters change with light for CdS and GaAs. Since light produces a change in the index of refraction, especially the effective permittivity (as stated in section 2.IV), a change in the electrical length and in the characteristic impedance of the microstrip will be produced, reflected in a change of the phase and amplitude reflection and transmission.

Looking to Figures 24a and b and 25a and b, one observes greater variation of the S_{11} and S_{21} parameters when light is applied for the CdS sample than for the GaAs sample. This was expected, since the concentration of clusters in the CdS sample is higher than the concentration of clusters in the GaAs sample. The absorption by the CdS sample from the white light source shows bigger values than for the GaAs sample (see Figures 20 and 21) as well. Also, considering that the GaAs sample has a much lower reflection coefficient than the CdS sample, the variation of the S-parameters in the GaAs sample should be more noticeable. The variations of the index of refraction from light to no light are reflected in a decrease in the linear magnitude and phase of the transmission and reflection coefficients.

As stated in equation (2.IV.3.2.2) and (2.IV.3.2.3) the S-parameters will change function of the increment in the index of refraction, and this will be reflected in a variation of the characteristic impedance and the electrical length of the microstrip, both as a function of the index of refraction.

The fact that Figures 24 and 25 show a decrease in phase and linear magnitude from dark to light and that the decrease is proportional to the amount of light incident in the microstrip, only suggested to us the variation of the parameters. Considering the imaginary part obtained that reflects capacitance and inductance effects, and that the real part of the reflection coefficient is not zero, we can not state that the variations in Figure 24 from dark to light of the S-parameters have not been attenuated and modified by the standing waves in the line. To determine the exact variation and true direction of the change of the S-parameters (increase or decrease with light), an ideal 50 Ohm microstrip would have to be fabricated where no capacitance and inductance affect the transmission. This could be accomplished by:

a) Measuring the relative permittivity as described in Sections 3.4 and 4.2,

b) Taking into consideration the changes of permittivity at higher frequencies as described in section 2.IV.3,

c) Redesigning the microstrip width/height ratio, taking into account the effective permittivity changes, for a 50 Ohm resistance, and allowing some extra length,

d) Measuring the S-parameters in the network analyzer for the working frequency of the system, then calculating the impedance and cutting the microstrip length until the imaginary part cancels, and

e) (At this stage the S11 parameter should be (0 + j0).) Applying light into the microstrip and inserting the variation into equation (2.IV.3.2.2.).

The result would give us the true direction and dimension of the variation of the phase and linear magnitude, and the variation of the index of refraction for the specific dielectric substrate used.

5.2 HOMODYNE DETECTION CONSIDERATIONS

5.2.1 PHASE RESPONSE FOR THE GaAs, Si AND CdS SAMPLES (LOCK-IN MEASUREMENTS).

5.2.1.1 MACH-ZEHNDER INTERFEROMETER

Looking at the response of the CdS and GaAs samples in Figure 25, we observe the repeatability of the detection over two periods. The maximum and minimum points and the crossings are well defined. Also shown are the phase and amplitude errors of the detection. The amplitude error is defined in (2.VI.1.4.2) as the difference in absolute value between the maximum positive and negative detected amplitudes, and is a function of the ratio between the amplitude of the reference channel and the amplitude in the information channel [4.6]. The amplitude error could be calculated by the normalized subtraction of the negative amplitude from the positive amplitude.

The results obtained for CdS and GaAs are:

Amp. error for CdS: (2.75 - 1.6) [nV]/ (2.75 + 1.6) [nV] = 0.265
Amp. error for GaAs: (32 - 8.5) [nV]/ (32 + 8.5) [nV] = 0.58

On the other hand, the detection phase error is defined as the phase difference between the zero crossing point in a detection curve with equal positive and negative amplitudes and the actual zero crossing. This error is proportional to the inverse of the sine of the ratio between the amplitudes of the reference and the information channels.

Phase error for CdS: $\phi(2.75 - 1.6/2) - \phi(0) = 30°$
Phase error for GaAs: $\phi(32 - 8.5) - \phi(0) = 60°$

The plots in Fig. 28 have the characteristic phase response of a homodyne detection system of DSBWC amplitude detection with amplitude and phase errors plus the deviation from a perfect sinusoidal signal and a shift of the extrema all of which could be due to some phase modulation as described in equations (2.VI.3.1) to (2.VI.3.7). The difference between the GaAs and CdS samples is also noticeable. While the GaAs shows a narrow positive and negative peaks amplitude and the extrema is slightly shifted backward, indicating that there is a combination of amplitude and phase modulation following equations (2.VI.3.4) and (2.VI.3.5). The CdS sample shows wider peaks, but the shifting is less appreciable, which may be due to a more pronounced amplitude modulation. The pronounced amplitude modulation in the CdS sample could be due to the fact that in the homodyne microwave circuit the SWR is much higher than in the network analyzer circuit, and since the CdS sample has a higher reflection coefficient than the GaAs sample it will contribute to a higher SWR, then the phase would be buried in the standing wave pattern.

If the carrier in the information channel is attenuated by 10 dBs as in Figure 29, the effects are obvious. Since the phase and amplitude errors are a function of the ratio of the amplitude of the carriers of the information channel and the reference channel, the attenuation of the information channel carrier will reduce the ratio and therefore the errors. As illustrated in the data obtained for CdS and GaAs, the GaAs sample in particular shows practically no error in phase and in amplitude, with crossings at 90 degrees and close positive and negative amplitudes. For the CdS sample, the error was improved but it still shows an appreciable error, which could be corrected by increasing the attenuation in the information channel. Also, in those two plots it can be seen that the amplitude obtained for GaAs is close to twice the amplitude obtained for the CdS (for the same variables in the system). This again could be due to the better SWR obtained in the GaAS microstrip. Since the reflection coefficient for the GaAs is 0.106 and for CdS is 0.267, the signal for the GaAs interferes with the reference signal with smaller SWR resulting in bigger interference.

The signal decreased proportionally more in the GaAs than in the CdS when the attenuation was applied, demostrating again that for the CdS sample interference was not as efficient as for the GaAs sample.

Figure 30 shows the response of the CdS sample to the laser and to the white light source. The two show similar position crossings and maxima and minima. This means that the amplitude and phase errors are a function of the ratio

of the carriers of the two branches in the interferometer, since the errors also improve linearly for the two sources as the information channel is attenuated. The difference between the two plots is the difference in amplitude obtained, since the white source has a much bigger amplitude than the blue light laser. This confirms the results obtained in the network analyzer where the high intensity white light obtained considerably bigger changes in phase and amplitude of the S-Parameters. The reason for the difference in amplitude is that the white light has more light intensity than the blue light laser and also, the white light has more absorptive frequencies than the blue light laser for the CdS, therefore more power could be absorbed.

At the moment of the experiment, no lasers were available in the absorption spectrum of the GaAs, therefore no comparison could be made to the data obtained with the white source.

For Figure 33 we can observe that the detection is in the square law detection region described in Section VI.1.3, since at 0 Db attenuation in the reference channel (the working point for all the experiments) the gain of detection keeps increasing. The response of the homodyne detection system is proportional to the amplitude of the reference signal up to a point. Beyond that point, the gain achieved by increasing the amplitude of the reference channel A ceases [4.11], and the detection is in the linear detection region.

Figure 34 shows the detection function of the carrier frequencies of 10 Ghz and 10.2 GHz. Observing the curve, one sees a shift in the phase front of about 60 degrees. This is due to the change in the length of the wavelength, with the result that interference occurs at a different phase front.

5.2.1.2 MICHELSON INTERFEROMETER CONSIDERATIONS

In the Mach-Zehnder interferometer the two channels (reference and information channels) were clearly identified. For the Michelson interferometer, the magic tee has the same function as the power divider and combiner of the Mach-Zehnder. The signal is equally divided and goes twice the length of the arm since reflections are produced in the short-circuits. The difference between the Mach-Zehnder and Michelson interferometer detections is that the equation for the total signal arriving at the detector for the Michelson system is

$$Et = A + b(1 + m \cdot \cos w_m \cdot t) \exp(-j \cdot 2\phi) \qquad (4.4.7.1)$$

whereas in the Mach-Zehnder (Equation 2.VI.1) a factor of one was multiplying the difference in phase between the information and reference signals ϕ.
Using the results obtained in section 2.VI.1 for amplitude modulation, one can state that the detected output at w_m is

$$Eout = K1 \cdot A \cdot b \cdot m \, [b/A + \cos(2\phi)] \cos(wm \cdot t) \qquad (4.4.7.1)$$

For linear amplitude modulation, phase modulation or the combination of amplitude and phase modulation the equations are the same as described in section 2.VI but with ϕ substituted for 2ϕ.

Figure 35 shows the different response of the Mach-Zehnder and the Michelson interferometers. The main advantage of the Michelson system over the Mach-Zehnder is that the reference signal A passes over the phase shifter twice. Then, when trying to find the maximum signal by adjusting the phase angle ($\cos 2\phi = \pm 1$) or the crossing ($\cos 2\phi = 0$), the values of 2ϕ will be :

for the crossings $2\phi = \pm(2n+1)\pi/2$
for the maximum $2\phi = \pm\ 2n\ \pi/2$

On the other hand, for the Mach-Zender those values were reached for ϕ. Thus, the change in the phase shifter setting in the Michelson is the same as the change of phase of the field. In contrast for the Mach-Zehnder the change in the phase shifted was half the phase of the field, and the phase shifter must have a range which is twice as large to measure the same variation in the phase of the field [4.11].

For the Michelson interferometer system, the phase shifter must have a minimum of 90° of differential phase shift to locate at least one zero or one maximum over the adjustable range of the phase of the shifter.

The plots illustrating the difference between Michelson and Mach-Zehnder detection are illustrated in Figure 35 for GaAs over two periods. There, the difference in the number of crossings as described above is evident.

Figure 36 shows the response for the Michelson and Mach-Zehnder detection for the CdS sample as well as the variation in detection as the information channel was attenuated.

Figure 37 shows the frequency response for the CdS sample in the Mach-Zehnder interferometer under the blue light and in the Michelson under the white light. One can observe the similar decay curve. Figure 38 shows the frequency response of the GaAs sample and the difference in detection at 50 and 200 Hz.

5.2.1.3 FREQUENCY RESPONSE CONSIDERATIONS

Figure 31 shows the frequency response of the CdS and GaAs substrates. The frequency response of the system was controlled for the generation and recombination time of the semiconductor used. After the electron-holes were created by the optical excitation, if the light is turned off during half of the cycle of the modulating frequency ($T/2 = \pi/w_m$), the semiconductor will try to restore the equilibrium of the carriers by non radiative recombination. Since GaAs and CdS are direct bandgap semiconductors, when excess carriers are introduced by the radiation, the electrons and holes will recombine directly since no additional crystal momentum is required or the transition across the bandgap. The time dependent expression for a direct recombination process as given for Sze [4.7] for a n-type sampler

$$pn(t) = pno + \tau c \cdot G_l \exp(-t/\tau_c) \qquad (4.4.4.1)$$

$p_n(t)$: number of minority carries function of time
p_{no}: number of minority carriers in equilibrium
τ_c: carrier lifetime
G_l: Generation rate of carriers under constant light
t: time past since the light was turned off

and the net recombination rate U is

$$U = (pn - pno) \cdot \tau c \qquad (4.4.4.2)$$

Both expressions are a function of the proportionality constant of the carrier lifetime, characteristic for every material.

The response time, extracted from [4.8], for the detection of light in GaAs and CdS detectors gives a response time for CdS of 0.53 seconds, and for GaAs of less than 10^{-6} seconds. Nevertheless those numbers are not indicative of the

samples being used since lifetime of the carrier is strongly sample dependent and changes from different concentration of inpurities and doppings in many orders of magnitud. From the curves however, one can state that the life time of the carriers for the CdS is much longer than the lifetime of the GaAs carriers as it shown by the fast decreasing response for the CdS frequency response curve and the slower slope in the curve of frequency response for the GaAs.

To study the influence of the carrier lifetime of the semiconductor in the detection of the optical field mixed with the microwave, followed by Yariv [4.9] for optical heterodyne detection systems, consider the signal field of the modulated light incident into the microstrip at frequency w_m

$$e_s(t) = E_m \cos w_m t \quad (4.4.4.3)$$

combined with the microwave carrier of amplitud E_1 and frequency $(w + w_m)$

$$e_1(t) = E_1 \cos(w + w_m)t \quad (4.4.4.4)$$

which gives a output field in the information channel

$$e(t) = Re(Em \exp(jw_m t) + E_1 \exp(j(w_m + w)) \equiv Re[v(t)] \quad (4.4.4.5)$$

The rate at which transitions are generated in the semiconductor is proportional to

$$W_{a \to b} : a\, V(t)\, V^*(t) \quad (4.4.4.6)$$

$V(t)$: $E(t) \exp j(w_m t)$ and is the approximate sinusoidal optical field

a: constant

The equation describing the number of excited carriers N_c is

$$\frac{dNc}{dt} = a\, V\, V^* - \frac{Nc}{\tau_c} \quad (4.4.4.7)$$

The term Nc/τ_c will correspond to the carrier's decay rate.
A solution for $N_c(t)$ is assumed in the form

$$N_c(t) = N_o + (N_1 \exp jwt + c.c.) \quad (4.4.4.8)$$

where c.c. stands for complex conjugate.
Substitution of (4.4.4.8) into (4.4.4.7) gives a solution of

$$Nc(t) = a\, \tau_c (E_m^2 + E_1^2) + a\tau_c \left[\frac{E_m\, E1\, \exp(jwt)}{1 + jw\tau_c} + c.c. \right] \quad (4.4.4.9)$$

Thus, the number of excited carriers under the sinusoidal optical field for the GaAs and CdS substrates will be determined by the carrier lifetime for all the other parameters of the same magnitude for both samples.
For a long carrier lifetime, the recombination does not occur at the half periods where light is not on for the high modulating frequencies, thus the clusters start being saturated with carriers and a smaller variation in the amount of concentration of carriers occurs. Then a smaller change in the index of refraction of the substrate will take place which is reflected in a decrease in the modulation signal of the microwave carrier.

Looking at the frequency response curves of the GaAs and CdS samples in Figure 31, the difference in the decay curves can be seen. CdS follows an exponential decay, and the GaAs follows a nearly straight line. Since the difference in response time between the two samples is so huge (on the order of 1 millionth), we believe that the detection system (mechanical chopper synchronized with the lock-in) had some loss of responsivity as the frequency was increased. Thus, the frequency response for the GaAs sample should have shown a straight horizontal line for the range of frequencies selected, and the CdS sample, a slower decay slope.

Curves in Figure 32 shows also the attenuation of the detection for increasing frequencies. However the position of the crossings and the maximum and minimum values don't change, only a decrease in the amplitude is observed. The small difference in the crossing is believed to be due to a small difference maximizing the signal in the lock-in amplifier. Also noticed is that the signal detected had less noise at the higher modulating frequency since the noise spectrum from the detector has a sizeable 1/f component [4.10]

5.2.2 PHASE MEASUREMENTS IN THE POWER METER

The mixer featured power splitting as shown in figures 16, 18 and 19 where power could be detected before the square law detection. The power attenuation between the input to the output power of the mixer was 9 Dbs, hence the low levels of powers obtained in comparison with the power in the generator.

Figure 39 shows the power detected for the GaAs and CdS samples as a function of phase shifted, in comparison with the data obtained in the lock-in amplifier. The readings in the power meter and in the lock-in were done at the same time and at the same position of the phase shifter.

The power meter reads a signal proportional to

$$E_t^2 = A^2 + b^2(1 + m\cdot \cos w_m)^2 + 2\ A\cdot b(1 + m\cdot \cos w_m\cdot t)\ \cos 2\phi$$

since the power meter reads the average of $E^2(t)$ over one period:

$$\langle P\rangle \quad \alpha \quad \int_0^T E^2(t)\cdot dt$$

while the lock-in has a reading as derived in Equation (4.4.7.1). Observe that the two equations have a DC factor and a factor proportional to the cos 2ϕ in the Michelson interferometer configuration.

The main reason for the difference between the maximums in the GaAs and CdS with respect to the maximums in readings in the lock-in (CdS leading and GaAs lagging) is the difference in length of the samples plus the qualitatively different response of the permittivity of the samples to incident light. One must also consider that some amount of error could have occurred due to the absence of isolation between the detector and the magic tee producing multiple reflections and creating standing waves in the output arm, or reflections in the reference channel due to an improperly calibrated phase shifter, or due to imperfections in the short circuits creating reflections at different angles.

Another experiment was performed by taking the reading in the power meter under illumination of the sample and then blocking the light and observe the difference in the readings. The readings were performed through the range of the phase shifter. The results are shown in Figure 40. One can observe the

matching in the crossings and in the maxima of the curve with the lock-in amplifier detection curve.

The difference in the sign of the subtraction between the power detected with and without illumination comes from the change of sign of the cosine function as the phase in the reference channel is shifted from zero to 2π.

As an illustrative example, consider the output function of the DC value plus a constant multiplying $\cos\phi$,

$$P = DC + K \cos 2\phi$$

The $\cos\phi$ term is the difference between the phase in the reference channel ϕr and the phase in the information channel ϕi. The variation of phase produced by the illumination of the microstrip in the information channel is $\delta\phi$. Therefore

$$\cos 2\phi = \cos 2(\phi r - \phi i) \text{ without illumination}$$
$$\cos 2\phi 1 = \cos 2(\phi r - (\phi i - \delta\phi)) \text{ with illumination}$$

For simplicity consider $\phi_i = 0$; then the difference between the power detection with and without illuminating the sample is a function of

$$\cos 2\phi - \cos 2\phi_1 = \cos 2\phi_r - \cos 2(\phi_r - \delta\phi)$$

If ϕ_r is varied from 0 to 2π with $\delta\phi$ constant, the curve obtained will have two cycles. If the value of ϕ_i is not zero the phase of the curve obtained will be shifted, as is the case in Figure 40.

The ratio between the difference in DC power obtained with and without illumination and the total DC power measured will give us the modulation index for each microstrip and the amount of light applied.

$$m = \frac{\text{Maximum Power in darkness - Maximum power under light}}{\text{Maximum Power in darkness}}$$

Then for CdS sample, the modulation index is:

$$m = \frac{5\ [uW]}{650\ [uW]} = 0.008$$

And for the GaAs sample, the modulation index is:

$$m = \frac{1.5\ [uW]}{700\ [uW]} = 0.002$$

This confirms the measurement in the network analyzer where the parameters of the GaAs sample varied less with light that for the CdS sample.

6. CONCLUSIONS AND SUGGESTIONS

Based on the discussions from the previous section, we can state that electrical and magnetic dipoles, optically generated in the semiconductor clusters, have changed the index of refraction of the microstrip's substrate, varying the characteristic impedance and the electrical length of the microstrip. Those variations have been used in a homodyne detection system to optically control a microwave signal.

Suggestions for future research:

Fabricate a microstrip of characteristic impedance of 50 Ohms and a value for the S11 parameter of (0 + j0). Then, if light is applied to the microstrip and the variation inserted into equation (2.IV.3.2.2.), the result would give the true direction and dimension of the variation of the phase and linear magnitude, as well as the variation of the index of refraction for the specific dielectric substrate used.

The use of more powerful light sources (above 10 mW), should increase the response, since the response is proportional to the light intensity applied. Also a narrower bandwidth laser will avoid thermal effects that may conflict with the conductivity of the clusters, since conductivity is inversely proportional to temperature.

Also, the phase could be better monitored if symmetrical arms (in length and in the class of cables and connectors) of the interferometer were used.

The strip adhesivity to the substrate offered some problems. This could be improved if another deposition of a very adhesive material (like chromium) were evaporated under the copper.

The carrier frequency in the experiment was subjected to the bandpass X-band microwave components used. However, the same experiment could be carried out with much lower frequencies, thereby avoiding dispersion in the microstrip.

The microstrip also could be isolated from external interference by casing it in a metallic structure. If a semiconductor laser with a high divergence angle is placed in a aperture in the case at 45° from the plane of the microstrip, a noiseless signal could be expected.

REFERENCES

1.1 Collin, *"Field theory of guided waves"*, McGraw-Hill, New York, 1960, chapter 10

1.2 Yariv, A. *"Optical Electronics"*, Holt, Rinehart and Winston Co., New York, 1985, chapter 9, p.132

2.1 Sze, S.M. *"Semiconductor Devices"*, Wiley, New York p. 513

2.2 Yariv, p.132

2.3 Harper, C.A. *"Handbook of Electronics Components"*, McGraw-Hill P. Co. New York, p 5-100

2.4 Seshadri, *"Fundamentals of transmissions linesand EM fields"*, Adison-Wesley P. Co. Inc., Reading MA. p.227

2.4b Ibid, p.224

2.5 Collin, *"Field theory of guided waves"*, McGraw-Hill, New York, 1960

2.6 Gupta K.C. *"Microstrip Lines and Slot Lines"*, Artech House Inc., Norwood, MA 1979, p. 4

2.7 Fooks, E.H.,*"Microwave Engineeing Using Microstrip Circuits"*, Prentice-Hall, New York, 1990, p.6

2.8 Hoffman, *"Microwave Integrated circuits"*, Artech House Inc., Norwood, MA

2.9 Balanis, C.A., *"Advance Engineering Electromagnetics"* Wiley & Sons, Inc, 1989 p. 452

2.10 Fooks, p. 79-80

2.11 Deulinger, E.J, *"A frequency dependent solution for microstrip transmission lines"*, IEEE Transactions of Microwave Theory and Techniques Vol MTT-19 , No 1, January 1971, p. 30

2.12 Bianco B. et all,*"Some considerations about the frequency dependence of the characteristic impedance of uniform microstrips"*, IEEE Transactions on Microwave Theory and Techniques, Vol MTT-26, No 3. March 1978, p.182

2.13 Balanis C., *"Advanced Engineering electromagnetics"*, Wiley, New York, 1989, p. 453
2.13b Fooks, p. 13
2.14 Jones R. & Wykes, *"Holographic and Speckle Interferometry"*,. Cambridge University Press, Cambridge, p. 11
2.15 King, R.J.*"Microwave Homodyne Systems"*, Peter Pellegrinus Ltd., Southgate House, Stevenage England 1978, P. 5 - 70
3.1 Polyscience,Inc *"Embedding with Methyl Methacrylate"* Data sheet No.104, June 1984, Poliscy, Warrington
3.2 Mohler, J.B. *"Electroplating and related Process"* Chemical Publishing Co. Inc, New York 1969, p.118
3.3 Blum, W at all, *"Electroplating and Electroforming"* McGraw-Hill, New York 1949, p. 290,
3.4 Balanis, p. 150
3.5 Hewlett-Packard, *"Measuring the relative permittivity and permeability of solids materials with the HP-Network Analyzer.*
3.6 Liao, S.Y. *"Microwave devices and circuits"* Prentice-Hall, 3rd Ed. Englewood Cliffs, NJ, p.146
3.7 Balanis, p. 445
3.8 Liao, p. 54
4.1 Liao, p. 34
4.2 Sze, p 513
4.3 Fooks, p.6
4.4 Harper, p. 5-95
4.5 Harper, p. 5-95
4.6 King, p. 11
4.7 Sze, p. 47
4.8 Harper, p. 5-98
4.9 Yariv, p. 361
4.10 King, p. 9
4.11 King, p. 19
4.12 King, p.133